Design of Time-Varying Hybrid Zero Dynamics Controllers for Exponential Stabilization of Agile Quadrupedal Locomotion

Joseph B. Martin V

Thesis submitted to the Faculty of the
Virginia Polytechnic Institute and State University
in partial fulfillment of the requirements for the degree of

Masters
in
Mechanical Engineering

Kaveh Akbari Hamed, Chair
Alexander Leonessa
Erik Komendera

October 1st, 2020
Blacksburg, Virginia

Keywords: Nonlinear Control, Quadrupedal Locomotion

Design of Time-Varying Hybrid Zero Dynamics Controllers for Exponential Stabilization of Agile Quadrupedal Locomotion

Joseph B. Martin V

ABSTRACT

This thesis explores the development of time-varying virtual constraint controllers that allow stable and agile gaits for full-order hybrid dynamical models of quadrupedal locomotion. Unlike time-invariant nonlinear controllers, time-varying controllers do not rely on sensor data for gait phasing and can initiate locomotion from zero velocity. Motivated by these properties, we investigate the stability guarantees that can be provided by the time-varying approach. More specifically, we systematically establish necessary and sufficient conditions that guarantee exponential stability of periodic orbits for time-varying hybrid dynamical systems utilizing the Poincaré return map. Leveraging the results of the presented proof, we develop time-varying virtual constraint controllers to stabilize bounding, trotting, and walking gaits of a 14 degree of freedom quadrupedal robot, Minitaur. A framework for selecting the parameters of virtual constraint controllers to achieve exponential stability is shown, and the feasibility of the analytical results is numerically validated in full-order model simulations of Minitaur.

Design of Time-Varying Hybrid Zero Dynamics Controllers for Exponential Stabilization of Agile Quadrupedal Locomotion

Joseph B. Martin V

GENERAL AUDIENCE ABSTRACT

This thesis extends a class of controllers designed to address the full dynamics of stable locomotion in quadrupedal robots. As of yet, there is no widely-accepted standard methodology for controlling the complex maneuvers of quadrupedal locomotion, as most strategies rely on simplified models to ease computational constraints. "Virtual constraint" controllers — also known as Hybrid Zero Dynamics controllers — are a class of controllers designed to address the full dynamics of legged locomotion by coordinating the links of a legged robot model to follow a periodic trajectory representing the desired gait pattern. However, the formalized "time-invariant" model of virtual constraint controllers relies on sensor data to track progress on the desired gait trajectory. This dependence on sensor data makes the resulting controllers unable to start from a state of zero velocity and sensitive to disturbances generated by high velocity impacts. The proposed "time-varying" virtual constraints controllers utilize the elapsed time to track gait progress and do not have the previously mentioned limitations. Motivated by these benefits, we develop a formalized methodology for designing time-varying virtual constraint controllers for quadrupedal robots. This includes extending time-invariant means of mathematically validating the stability of the gait controllers to time-varying systems. With strategies of designing and validating time-varying virtual constraint controllers formalized, the methodology is implemented on numerical simulations of bounding, trotting, and walking gaits for the quadrupedal robot Minitaur which validates the stability and feasibility of the developed controllers.

Acknowledgments

The research and writing of this thesis was built on a foundation of support for which I continue to be grateful.

First, I would like to thank my advisor Dr. Kaveh Akbari Hamed for his guidance, wealth of knowledge, support of my work, and the opportunity to have an impact on the greater robotics community. I am thankful to be a part of the early foundation of this lab and I am looking forward to what its future holds.

I would also like to acknowledge the work of my colleagues in the Hybrid Dynamic Systems and Robot Locomotion Lab. Not only was your work integral in achieving publication of this research, but your collaborations and insight were instrumental to the development of my technical understanding of the work and my confidence in my contributions.

I thank my family: my father JoeB, my mother Jodi, my brother Benjamin, grandparents, aunts, uncles, cousins, and beyond. You have supported me through all the challenges and victories of my life, including chemotherapy, physical and mental well-being, and academic success. In the truest sense of the idiom, I would not be here without you. I hope one day to pay forward even a fraction of what you've given me to the future generations.

Finally, I would be remiss not to thank my friend Dana Cohen, who offered her time and heart during the longest nights and the toughest challenges of research. May our next decades of friendship be just as great as the last.

Contents

List of Figures

List of Tables

Chapter 1

Introduction

1.1 Overview

Robust legged locomotion provides robots access to a diverse range of environments, thus making legged machines the subject of intense study. Every day, bipedal and quadrupedal animals expertly navigate both unpredictable natural terrain and systematically manufactured spaces. Robots which take advantage of this locomotion structure offer the versatility to navigate almost any land environment [11] with an energy efficient model that has found success both in nature and the robotics community.

The access that legged robots have to these natural and man-made environments makes such machines more suitable for applications in fields like natural disaster relief, search and rescue efforts, and industrial maintenance over wheeled transportation which is limited to about half of land terrain [12] despite a greater energy efficiency [13]. The study of robotic legged locomotion is also intertwined with the study of biological locomotion, with applications ranging to prostheses with control feedback and functional exoskeletons. While robotic bipedal locomotion has over several decades of academic application, extension to the wide range of quadrupedal gait patterns is a relatively unexplored area of the legged locomotion field. Quadrupedal robotics is certainly not without its own impressive accomplishments with dynamic, quadrupedal gaits having been designed for robots such as Spot [1], Big Dog [11], ANYmal [10], MIT Cheetah [14], Vision 60 [5], and IIT HyQ [15] (see Fig. 1.1). Still, there is ample room for growth in the field.

In order for both bipedal and quadrupedal robots to become practical choices for day-to-day application, we must be able to quickly produce robots with reliable, stable gait trajectories with robust control. These robots must be able to act in a wide range of environments and employ complex, dynamic maneuvers. The end goal is not just to have robots which can engage in environments too dangerous for humans, but to also have a class of controllers which allow for the safe and seamless integration of legged machines into human daily life.

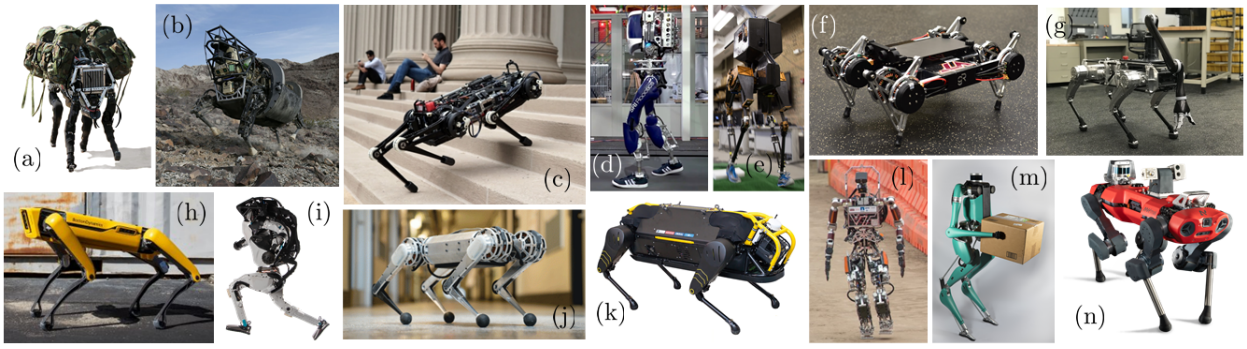

Figure 1.1: A diverse sampling of state-of-the-art legged robots. (a) Big Dog (Boston Dynamics) [1], (b) LS3 (Boston Dynamics) [1], (c) Cheetah (MIT) [2], (d) DURUS (AMBER Lab) [3], (e) ATRIAS (University of Michigan/Oregon State University) [4], (f) Minitaur (Ghost Robotics) [5], (g) Vision 60 (Ghost Robotics) [5], (h) SpotMini (Boston Dynamics) [1], (i) Atlas (Boston Dynamics) [1], (j) Mini Cheetah (MIT) [6], (k) HyQReal (Italian Institute of Technology) [7], (l) ESCHER (Virginia Tech) [8], (m) Digit (Agility Robotics) [9], (n) ANYmal (ETH Zurich) [10].

Many steps have been taken toward this end, but a standard approach to generally address the full dynamics of legged machines has yet to solidify itself in the field.

1.2 Literature Review

1.2.1 Zero-Moment Point Control and the Foot-Rotation Indicator

As a legged locomotion framework with over four decades of history and as the origin of experimental bipedal locomotion, Zero-Moment Point (ZMP) control is a clear bench-marking point for all other legged locomotion approaches [16, 17]. This framework defines the ZMP as the point on the locomotion surface where the summation of all relevant forces on the robot body can be represented by a single linear force vector. This control method ensures the walking robot is fully-actuated and balanced over the course of the entire gait cycle by preventing the ZMP from exceeding the interior of the convex support region made by the contact foot or feet. ZMP based locomotion and extensions thereof have seen success with single-leg [18], bipedal [19, 20, 21, 22, 23, 24, 25, 26, 27, 28, 29, 30, 31] and quadrupedal [32] models. However, if the ZMP falls outside of the support region, the system will become underactuated and no longer meet the dynamic balance condition. In these cases, additional recovery control methods must be performed to return the robot to its ideal orientation. Despite its longevity and proliferation, ZMP control fails to robustly address the underactuation inherent in biological legged locomotion by enforcing the dynamic balance condition at all

stages of the gait. This causes robots which rely on ZMP control to struggle in more complex terrain and to be much less energy efficient than other control methodologies. Researchers often rely on reduced-order models for ZMP control implementations as well. Nevertheless, the principles of the ZMP provide intuitive understanding of the performance of other gait controllers even if they do not explicitly maintain the support region condition.

Similar in concept to the ZMP, the foot-rotation indicator (FRI) can be used to establish criteria for dynamic stability. The FRI point describes the location where the net ground reaction force (GRF) would have to act to keep the target foot stationary [33]. Unlike ZMP, the FRI point does not need to remain within the foot support polygon for the robot to be in a state of stability. The FRI point can be used to measure the degree of unbalanced torque on the support frame, as opposed to the more binary application of the ZMP in defining instability.

1.2.2 Reduced-Order Models

Legged locomotion naturally poses the challenge of controlling high degree of freedom (DOF) systems. Therefore, control strategies have been developed to reduce the scope of the stability problem. These reduced-order strategies tend to focus on modeling the trajectory of the center of mass (COM) in biological locomotion while eliminating symmetries and redundancies present in biological systems, such as parallel musculature [34]. The Linear Inverted Pendulum (LIP) model is a single DOF model which treats the contact of a stance leg as a pivot which the COM vaults over in an appropriate exchange of kinetic and gravitational potential energy [34]. Though the COM trajectory does not accurately model that of the biological human walking gait [35], the technique has retained longevity with a solid foundation of success including approaches found in the DARPA Robotics Challenge [36, 37, 38]. However, in order to apply these models to physical implementations, the COM must have full actuation which in turn typically necessitates a fully-actuated foot design. In contrast, many agile machines make use of the point foot model which leads to underactuation during dynamic gaits [9, 4, 5]. The LIP can also be extended to the Spring Loaded Inverted Pendulum (SLIP) model, where a compression spring is added to the pendulum model of the leg. In addition to the previous dynamics, the COM will store elastic potential energy during the first half of the contact phase, and release this energy in the second half [34]. As well as being able to accurately track the COM of human runners [39], this simple model can be implemented on a wide variety of leg structures including multi-link single, bipedal, and quadrupedal contact models by mapping the forces of a set of contact legs to a single virtual leg [40, 41, 12]. SLIP dynamics can also be extended to capture additional target dynamics. The Asymmetric Spring Loaded Inverted Pendulum (ASLIP) nontrivially couples torso pitch with the virtual leg dynamics [40]. The Lateral Leg Spring (LSS) model includes additional modeled linear springs to account for the effects of GRF perpendicular to the sagittal plane. This model adds a yaw angle to the 2D translation of the body mass to allow for 3D steering of the otherwise planar dynamics [34].

In some cases, the leg dynamics are ignored completely by the controller, treating the robot as a floating base link subject to forces based on the positions of contact feet attached to zero-mass virtual legs [41]. This strategy can be used to address a wide variety of quadrupedal gaits as demonstrated by the MIT Cheetah 3 which had a combined leg mass of roughly 10% of its total mass [42]. Along with leg mass limitations, the orientation of the single rigid body must be represented by global coordinates to avoid issues of singularity and inconsistent behaviors across operating configurations [43]. Nontrivial leg dynamics have also been explored [44], but such models still offer a significant reduction in scope from a full-order model.

1.2.3 Model Predictive Control

In the context of legged locomotion, Model Predictive Control (MPC) determines the current optimal control input by solving for the optimal sequence of control inputs acting on the state model for a finite prediction range. Optimality is determined by comparison to a reference trajectory of the supplied state model subject to state and actuation constraints. Once an optimal sequence is determined, the first iteration of the sequence is used as the control input. The process then repeats, solving the optimization problem at each iterative step. MPC also utilizes a least-squares approach to determine the best control sequence if the reference trajectory becomes infeasible due to a state of underactuation or constraint limitations. In addition to directly computing actuated joint torques, MPC has also been used to determine desired ground reaction forces for the trajectory of a reduced-order model floating base [42, 43, 45]. Other applications of MPC include policy regularized MPC [46], nonlinear MPC [47] and event-triggered control [48]. Since MPC requires predictive simulation at every iteration, it must employ simplifications to the problem scale such as implementing reduced-order models and taking advantage of the structure of a linear program (LP) or quadratic program (QP) formulation of the optimization problem [49, 43, 50]. Additionally, real-time computation constraints can be reduced if MPC is not solved at every time sample [51]. MPC has recently been extended to full-order systems [52, 53], but the approach still suffers from issues of scalability even with QP formulation.

1.2.4 Hybrid Systems Theory

Hybrid systems theory is a versatile technique for formalizing the dynamics of legged locomotion into a directed graph structure addressable by several paradigms of feedback control. Models of legged robots are hybrid with continuous-time domains (i.e., phases) to represent the Lagrangian dynamics and discrete-time transitions between continuous-time models to represent the changes in physical constraints (e.g., a new contact point with the environment is added to the existing set of contact points or an existing contact point is broken). Steady state locomotion corresponds to periodic solutions of these hybrid models. The

Lagrangian dynamics are also subject to holonomic physical constraints locking the contact feet in place. The forces from the contact constraints are applied to the dynamics of the robot model and are used to calculate the feasibility of the ground reaction forces. Hybrid systems theory has been successfully applied to a wide range of control strategies [54, 55, 56, 57, 58, 59, 60, 61, 62, 63, 64, 65, 66, 67, 68, 40, 69, 70, 71, 72, 73, 74, 75, 76, 77, 78] such as hybrid zero dynamics (HZD) [79, 68, 80, 56, 81, 82, 83], Lyapunov functions [84, 85], transverse linearization [59, 86], hybrid reduction [87, 88, 89, 90], and controlled symmetries [57].

1.2.5 Transverse Linearization

One methodology which can address the underactuation inherent to dynamic legged locomotion is transverse linearization. Any arbitrary desired motion in the vicinity of a periodic orbit can be split into coordinate subsystems which represent the dynamics along the periodic orbit and the dynamics transverse to the orbit respectively [91]. Regardless of the level of underactuation, the transverse dynamics can be linearized and then driven appropriately. Notably, a linearization cannot be asymptotically stable about an entire periodic solution, so the transverse dynamics must be linearized locally [86]. However, the control strategy does not scale well with the high DOF systems of quadrupeds, which can have 2-4 DOF per leg [83, 11]. Additionally, while the theory of transverse linearization applies to arbitrary, nontrivial maneuvers of any level of underactuation, it may not systematically address robustness against uncertainty in full-order nonlinear models of locomotion that which can cause the methodology to break down in practice. Furthermore, the simplifications of linearization may eliminate potentially advantageous nonlinear dynamics.

1.2.6 Hybrid Reduction

Hybrid reduction seeks to take advantage of the symmetries of systems which have Lagrangians that are only dependent on a subset of the coordinates of the configuration space by identifying coordinates which do not appear in the Lagrangian, referred to as "cyclic" variables [92]. By applying Routhian techniques of reduction to Lagrangians which are cyclic save for one non-cyclic variable in the potential energy, the dynamics of the resulting reduced-order Lagrangian can be used to reconstruct full-order dynamics [93]. Further theory applies these reduction strategies for hybrid dynamics [88]. This approach has been used to address both 2D and 3D models of bipedal walking [94], including using a 2D control law to control a 3D walker [93].

1.2.7 Passivity Approaches

Passivity approaches seek to exploit passive dynamics in walking to minimize controller effort. This research extends the fundamental work of McGeer in developing a biped which could stably walk down a shallow incline without control or energy input [95]. Research in planar mechanisms has shown that purely passive gaits are limited to shallow slopes [95, 96, 97, 98]. These passive gaits may also exhibit dynamic behavior, where the COM is not limited to the foot support region. Three-dimensional passive walking has been achieved through the use of specialized feet to stabilize the lateral motion of the gait [99]. From the passive walkers came explorations of feedback, such as introducing gravity compensation which adjusts the gait for different slopes by shaping the potential energy [100, 101], and applying passive gait trajectories to the gait design of actuated trajectories on level ground [102]. More recent research in this domain has focused on full Lagrangian shaping to induce controlled symmetries [57, 58] and utilizing virtual holonomic constraints to ease the computational burden of finding stable gaits for passive walkers [103].

1.2.8 Hybrid Zero Dynamics

Hybrid zero dynamics (HZD) is an extension of Byrnes-Isidori zero dynamics [104] to hybrid models of legged locomotion and has become a powerful approach which addresses the inherent underactuation of dynamic legged locomotion [79, 80]. However, the current state-of-the-art of HZD is mainly tailored to address bipedal robots. In this approach, the coordination of the links is based on the description of output functions—known as virtual constraints [54, 105, 106]—which are imposed via the action of a feedback controller (e.g., input-output (I-O) linearization). These virtual constraints map the error of the state variables with respect to a desired trajectory to an output vector which defines a nontrivial subset of the state space where the virtually constrained robot evolves (the zero dynamics manifold). Virtual constraint controllers have been successfully implemented in simulation and practice on a wide variety of 2D and 3D bipedal robots [54, 67, 55, 107, 77, 108, 109, 110, 69, 111, 83, 112, 56, 113, 66, 114, 82], lower-extremity prosthesis [115, 116, 65], exoskeletons [117, 118, 119], monopedal robots [40, 120], reduced-order models of quadruped locomotion [44], and full-order models of trotting, ambling, and walking gaits [121, 122].

1.2.9 Time-Invariant HZD Controllers

Time-invariant parameterization is the most common method for tracking progress on the evolution of a gait subject to virtual constraint control. A combination of state parameters which strictly monotonically increases over desired evolution of the gait is selected. This term is often referred to as the "phasing variable." During continuous-time evolution, the value of the time-invariant phasing variable determines the reference signal from the desired

periodic orbit supplied to the HZD controller. While asymptotic (exponential) stability of the desired periodic orbit is guaranteed by the theory of state-varying HZD controllers, in practice the reliance on state-based phasing variable introduces a reliance on precise sensor feedback and accurate physical models [123, 124]. In particular, time-invariant approaches do *not* account for sensor aggravations due to the impacts inherent in dynamic locomotion. This issue is exacerbated in the cases of gaits with extended flight phases such as bounding and galloping. Another practical concern is the initial perturbation of the robot required to begin a time-invariant control trajectory. The evolution of the HZD controller output requires the time-invariant phasing variable to be evolving, which precludes a static initial condition. Thus, robots which utilize time-invariant HZD control must be perturbed to begin locomotion, often by a push from a human operator. This condition increases the difficulty of providing consistent and viable initial conditions that will approach the limit cycle of the desired gait. Time-varying controllers do *not* need the initial state to be perturbed in this way, giving such controllers a clear advantage in this case.

1.2.10 Event-Based Controllers

Event-based controllers act on outputs which are sampled based on discrete criteria rather than a constant sampling, and such controllers have a long history in a variety of controller applications beyond legged locomotion. Strategies can be grouped into controllers which sample the output based on measured events ("event-triggered control") and controllers which sample the output based on predicted dynamics ("self-triggered control") [125]. These controllers are often used in decentralized systems, where multiple controllers act in tandem without access to global information.

Event-based controllers for legged locomotion are event-triggered controllers implemented in a multi-level control structure, where parameters held constant over the course of continuous time phases are adjusted at each impact event based on the ground reaction forces with the goal of generating eigenvalues of the Jacobian linearization of the Poincaré return map which form a Hurwitz matrix [66, 126, 127, 128, 129, 130, 131, 132, 62, 133, 108, 111]. An impulse-based controller was developed for the Cheetah quadruped but was shown to be insufficient to drive the periodic orbit of its hybrid bounding gait to stability without the addition of continuous time feedback control [14]. Additionally, event-triggered controllers suffer from the delay between the discrete event and the appropriate augmentation of the controller effort. There have been attempts to achieve locomotive stability at the first level [67, 134, 83, 135, 121] by solving offline optimization problems.

1.2.11 Direct Collocation for Gait Planning

The process of generating an optimal locomotive gait for a full-order model subject to HZD control can be formatted into a nonlinear program (NLP), where the contact requirements

can be formatted as equality constraints and the control input can be modeled as a cost function. While both direct single-shooting [136, 80] and multiple-shooting [137, 138] approaches have been implemented to solve the gait planning NLP, these methods face scalability issues when applied to high DOF systems and systems with high degrees of underactuation [139]. This scalability problem has been addressed with the direct collocation method [77, 140, 141, 142, 143], which is the foundation of the optimization process in the Fast Robot Optimization and Simulation Toolkit (FROST) [144]. These direct collocation methods discretize the dynamics of continuous phases of the hybrid gait and treat the state variables as optimization variables, seeking to generate a piecewise trajectory that satisfies the NLP. Direct collocation has been used to generate optimal gait trajectories for a variety of systems including bipeds [77, 144], quadrupeds [122], and prostheses [145], making it a versatile tool for legged locomotion.

1.3 Motivations and Challenges

While there has been terrific progress in the extension of bipedal gait controller methodologies to quadrupedal locomotion, quadrupeds still lag behind in a few key areas of the state-of-the-art. There are few strategies that can address the full-order dynamics of the inherently high DOF systems, and methods that do can still suffer from issues of scalability. Implementations of HZD controllers show promise in addressing high DOF systems, but current time-invariant approaches need to be supplemented with additional strategies to enlarge domains of attraction and robustness. While reduced-order models and hierarchical control strategies provide valuable insight into the challenges and streamlining strategies for control of high DOF systems, quadrupedal locomotion needs a straightforward and robust formal methodology to address the full-order dynamics of modern robotic quadrupeds.

1.4 Goals, Objectives, and Contributions

The ***overarching goal*** of this thesis is to establish a formal foundation to generate and stabilize dynamic quadrupedal gait controllers via time-varying HZD controllers. Through the development of bounding, trotting, and walking gaits for a full-order hybrid model of an advanced quadrupedal robot, Minitaur, the work of this thesis provides the following ***key objectives*** and ***contributions*** to the research of quadrupedal legged locomotion and HZD controllers:

1. **Extension of the Poincaré analysis to exponentially stabilize dynamic gaits via time-varying nonlinear controllers**

   Poincaré sections analysis is the most powerful approach to investigate the existence and stability of periodic solutions to time-invariant nonlinear dynamical systems [54,

146, 147, 148, 83, 66, 65]. In this approach, the stability of periodic solutions (i.e., periodic orbits) for hybrid dynamical systems is translated into that of a fixed point for a discrete-time nonlinear system, referred to as the Poincaré return map. The Poincaré return map maps the evolution of the hybrid dynamical system from a point on a hyperplane transversal to the orbit, referred to as the Poincaré section, back to the hyperplane. This analysis addresses the asymptotic and exponential stability of gaits for legged robots under time-invariant controllers by studying the Jacobian linearization of the Poincaré return map. In particular, if all eigenvalues of the Jacobian matrix lie in the complex unit circle, the periodic orbit is exponentially stable. This thesis provides necessary and sufficient conditions to utilize this analysis on periodic gaits using time-varying controllers. The results show that the Poincaré section analysis can be extended to investigate the stability of periodic solutions for *periodic* and *time-varying* hybrid systems.

2. **Time-varying virtual constraint design for full-order quadrupedal gaits**

   Time-varying HZD controllers are developed in this thesis to achieve stable bounding, trotting, and walking gaits for full-order hybrid models of quadrupedal locomotion. Direct collocation and HZD-based gait planning methods using FROST are first used to generate optimal, feasible, and periodic trajectories for each desired gait. The intuition and procedure for determining the virtual constraints corresponding to these trajectories are then discussed to synthesize time-varying HZD controllers to exponentially stabilize the optimal gaits. The effects of output (i.e., virtual constraints) selection are analyzed with respect to the available outputs to insure exponential stability in the presence of overactuation, full actuation, and underactuation in the gait cycles. Additional considerations are made through understanding the dynamics of each gait and the defined robot model.

3. **Numerical verification of the analytical results using full-order simulations**

   Analytical results of the paper are numerically verified on a full-order simulation model of bounding, walking, and trotting gaits for a quadrupedal platform, Minitaur, with 14 degrees of freedom. The closed-loop simulation demonstrates the convergence to the desired gaits with perturbed initial conditions. The limit cycles of each gait are shown to be exponentially stable by demonstrating that the eigenvalues of the Jacobian matrix of the Poincaré return map are within the complex unit circle and by visualizing the resulting gait trajectories.

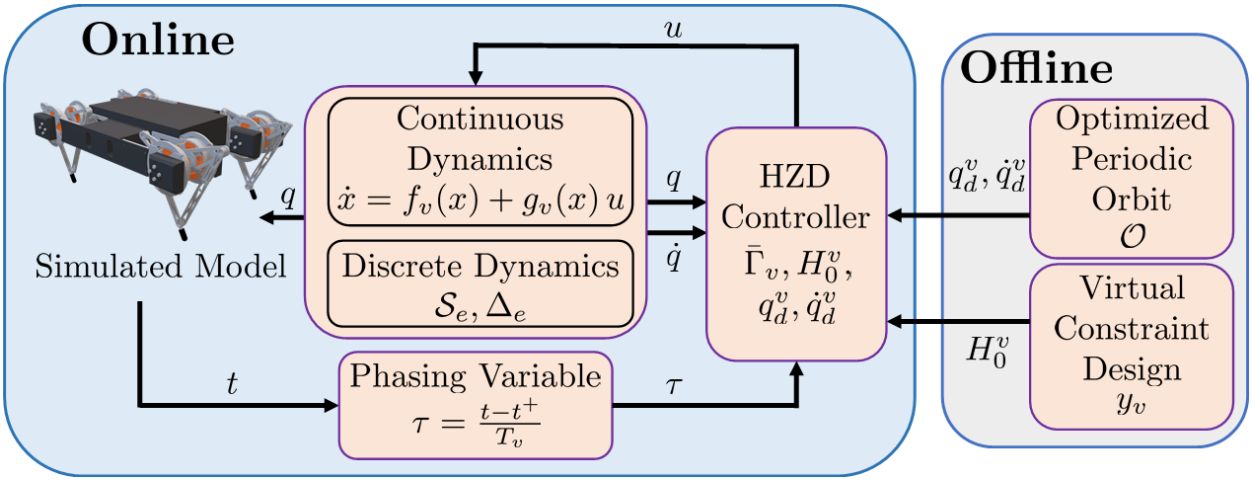

Figure 1.2: Illustration of the single-level time-varying HZD control algorithm. The continuous and discrete dynamics are discussed in Chapter 2, the HZD controller and virtual constrain design process are covered in Chapter 3, the extension of the Poincaré sections analysis to time-varying and periodic hybrid systems is provided in Chapter 4, and the optimization procedure for developing the ideal periodic orbit is described in Chapter 5. Chapter 6 covers the results of the controllers implemented on the simulated model of Minitaur.

A portion of the results of this research has been accepted to appear and presented in the 2020 IEEE/RSJ International Conference on Intellignet Robots and Systems (IROS) [149], that is,

- **J. Martin**, V. R. Kamidi, A. Pandala, R. Fawcett, and K. Akbari Hamed, "Exponentially stabilizing and time-varying virtual constraint controllers for dynamic quadrupedal bounding," *IEEE/RSJ International Conference on Intelligent Robots and Systems (IROS)*, Accepted to Appear, Las Vegas, NV, October 2020

In particular, the described methodology is applied to develop a bounding gait for Minitaur in the above-mentioned paper. This thesis provides an expanded analysis of the results of the bounding gait and extends the methodology to the development of trotting and walking gaits for Minitaur.

1.5 Outline of Thesis

The remaining material of this thesis is organized as follows. Chapter 2 covers the background of hybrid models and provides hybrid gait descriptions for quadrupedal bounding, trotting, and walking gaits for a described model of the robot Minitaur. Chapter 3 discusses the theories of HZD and virtual constraints and show how they are applied to the controllers for

the hybrid gaits discussed in the previous chapter. Chapter 4 demonstrates how exponential stability for a hybrid gait with a time-based phasing parameter can be evaluated through an adaptation of the Poincaré sections analysis developed for time-invariant designs. The methods by which optimal gait trajectories of the hybrid systems are generated are described in Chapter 5, with a primary focus on the FROST methodology and its implementation of direct collocation. Chapter 6 presents the simulated results of the closed-loop hybrid system. Chapter 7 finally summarizes the implications of these results and the future work they provide a platform for. Figure 1.2 provides a visual representation of how the components of each chapter are utilized in the overall design of the controller.

Chapter 2

Mutli-Contact Quadrupedal Locomotion via a Hybrid Systems Approach

2.1 Background

The initial step in developing controllers using the HZD framework is to convert the real-world dynamics of robotic locomotion into hybrid dynamic models. First, we will introduce the simplified model of the quadrupedal robot Minitaur from Ghost Robotics [5]. The resulting model is full-order, but removes unnecessary holonomic constraints to aid in the computation of the NLP. A summary of the general mathematics and conventions of hybrid systems formulation will then be provided, defining the fundamental continuous-time and discrete-time phases that make up a hybrid gait trajectory. This formulation will be used to define hybrid trajectories for the quadrupedal bounding, trotting, and walking gaits. Table 2.1 provides a list of definitions for the symbols and terms introduced in this chapter.

2.2 Robot Model

Minitaur is a quadrupedal robot developed by Ghost Robotics [5] and serves as the model testbed for the series of quadrupedal gait controllers developed in this work. The robot has a rectangular chassis which contains the power supply, microprocessor, and on-board computer (see Fig. 2.1). Eight motors positioned in pairs at each corner of the chassis control the four legs of Minitaur. Each of the four legs is composed of a four-bar linkage which meets at the toe joint of the respective foot. As an intend result of this design, each of the legs is constrained to the sagittal plane. The eight motor angles are encoded

Table 2.1: Definitions of terms introduced in Chapter 2

Term	Definition	Term	Definition
q_m	motor angles	$\mathcal{D}$	domains of admissibility
q_{i1}	motor 1 of leg i	$\mathcal{S}$	switching surface
q_{i2}	motor 2 of leg i	Δ	discrete time dynamics
p_i	contact point foot of leg i	$\mathcal{FG}$	continuous time dynamics
$\mathcal{B}$	base frame	$\mathcal{V}$	continuous time domain vertices
q_b	position/orientation of base frame	$\mathcal{E}$	discrete time domain edges
q_x	horizontal x position of base frame	D	mass-inertial matrix
q_y	horizontal y position of base frame	v	individual continuous-time domain
q_z	vertical position of base frame	e	individual discrete-time edge
q_ϕ	roll rotation of base frame	n	dimension of state space
q_θ	pitch rotation of base frame	m	dimension of input space
q_ψ	yaw of base frame	C	Coriolis\ Centrifugal matrix
q_{Hi}	hip joint of simulated leg i	G	gravity vector
q_{Ki}	knee joint of simulated leg i	B	input distribution matrix
q_{Kei}	length extension knee joint i	H	Coriolis, centrifugal, and gravity terms
l_1/l_2	length of leg bar 1 and 2	λ	Lagrange multiplies
q	generalized coordinate vector	J	Jacobian of holonomic constraints
$\mathcal{Q}$	configuration space	proj	constrained dynamics projection
x	state vector	F	projected gravity and Coriolis terms
Σ	hybrid systems formulation tuple	T	projected input distribution matrix
$\mathcal{G}$	directed cycle of hybrid system	p_v	point foot of contact event
$\mathcal{X}$	state manifolds	$\delta\lambda$	discrete force vector
$\mathcal{U}$	admissible controls	R	reflection transformation matrix
$\circ_v \backslash \circ^v$	of the domain $v \in \mathcal{V}$	$\circ_e \backslash \circ^e$	of the edge $e \in \mathcal{E}$
$\circ^-$	value before discrete transition	$\circ^+$	value after discrete transition
$\circ^{\mathrm{H}}$	horizontal	$\circ^{\mathrm{V}}$	vertical

in the vector q_m, and each motor pair in q_m is further parameterized by q_{i1} and q_{i2} for all $i \in \{0, 1, 2, 3\}$, where i denotes the leg number. The point foot at the end of each leg i is similarly marked as p_i. Additionally, a base frame $\mathcal{B}$ is attached to the geometric center of the robot. The base frame $\mathcal{B}$ and the leg labling can be seen in Fig. 2.2. The position and orientation of the frame $\mathcal{B}$ with respect to an inertial world frame is then represented by $q_b := \mathrm{col}(q_x, q_y, q_z, q_\phi, q_\theta, q_\psi)$, in which $\mathrm{col}(q_x, q_y, q_z)$ and $\mathrm{col}(q_\phi, q_\theta, q_\psi)$ denote the Cartesian coordinates and absolute orientation of the robot, respectively. In our notation, "col" represents the column vector. As the closed kinematic chain of the four-bar linkage leg structure produces modeling complexities, we use a coordinate transformation which

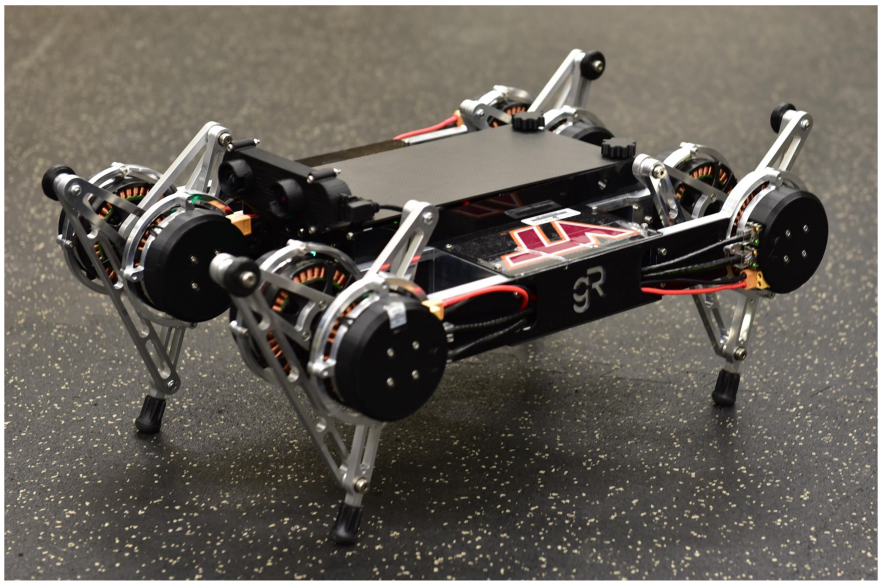

Figure 2.1: Planar quadrupedal robot, Minitaur, designed by Ghost Robotics [5]. A full-order hybrid dynamical model is considered for the development of the controllers as well as the numerical studies.

maps the states of the motor pairs q_{i1} and q_{i2} to respective hip rotation and knee extension coordinates of an equivalent two DOF structure for leg $i \in \{0, 1, 2, 3\}$. We perform the linear transformations $q_{\mathrm{H}i} := \frac{1}{2}(q_{i1} + q_{i2})$ and $q_{\mathrm{K}i} := \frac{1}{2}(q_{i1} - q_{i2})$, where the subscripts "H" and "K" denote the rotational hip and knee joints, respectively. The rotational knee coordinate can be related to a linear extension coordinate denoted by the subscript "Ke" by the equations

$$q_{\mathrm{Ke}} = \sqrt{l_2^2 - l_1^2 + (l_1 \cos(q_{\mathrm{K}})^2)} - l_1 \cos(q_{\mathrm{K}}) - l_2 - l_1 \tag{2.1}$$

$$q_{\mathrm{K}} = \cos^{-1}\left(\frac{l_2^2 - l_1^2 - (q_{\mathrm{Ke}} + l_1 + l_2)^2}{2\, l_1 (q_{\mathrm{Ke}} + l_1 + l_2)}\right), \tag{2.2}$$

where l_1 and l_2 represent the lengths of Minitaur's upper and lower leg bars respectively,

$$l_1 = 0.1036\mathrm{m}$$
$$l_2 = 0.216\mathrm{m}.$$

We can now introduce the generalized coordinates vector as follows:

$$q := \mathrm{col}\{q_b, q_{\mathrm{H}i}, q_{\mathrm{Ke}i} \,|\, i = 0, 1, 2, 3\} \in \mathcal{Q} \tag{2.3}$$

for some configuration space $\mathcal{Q} \subset \mathbb{R}^{14}$. The state vector of the robot is taken as $x := \mathrm{col}(q, \dot{q}) \in \mathrm{T}\mathcal{Q} := \mathcal{Q} \times \mathbb{R}^{14}$. To distinguish between the simulated model of Minitaur and the actual configuration of the physical platform, we refer to the former as the "leg space" model

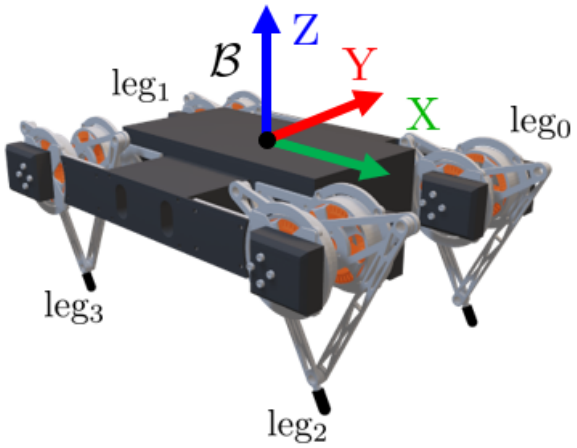

Figure 2.2: The floating base model $\mathcal{B}$ superimposed over a diagram of Minitaur, along with the leg enumeration convention.

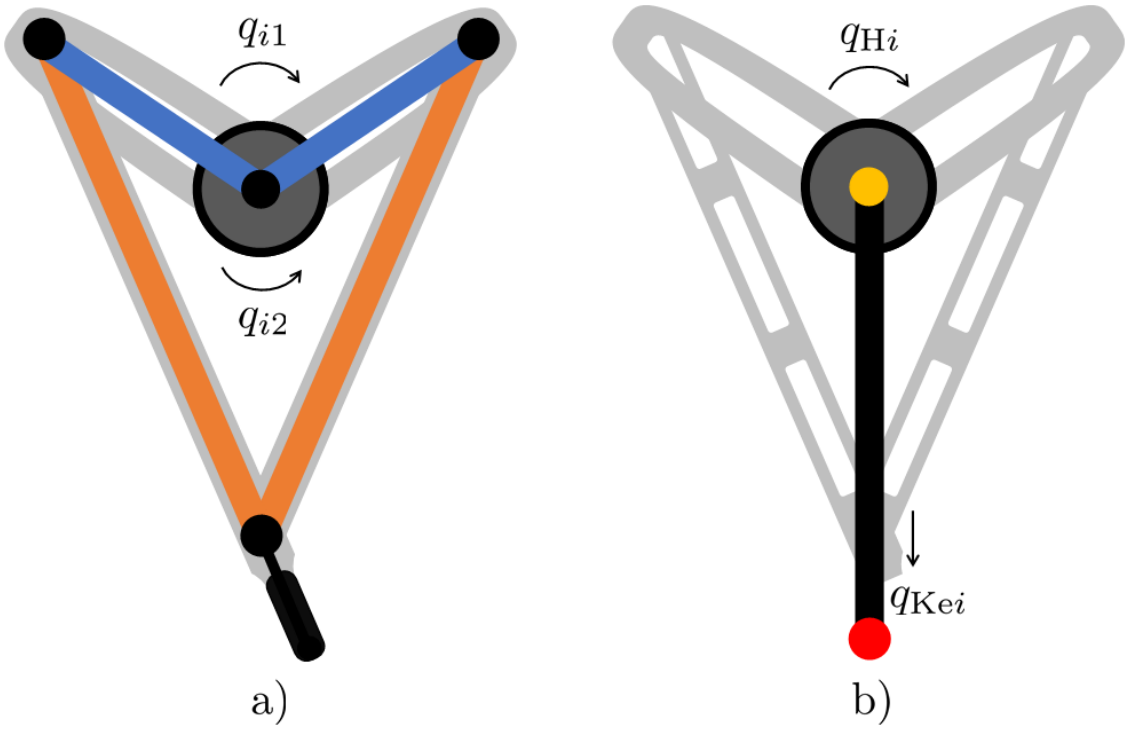

Figure 2.3: Configuration models of an arbitrary leg i superimposed over a representation of Minitaur's leg. While sign conventions differ between legs, the relationships between the configuration parameters are consistent. a) Motor space configuration defining q_{i1} and q_{i2} which have opposite sign conventions. b) Leg space configuration defining $q_{\text{H}i}$ rotation and $q_{\text{Ke}i}$ extension parameters.

Table 2.2: The mass of Minitaur's links as defined by the SDK of Ghost Robotics and the simplified model designed by Google, respectively.

Link	Minitaur Mass (kg)	Simple Mass (kg)
base chassis link	3.516 (1)	3.353 (1)
frame	0.016 (4)	0 (0)
chassis	0.2 (2)	.322 (2)
motor bracket	0.1 (4)	0.16 (4)
motor link	0.25 (8)	0.482 (4)
upper leg	0.05 (8)	0.034 (4)
lower leg	0.05 (8)	0.086 (4)
toe	0.01 (4)	0 (0)
total mass	7.22	7.045

and the latter as the "motor space" model. Figure 2.3 displays the respective configurations of each leg model.

In order to utilize this leg model structure, we implement a robot description for Minitaur developed by Google and implemented in [150]. For comparison sake, Table 2.2 highlights the differences between the simplified model and the original Minitaur description file provided by the Ghost Robotics SDK, which includes the fourbar linkage. In addition to the change in leg structure, the simplified model also reduces the number of links while taking into account differences in mass. The static "frame" links are treated as part of the base chassis link, and the toes are combined into the lower leg links. The differences in mass distribution between the two leg structures are practically inconsequential, as the combined masses of the legs in both models are less than 7% of the respective total masses. As mentioned in the previous chapter, leg dynamics can be considered to be trivial if the total leg mass is less than 10% of the total mass [42]. Thus, we consider the simplified model to be an acceptable full-order representation of Minitaur.

2.3 Hybrid Dynamics

This section describes the general mathematical model of hybrid locomotion which will be adapted to the bounding, trotting, and walking hybrid gaits in the following section. Readers interested in the general foundation of hybrid systems theory for legged locomotion are directed to [80, Chapter 3]. The level locomotion surface is defined at the vertical zero with respect to the base frame $\mathcal{B}$. The model assumes that each leg has a point foot; only a single point at the end of each leg is considered for contact. The dynamics of each gait are separated into two categories: continuous-time "swing" phases and discrete-time "impact"

or "takeoff" phases.

2.3.1 Hybrid Systems Formulation

The hybrid systems formulation for the quadrupedal gaits of Minitaur are defined with the following tuple

$$\Sigma := (\mathcal{G}, \mathcal{X}, \mathcal{U}, \mathcal{D}, \mathcal{S}, \Delta, \mathcal{FG}), \tag{2.4}$$

where $\mathcal{G} := (\mathcal{V}, \mathcal{E})$ represents a directed cycle of the continuous time domain vertices $\mathcal{V}$ and the discrete time domain edges $\mathcal{E} \subset \mathcal{V} \times \mathcal{V}$. The state manifolds and set of admissible controls are represented by $\mathcal{X} := \{\mathcal{X}_v\}_{v\in\mathcal{V}}$ and $\mathcal{U} := \{\mathcal{U}_v\}_{v\in\mathcal{V}}$, respectively, with $\mathcal{X}_v \subset \mathbb{R}^n$ and $\mathcal{U}_v \subset \mathbb{R}^m$, where $n = 28$ and $m = 8$. Moreover, $\mathcal{D} := \{\mathcal{D}_v\}_{v\in\mathcal{V}}$ with $\mathcal{D}_v \subset \mathcal{X}_v \times \mathcal{U}_v$ denotes the domains of admissibility on which 1) the ground reaction forces are feasible and 2) the unilateral constraints are satisfied. The set of guards, i.e., $\mathcal{S} := \{\mathcal{S}_e\}_{e\in\mathcal{E}}$, defines the set of states and controls $(x, u) \in \mathcal{D}$ on which the state trajectories encounter a discrete transition for the edge $e = (v \to v + 1)$. The set of discrete-time dynamics corresponding to these events can be given by $\Delta := \{\Delta_e\}_{e\in\mathcal{E}}$, where upon intersection with $\mathcal{S}_e$ the state vector x evolves according to the discrete dynamics $x^+ = \Delta_e(x^-)$ [151], where x^- represents the state vector right before the discrete phase and x^+ refers to the state vector right after the discrete transition. The set of continuous-time dynamics is finally denoted by the set $\mathcal{FG} := \{(f_v, g_v)\}_{v\in\mathcal{V}}$. In particular, the evolution of the system during the continuous-time domain $v \in \mathcal{V}$ is represented by the input-affine state equation $\dot{x} = f_v(x) + g_v(x)\, u$ for all $(x, u) \in \mathcal{D}_v$.

2.3.2 Continuous-Time Dynamics

The group of continuous-time domains are collected in the set $\mathcal{V}$, with $v \in \mathcal{V}$ representing a particular continuous-time domain. By the method of Lagrange [80, Appendix B.4.4], we can generalize the dynamics of the unconstrained floating-base model as follows:

$$D(q)\,\ddot{q} + C\,(q, \dot{q})\,\dot{q} + G(q) = B\,u, \tag{2.5}$$

where $D(q) \in \mathbb{R}^{14\times14}$ is the positive definite mass-inertia matrix, $C(q, \dot{q}) \in \mathbb{R}^{14\times14}$ represents the Coriolis matrix, $G(q) \in \mathbb{R}^{14}$ is the gravity vector, and B is the input distribution matrix with the property $\operatorname{rank} B = 8$. However, these dynamics do not account for the constraints on the system by the contact feet of a given domain. When a foot is in contact with the ground, the dynamics are constrained as if the foot was locked in place and exerting forces appropriately. The feasibility of the ground reaction forces required to maintain these constraints are considered at the gait development stage (see Chapt. 5). Along a simplifying step of defining $H(q, \dot{q}) := C\,(q, \dot{q})\,\dot{q} + G(q)$, the forces extorted due to the holonomic foot

constraints are factored into the dynamics as follows:

$$\begin{aligned} D(q)\,\ddot{q} + H\,(q,\dot{q}) \quad &= B\,u + J_v^{\top}(q)\,\lambda_v \\ J_v(q)\,\ddot{q} + \dot{J}_v\,(q,\dot{q})\,\dot{q} &= 0, \end{aligned} \tag{2.6}$$

where λ_v and $J_v(q)$ represent the Lagrange multipliers (i.e., ground reaction forces) and Jacobian matrix of the holonomic constraints corresponding to the continuous-time domain $v \in \mathcal{V}$, respectively. To define the evolution of the state space x, the Lagrange multipliers from (2.6) are removed to produce the *constrained dynamics* [121] of the domain v as

$$D(q)\,\ddot{q} + F_v\,(q,\dot{q}) = T_v(q)\,u, \tag{2.7}$$

where

$$F_v\,(q,\dot{q}) := \mathrm{proj}_v H + J_v^{\top}(J_v D^{-1} J_v^{\top})^{-1}\tfrac{\partial}{\partial q}(J_v\,\dot{q})\dot{q} \tag{2.8}$$

$$T_v\,(q) := \mathrm{proj}_v B \tag{2.9}$$

$$\mathrm{proj}_v\,(q) := I - J_v^{\top}(J_v D^{-1} J_v^{\top})^{-1} J_v D^{-1}. \tag{2.10}$$

From (2.7), the evolution of the mechanical system can be described by

$$\dot{x} = \begin{bmatrix} \dot{q} \\ D^{-1}(q)(-F_v(q,\dot{q}) + T_v(q)\,u) \end{bmatrix} \tag{2.11}$$

$$=: f_v(x) + g_v(x)\,u, \tag{2.12}$$

where $\dot{x} = f_v(x) + g_v(x)\,u$ is the input-affine state equation.

2.3.3 Discrete-Time Dynamics

When the state trajectory of the domain $v \in \mathcal{V}$ encounters the switching surface $\mathcal{S}_e$, the system can experience a discontinuity in the velocity vector $\dot{q}$ corresponding to Δ_e. As the phases of locomotion are delineated by either the removal or addition of a contact constraint, let us define $p_v = \mathrm{col}(p_v^H, p_v^V)$ as the global position of the point foot which will undergo a change of contact state at the end of the domain $v \in \mathcal{V}$. There are two types of guards considered. An "impact" occurs when p_v reaches a vertical height of zero and is thus at the level locomotion surface, and a "takeoff" occurs when the vertical GRF at p_v is zero. If an edge $e \in \mathcal{E}$ corresponds to a takeoff, there is no discrete change in the state vector x, therefore $x^+ = \Delta_e(x^-) = x^-$. However, if e corresponds to an impact, the system will experience a discontinuity in the velocity component of the state vector due to the impulsive forces exerted at p_v [151]. This discrete change in $\dot{q}$ is described by the plastic input model [121]

$$\begin{bmatrix} D(q) & -J_{v+1}^{\top}(q) \\ J_{v+1}(q) & 0 \end{bmatrix} \begin{bmatrix} \dot{q}^+ \\ \delta\lambda \end{bmatrix} = \begin{bmatrix} D(q)\,\dot{q}^- \\ 0 \end{bmatrix}, \tag{2.13}$$

which can be solved for $\dot{q}^+$ and $\delta\lambda$. The intensity of the impulsive forces associated with maintaining the holonomic constraints due to J_{v+1} stored in $\delta\lambda$ are unnecessary for describing the state trajectory but can be used to determine the feasibility of the discrete dynamics at the gait optimization stage. Finally, by assuming the continuity of position, i.e., $q^+ = q^-$, one can express the impact map as $x^+ = \mathrm{col}(q^+, \dot{q}^+) = \Delta_e(q^-, \dot{q}^-) = \Delta_e(x^-)$.

2.4 Locomotion Patterns

The following section describes the hybrid formulation of the bounding, trotting, and walking gaits and presents a visual representation of the directed graph $\mathcal{G}$ for each gait. The trotting and walking gaits each take advantage of symmetries in their respective gait patterns by performing a coordinate reflection $R\,q$ halfway through each respective gait. The bounding gait has no such symmetry to take advantage of. Each gait is therefore visualized in Figs. 2.4, 2.5, and 2.6, with the coordinate reflection marked where appropriate. The transformation matrix R is defined as follows:

$$R = \begin{bmatrix} 1 & 0 & 0 & 0 & 0 & 0 & 0 & 0 & 0 & 0 & 0 & 0 & 0 & 0 \\ 0 & -1 & 0 & 0 & 0 & 0 & 0 & 0 & 0 & 0 & 0 & 0 & 0 & 0 \\ 0 & 0 & 1 & 0 & 0 & 0 & 0 & 0 & 0 & 0 & 0 & 0 & 0 & 0 \\ 0 & 0 & 0 & -1 & 0 & 0 & 0 & 0 & 0 & 0 & 0 & 0 & 0 & 0 \\ 0 & 0 & 0 & 0 & 1 & 0 & 0 & 0 & 0 & 0 & 0 & 0 & 0 & 0 \\ 0 & 0 & 0 & 0 & 0 & -1 & 0 & 0 & 0 & 0 & 0 & 0 & 0 & 0 \\ 0 & 0 & 0 & 0 & 0 & 0 & 0 & 0 & 1 & 0 & 0 & 0 & 0 & 0 \\ 0 & 0 & 0 & 0 & 0 & 0 & 0 & 0 & 0 & 1 & 0 & 0 & 0 & 0 \\ 0 & 0 & 0 & 0 & 0 & 0 & 1 & 0 & 0 & 0 & 0 & 0 & 0 & 0 \\ 0 & 0 & 0 & 0 & 0 & 0 & 0 & 1 & 0 & 0 & 0 & 0 & 0 & 0 \\ 0 & 0 & 0 & 0 & 0 & 0 & 0 & 0 & 0 & 0 & 0 & 0 & 1 & 0 \\ 0 & 0 & 0 & 0 & 0 & 0 & 0 & 0 & 0 & 0 & 0 & 0 & 0 & 1 \\ 0 & 0 & 0 & 0 & 0 & 0 & 0 & 0 & 0 & 0 & 1 & 0 & 0 & 0 \\ 0 & 0 & 0 & 0 & 0 & 0 & 0 & 0 & 0 & 0 & 0 & 1 & 0 & 0 \end{bmatrix}. \tag{2.14}$$

We remark that the transformation matrix has the property $R\,R = I$.

2.4.1 Bounding Gait

Bounding is a fast dynamic gait during which the quadruped becomes airborne in-between steps. The hybrid model of a bounding gait is represented by a four-domain directed cycle of alternating stance and flight phases. Since Minitaur is a planar robot, we are interested in studying the bounding gaits in the sagittal dynamics. For this purpose, we need to consider the Lagrangian dynamics (2.6) subject to some additional holonomic constraints arising from

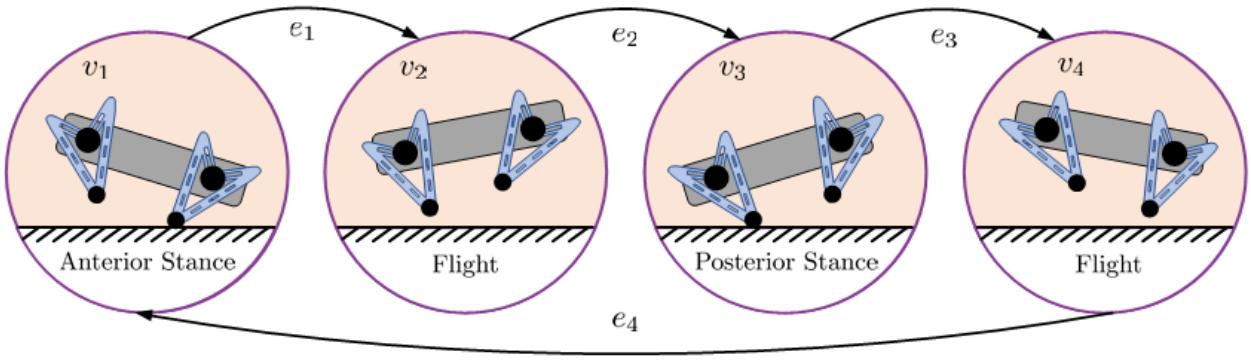

Figure 2.4: Illustration of the directed cycle which represents the four-domain bounding gait. As this bounding is a planar gait, the front and rear pairs of legs move in parallel.

the confinement of the motion in the frontal and transversal planes. These conditions are expressed as $\ddot{q}_y = \ddot{q}_\phi = \ddot{q}_\psi = 0$ and can be augmented to the Jacobian matrix $J_v(q)$ for all domains. In this planar model, the front set of legs and rear set of legs are constrained to move in tandem.

The gait begins in the anterior stance phase, where the front two legs are in contact with the ground. The two legs then takeoff as the robot enters the first flight phase. Then, the back legs impact to begin the posterior stance phase. The robot enters the second flight phase before returning to the beginning of the cycle with the impact of the front leg pair. Since the switching surface $\mathcal{S}_e$ is defined by a single event, p_v is arbitrarily selected from the corresponding leg pair. The front left foot p_0 is selected for front leg events, and the back left foot p_1 is selected for back leg events.

2.4.2 Trotting Gait

A general understanding of trotting sees the gait as a series of double stance phases alternating between the two diagonal sets of legs of the quadruped. However, since the switching surface $\mathcal{S}_e$ must be defined by a single event and since the foot selection is not arbitrary as in the case of bounding, the hybrid model is represented by an eight-domain cycle. Rather than impacting at the same time, a leg is selected to impact and have a short single stance phase before the impact of the other leg in the double stance pair. A similar convention is used for the corresponding takeoffs leading to a short flight phase.

The robot begins in a signal stance phase of the front right foot p_2, after which the back left foot p_1 impacts. The resulting double stance will take up the majority of the continuous evolution of the gait before p_2 lifts off to enter the second single stance domain, after which p_1 will takeoff resulting in a short flight phase. Once the front left foot p_0 impacts the ground, the system repeats its trajectory reflected across the sagittal plane to define the remaining

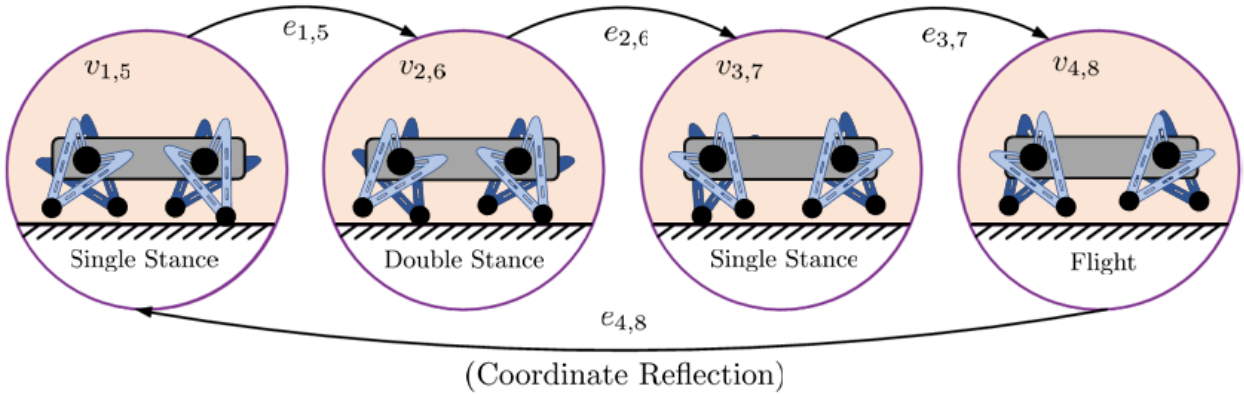

Figure 2.5: Illustration of the directed cycle which represents the eight-domain trotting gait. The final four domains are a coordinate reflection of the first four domains.

four continuous-time domains.

2.4.3 Walking Gait

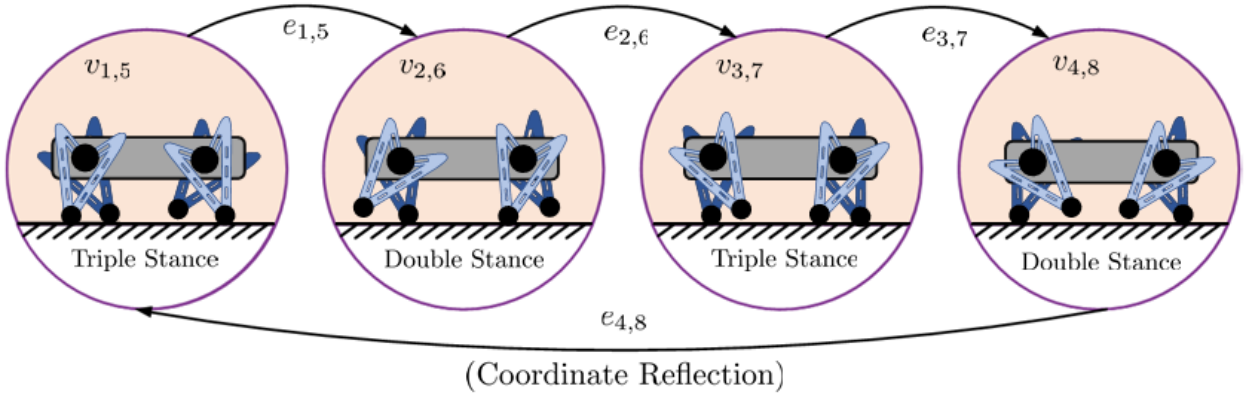

Figure 2.6: Illustration of the directed cycle which represents the eight-domain walking gait. The final four domains are a coordinate reflection of the first four domains.

Quadrupedal walking is a slower gait defined as a series of alternating double and triple stance phases. Like the trotting gait, it also has hybrid model with an eight-domain cycle where the last four domains are a sagittal reflection of the first four.

The gait begins in a triple stance with the front left foot p_0 in swing. Then, the back right foot p_3 lifts off to begin the first double stance phase. The second triple stance phase begins when p_0 impacts, and the second double stance begins when the front right foot p_2 enters the swing state. The impact of p_3 begins the reflected portion of the hybrid model.

Chapter 3

Virtual Constraint Controllers

Table 3.1: Definitions of terms introduced in Chapter 3

Term	Definition
y	virtual constraints
h	controlled variables
H_0	output matrix
τ	time-varying phasing variable
t	simulation time
t^+	initialization time
T_v	time length of domain
$\mathcal{L}$	Lie derivative
$\mathcal{L}_{g_v}\mathcal{L}_{f_v}y_v$	decoupling matrix
K_p	proportional gain matrix
K_d	derivative gain matrix
Γ	control law
$\mathcal{Z}$	zero dynamics manifold
z	zero dynamics state space
$\alpha_i \backslash \beta_i$	tunable parameters
$\circ^\dagger$	pseudoinverse operator

3.1 Background

The objective of this section is to present a formal methodology for designing time-varying virtual constraint controllers that exponentially stabilize agile and dynamic quadrupedal

gaits. Interested readers are directed to [80, Chapter 5] for the corresponding design of traditional time-invariant virtual constraint controllers. First, the principles of time-variant virtual constraint controllers are described. Next, the zero dynamics manifold is defined and the behavior of the zero dynamics under virtual constraint control is explored, particularly with regards to how the zero dynamics limit the available outputs for control. Previous work in HZD [83, 135, 81, 55] shows that the proper selection of the outputs directly affects the stability of dynamic gaits, so a systematic process for selecting these outputs is presented. The output functions for each continuous-time domain of each gait are defined along with a series of parameters that allow for the fine-tuning necessary to ensure stability. Table 3.1 provides a list of definitions for the symbols and terms introduced in this chapter.

3.2 Virtual Constraints

Virtual constraints are kinematic constraints defined to coordinate the limbs of legged machines within strides [54, 80, 152]. They are imposed by the action of feedback control algorithms such as I-O linearization [104]. Virtual constraints can be defined by mapping a desired trajectory to a series of output functions as follows:

$$y_v(\tau, x) := h^v(\tau, q) := h_0^v(q) - h_d^v(\tau) := H_0^v(q - q_v^d(\tau)), \tag{3.1}$$

where $h_0^v(q) := H_0^v\, q$ denotes the set of holonomic variables to be controlled during the continuous-time domain v, referred to as the *controlled variables*, H_0^v represents the *output matrix* to be determined, $h_d^v(\tau) := H_0^v\, q_v^d(\tau)$ denotes the desired evolution of the controlled variables on the gait in terms of a time-varying gait phasing variable denoted by τ, and $q_d^v(\tau)$ represents the desired evolution of the configuration variables on the gait. In addition, the phasing variable τ represents the progress of the robot on the gait and can be defined as follows:

$$\tau := \frac{t - t^+}{T_v} \tag{3.2}$$

where t is the current time, t^+ denotes the time of the previous discrete event, and T_v refers to the expected duration of the current domain $v \in \mathcal{V}$ defined by the ideal trajectory. The parameterization of q_d^v by τ represents the key distinction in the derivation of the time-varying output dynamics from the derivation of the time-invariant output dynamics. Through this design, the controller selects the target state of the periodic orbit based upon how much time has passed during the current continuous-time domain.

By driving the outputs y_v to zero, the controller is essentially constraining the system just as a physical holonomic constraint would, hence the term "virtual constraint." Differentiating the outputs (3.1) along the continuous-time dynamics of domain v results in the following

definitions of output dynamics

$$
\begin{aligned}
y_v &= h^v \\
\dot{y}_v &= \underbrace{\frac{\partial h^v}{\partial q}\dot{q}}_{=:\mathcal{L}_{f_v} y^v(\tau,x)} + \frac{\partial h^v}{\partial \tau}\dot{\tau} \\
&= H_0^v \dot{q} - H_0^v \frac{\partial q_d^v}{\partial \tau}(\tau)\,\frac{1}{T_v} \\
\ddot{y}_v &= \frac{\partial h^v}{\partial q}\ddot{q} + \underbrace{\frac{\partial}{\partial q}\left(\frac{\partial h^v}{\partial q}\dot{q}\right)\dot{q}}_{=0} + \underbrace{\frac{\partial}{\partial \tau}\left(\frac{\partial h^v}{\partial q}\dot{q}\right)\dot{\tau}}_{=0} + \frac{\partial^2 h^v}{\partial \tau^2}\,(\dot{\tau})^2 + \underbrace{\frac{\partial}{\partial q}\left(\frac{\partial h^v}{\partial \tau}\dot{\tau}\right)\dot{q}}_{=0} \\
&= \underbrace{-\frac{\partial h^v}{\partial q}D^{-1}H}_{=:\mathcal{L}_{f_v}^2 y_v(\tau,x)} + \underbrace{\frac{\partial h^v}{\partial q}D^{-1}B}_{=:\mathcal{L}_{g_v}\mathcal{L}_{f_v} y_v(\tau,x)}\; u + \frac{\partial^2 h^v}{\partial \tau^2}(\dot{\tau})^2, \\
&= -H_0^v\, D^{-1}\, H + H_0^v\, D^{-1} B\, u + H_0^v \frac{\partial^2 q_d^v}{\partial \tau^2}(\tau)\,\frac{1}{T_v^2},
\end{aligned}
\tag{3.3}
$$

where "$\mathcal{L}$" denotes the Lie derivative. We then set the output dynamics (3.3) to a desired output dynamics as follows:

$$
\begin{aligned}
\ddot{y}_v &= \mathcal{L}_{g_v}\mathcal{L}_{f_v} y_v(\tau,x)\, u + \mathcal{L}_{f_v}^2 y_v(\tau,x) + \frac{\partial^2 y_v}{\partial \tau^2}(\dot{\tau})^2 \\
&= -K_p\, y_v - K_d\, \dot{y}_v
\end{aligned}
\tag{3.4}
$$

in which K_p and K_d are positive definite matrices and hence, the origin is exponentially stable for (3.4). From the output dynamics (3.4), one can solve for the minimum 2-norm (i.e., minimum power) I-O linearizing controller, that is,

$$
\begin{aligned}
u &= \Gamma_v\,(\tau,x) \\
&:= -\left(\mathcal{L}_{g_v}\mathcal{L}_{f_v} y_v\right)^{\dagger}\left(\mathcal{L}_{f_v}^2 y_v + \frac{\partial^2 y_v}{\partial \tau^2}(\dot{\tau})^2 + K_p\, y_v + K_d\, \dot{y}_v\right),
\end{aligned}
\tag{3.5}
$$

where the superscript "$\dagger$" represents the pseudoinverse operator. The pseudoinverse is used so that (3.5) can be applied generally to all domains of the proposed gaits, as the decoupling matrix $\mathcal{L}_{g_v}\mathcal{L}_{f_v} y_v$ is 6×8 during the stance phases of the bounding gait due to the closed kinematic chain created by the parallel stance legs.

3.3 Zero Dynamics

The *zero dynamics manifold* is a subset of the state space on which the virtual constraints are met, i.e.,

$$\mathcal{Z}_v := \left\{ x \in \mathcal{X}_v \,|\, y_v(\tau, x) = \mathcal{L}_{f_v} y_v(\tau, x) + \frac{\partial y_v}{\partial \tau}(\tau, x)\, \dot{\tau} = 0 \right\}. \tag{3.6}$$

The controller defined in (3.5) asymptotically drives the state trajectory to the zero dynamics manifold defined by the virtual constraints and thus renders the zero dynamics manifold forward-invariant and attractive. The internal dynamics compatible with the output functions being identically zero are referred to as the *zero dynamics*. More specifically, the zero dynamics describe the evolution of the mechanical system on the zero dynamics manifold as follows:

$$\dot{z} = f_v^{\text{zero}}(\tau, z), \tag{3.7}$$

where $f_v^{\text{zero}} := f_v^{\text{cl}}|_{\mathcal{Z}_v}$ and $f_v^{\text{cl}}(\tau, x) := f_v(x) + g_v(x)\, \Gamma_v(\tau, x)$ represents the closed-loop vector field for the domain $v \in \mathcal{V}$. We remark that

$$\dim \mathcal{Z}_v = \dim \mathcal{X}_v - 2 \dim y_v, \tag{3.8}$$

and hence, along with the physical holonomic constraints, each virtual constraint additionally reduces the number of degrees of freedom by two, as each constraint on the coordinate vector q has a corresponding constraint on the velocity vector $\dot{q}$. This process allows for a controlled system operating in a significantly reduced dimensional space. However, just as a system will have trivial dynamics if the number of physical constraints is equal to its unconstrained degrees of freedom, imposing too many virtual constraints will force motion to be infeasible if the number of constraints corresponds a trivial zero dynamics manifold with dimension zero. In particular, a trivial zero dynamics manifold will cause the decoupling matrix of (3.5) to become singular. Therefore, the number of virtual constraints selected for a given domain must allow for a zero dynamics manifold of dimension one at minimum, i.e.,

$$\dim \mathcal{Z}_v \geq 1. \tag{3.9}$$

The minimum dimension of the zero dynamics manifold is also affected by the rank of the projected input distribution matrix T_v—defined in (2.9)—as there must be an equivalent input to correspond with the I-O linearization problem, that is,

$$\dim y_v \leq \text{rank} T_v. \tag{3.10}$$

In practice, an HZD controller will have outputs selected to minimize the dimension of the zero dynamics manifold in order to simplify the control of the constrained dynamics as much as possible. Table 3.2 displays the dimensional limitations of each continuous-time domain for Minitaur and the resulting dimension of the virtual constraints y_v according to the relations (3.8)-(3.10) to minimize the dimension of the zero dynamics manifold $\mathcal{Z}_v$. Fig. 3.1 provides a geometric illustration of the zero dynamics manifolds and guards of the multi-domain hybrid model of the locomotion patterns.

Table 3.2: Table showing the dimension of the state manifold $\mathcal{X}_v$, the dimension of the constrained configuration space $\mathcal{Q}_v$, the rank of the projected input distribution matrix T_v in (2.9), the maximum possible dimension of the output function vector y_v, and the resulting dimension of the corresponding zero dynamics manifold $\mathcal{Z}_v$ given a contact state of the domain v.

Flight Phase	Single Contact	Double Contact	Triple Contact
$\dim \mathcal{X}_v = 28$	$\dim \mathcal{X}_v = 22$	$\dim \mathcal{X}_v = 16$	$\dim \mathcal{X}_v = 10$
$\dim \mathcal{Q}_v = 14$	$\dim \mathcal{Q}_v = 11$	$\dim \mathcal{Q}_v = 8$	$\dim \mathcal{Q}_v = 5$
$\operatorname{rank} T_v = 8$	$\operatorname{rank} T_v = 8$	$\operatorname{rank} T_v = 7$	$\operatorname{rank} T_v = 5$
$\dim y_v = 8$	$\dim y_v = 8$	$\dim y_v = 7$	$\dim y_v = 4$
$\dim \mathcal{Z}_v = 12$	$\dim \mathcal{Z}_v = 6$	$\dim \mathcal{Z}_v = 2$	$\dim \mathcal{Z}_v = 2$

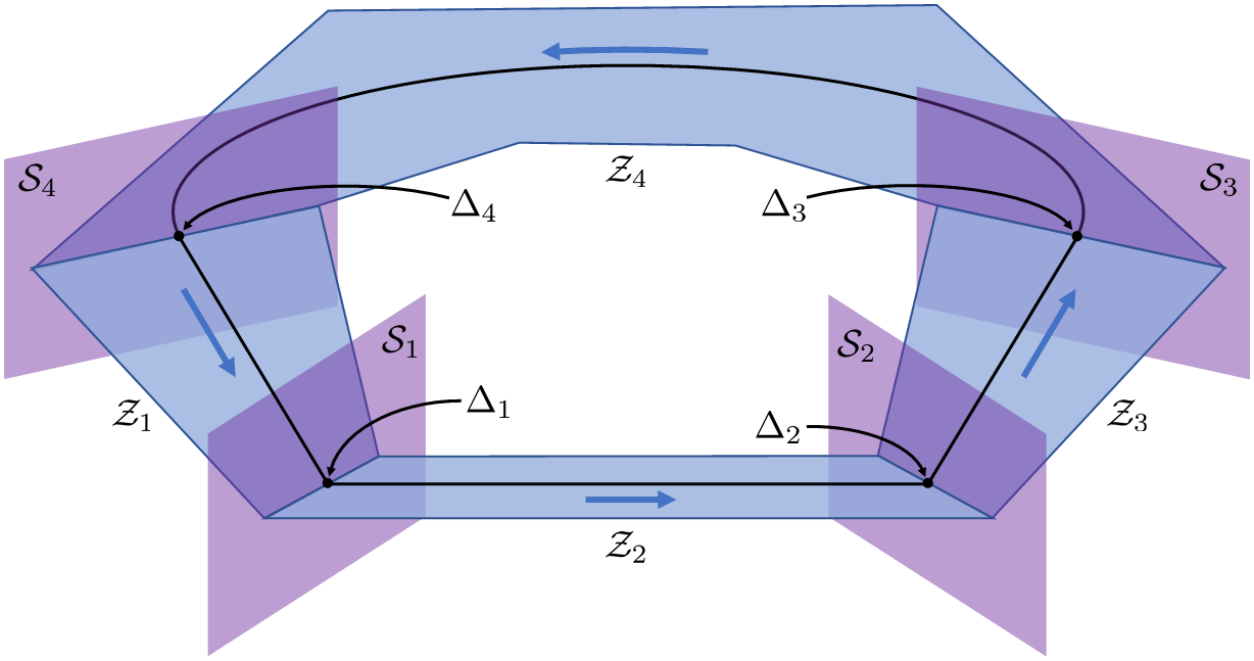

Figure 3.1: Geometric illustration of HZD for a four-domain model of locomotion. The eight-domain systems described in this research can be achieved by applying a coordinate transformation in the discrete dynamics Δ_4 upon intersection of the switching surface $\mathcal{S}_4$.

3.4 Virtual Constraint Design

This section covers the output functions designed for the bounding, trotting, and walking gaits respectively, along with their respective tuneable parameters. The basic design process applied to all gaits is as follows: First, the internal actuated degrees of freedom are set as the

baseline control strategy, which creates a set of virtual constraints of dimension 8. If these virtual constraints cause the zero dynamics manifold to be trivial, selected internal degrees of freedom are removed or combined with a heuristic approach focusing on intuition and simulation performance. Finally, tuneable parameters are added to the outputs to control the asymptotic convergence to the desired trajectory (i.e., asymptotic stabilization problem). While simulation has access to all position and rotation data, controllers are limited by the accuracy of measurements from an internal IMU in practice. Therefore, only roll and pitch angles of the floating base are factored into virtual constraints. From this stage, the roll and pitch parameters are tuned until the constrained dynamics meet the asymptotic stability requirements described in Chapter 4.

3.4.1 Bounding Virtual Constraints

The bounding gait is a series of alternating fully-actuated double contact and underactuated flight phases. As described in Chapter 2, since the hybrid model of bounding for Minitaur is a planar gait, the body roll q_ϕ is held constant by a holonomic constraint and therefore cannot be factored into the virtual constraints. Therefore, tunable parameters are added to control the pitch angle q_θ. During flight phases, this controller design allows the robot to land at proper angles to recover from instability. This procedure is implemented mathematically by adding the pitch angle to the internal controlled variables via some weighting factors α_v and β_v that will be tuned using the validation method described in Chapter 4 through Theorem 1. Additionally, the dimension of the virtual constraints for stance phases is reduced from 8 to 6 due to the closed kinematic chain formed by the two front or the two rear stance legs. Therefore we choose to average the outputs associated with the stance hips and knees respectively. The four output matrices H_0^v for the bounding gait are provided below.

$$H_0^1 q := \begin{bmatrix} \frac{1}{2}q_{\mathrm{H0}} + \frac{1}{2}q_{\mathrm{H2}} + \alpha_1 q_\theta \\ q_{\mathrm{H1}} \\ q_{\mathrm{H3}} \\ \frac{1}{2}q_{\mathrm{Ke0}} + \frac{1}{2}q_{\mathrm{Ke2}} + \beta_1 q_\theta \\ q_{\mathrm{Ke1}} \\ q_{\mathrm{Ke3}} \end{bmatrix}, H_0^2 q := \begin{bmatrix} q_{\mathrm{H0}} + \alpha_2 q_\theta \\ q_{\mathrm{H2}} + \alpha_2 q_\theta \\ q_{\mathrm{H1}} \\ q_{\mathrm{H3}} \\ q_{\mathrm{Ke0}} + \beta_2 q_\theta \\ q_{\mathrm{Ke2}} + \beta_2 q_\theta \\ q_{\mathrm{Ke1}} \\ q_{\mathrm{Ke3}} \end{bmatrix} \tag{3.11}$$

$$H_0^3 q := \begin{bmatrix} q_{\mathrm{H0}} \\ \frac{1}{2}q_{\mathrm{H1}} + \frac{1}{2}q_{\mathrm{H3}} + \alpha_3 q_\theta \\ q_{\mathrm{H2}} \\ q_{\mathrm{Ke0}} \\ \frac{1}{2}q_{\mathrm{Ke1}} + \frac{1}{2}q_{\mathrm{Ke3}} + \beta_3 q_\theta \\ q_{\mathrm{Ke2}} \end{bmatrix}, H_0^4 q := \begin{bmatrix} q_{\mathrm{H0}} \\ q_{\mathrm{H2}} \\ q_{\mathrm{H1}} + \alpha_4 q_\theta \\ q_{\mathrm{H3}} + \alpha_4 q_\theta \\ q_{\mathrm{Ke0}} \\ q_{\mathrm{Ke2}} \\ q_{\mathrm{Ke1}} + \beta_4 q_\theta \\ q_{\mathrm{Ke3}} + \beta_4 q_\theta \end{bmatrix}.$$

During stance phases, we control the average knee and hip terms for the stance legs, while allowing feedback from the pitch angle via the coefficients $\alpha_{1\backslash 3}$ and $\beta_{1\backslash 3}$ respectively. The terms of the swing legs are controlled individually and without influence from the pitch angle as their small mass has little effect on the trajectory of the floating base. During flight phases, each hip term of the incoming contact legs experiences identical pitch feedback via $\alpha_{2\backslash 4}$, and the knee terms of the incoming contact legs are controlled in the same manner with respect to $\beta_{2\backslash 4}$. The controlled variables of the legs which will remain in the air at the end of the flight phase are uninfluenced by the pitch angle.

3.4.2 Trotting Virtual Constraints

The trotting gait designed for Minitaur is composed of a set of shorter single stance and flight phases and longer double stance phases which take up the majority of the gait. Therefore, roll and pitch control is performed during the longer double stance phases. Since Minitaur is underactuated during flight and single stance phases, the output matrices H_0^v for the flight phase and single stance phases can map each of the eight actuators to the outputs while maintaining nontrivial zero dynamics. The first double stance phase—which is fully-actuated and must have fewer than seven outputs to have a non-trivial zero dynamics—is mapped by the following relation.

$$H_0^2 q = \begin{bmatrix} q_{\mathrm{H0}} \\ q_{\mathrm{H2}} \\ q_{\mathrm{H3}} \\ q_{\mathrm{Ke0}} + \alpha_0 q_\theta + \beta_0 q_\phi \\ q_{\mathrm{Ke1}} + \alpha_1 q_\theta + \beta_1 q_\phi \\ q_{\mathrm{Ke2}} + \alpha_2 q_\theta + \beta_2 q_\phi \\ q_{\mathrm{Ke3}} + \alpha_3 q_\theta + \beta_3 q_\phi \end{bmatrix}. \tag{3.12}$$

The second double stance phase uses the same design after being appropriately reflected by the transformation matrix R. The set of tuneable parameters α_i and β_i are used to control the response of the knee joints to pitch and roll deviations respectively, as heuristic testing found that the stability of the gait was most sensitive to adjustments to the control of the knee joint.

3.4.3 Walking Virtual Constraints

The hybrid gait for quadrupedal walking is a set of alternating double contact and triple contact states. As the only of the three presented gaits to have a triple contact phase, the walking gait is also the only of the presented gaits to be overactuated during a portion of its trajectory. This significantly limits the available outputs for the triple contact phases, so control of the floating base DOF is limited to the fully-actuated double contact phases.

Control of the pitch and roll angles are factored into the coordinates of the swing leg which will impact at the discrete transition between the double and triple stance phases. The output matrices for the first four domains of the walking gait are provided below, with the matrices for the latter four domains operating identically on the reflected coordinates.

$$H_0^1 q = \begin{bmatrix} q_{\mathrm{H0}} \\ q_{\mathrm{Ke0}} \\ q_{\mathrm{Ke1}} \\ q_{\mathrm{Ke2}} \end{bmatrix}, H_0^2 q = \begin{bmatrix} q_{\mathrm{H0}} + \alpha_0 q_\theta + \beta_0 q_\phi \\ q_{\mathrm{H1}} \\ q_{\mathrm{H2}} \\ q_{\mathrm{Ke0}} + \alpha_1 q_\theta + \beta_1 q_\phi \\ q_{\mathrm{Ke1}} \\ q_{\mathrm{Ke2}} \\ q_{\mathrm{Ke3}} \end{bmatrix}, \tag{3.13}$$

$$H_0^3 q = \begin{bmatrix} q_{\mathrm{H3}} \\ q_{\mathrm{Ke1}} \\ q_{\mathrm{Ke2}} \\ q_{\mathrm{Ke3}} \end{bmatrix}, H_0^4 q = \begin{bmatrix} q_{\mathrm{H0}} \\ q_{\mathrm{H1}} \\ q_{\mathrm{H3}} + \alpha_2 q_\theta + \beta_2 q_\phi \\ q_{\mathrm{Ke0}} \\ q_{\mathrm{Ke1}} \\ q_{\mathrm{Ke2}} \\ q_{\mathrm{Ke3}} + \alpha_3 q_\theta + \beta_3 q_\phi \end{bmatrix}.$$

Similar to bounding, heuristic analysis found that using α_i and β_i to tune the response of incoming impact legs provided the best results for stability.

Chapter 4

Exponential Stability Analysis via Time-Varying Nonlinear Controllers

Table 4.1: Definitions of terms introduced in Chapter 4

Term	Definition
$\mathcal{O}$	periodic orbit
φ^*	periodic solution
T	fundamental period
P	Poincaré return map
Π	saltation matrix
Φ	trajectory sensitivity matrix
s	switching surface differential function
A	Jacobian linearization of the augmented vector field
$\circ^*$	of the periodic solution
$\circ^{cl}$	of the closed-loop system
$\circ_a$	of the augmented system
$\circ_x$	of the state system
$\circ_\tau$	of the time system
$\circ_{\text{half}}$	of the half-orbit

4.1 Background

The Poincaré sections analysis is the most basic mathematical tool for investigating the existence and stability of periodic solutions to time-invariant nonlinear dynamical systems

[54, 148, 147, 146]. It translates the stability of limit cycles into that of a fixed point for a discrete-time system, defined as the Poincaré return map. The Poincaré map maps the evolution of the system from a hyperplane transversal to the orbit, referred to as the Poincaré section [147, 146, 153], back to the hyperplane [54]. The objective of this section is to extend the Poincaré analysis for use in verifying the exponential stability of limit cycles for dynamical systems with periodic and time-varying controllers. In order to use this powerful mathematical tool in validating the proposed HZD controllers, we formally extend the analysis to general time-varying periodic systems. In particular, we show that the criteria of exponential stability of limit cycles for a time-varying periodic hybrid system is identical to that of the time-invariant systems. Finally, we will describe the application of the Poincaré sections analysis to time-varying HZD controllers for hybrid quadrupedal locomotion and provide details on the specific implementation used to verify the asymptotic stability of our periodic solutions (i.e., gaits). Table 4.1 provides definitions of the terms and symbols introduced in this section.

4.2 Extending Poincaré to Time-Varying Systems

We will consider robot gaits as periodic solutions of the hybrid system Σ in (2.4). We investigate time-varying feedback controllers as follows:

$$u = \Gamma_v(\tau, x) \tag{4.1}$$

during the continuous-time domain $v \in \mathcal{V}$. Here, τ denotes the gait timing (i.e., phasing) variable which represents the progress of the robot on the gait. More specifically, it is taken as zero at the beginning of each domain (i.e., $\tau^+ = 0$) and evolves according to

$$\dot{\tau} = \frac{1}{T_v}, \tag{4.2}$$

where T_v is the desired elapsed time for the domain v. In (4.1), Γ_v is a continuously differentiable (i.e., $\mathcal{C}^1$) state law in terms of (τ, x). We assume that by employing the feedback controller (4.1), there is a periodic orbit for the closed-loop hybrid system. More specifically,

$$\mathcal{O} := \{x = \varphi^*(t) \,|\, 0 \leq t < T\} \tag{4.3}$$

denotes a periodic orbit for Σ, for some fundamental period $T > 0$ and some periodic solution $\varphi^*(t)$ with the property $\varphi^*(t + T) = \varphi^*(t)$ for all $t \geq 0$. According to the construction procedure, the state feedback law (4.1) is assumed to be periodic in τ with the period taken as 1, that is,

$$\Gamma_v(\tau + 1, x) = \Gamma_v(\tau, x) \tag{4.4}$$

for all $\tau \geq 0$, $x \in \mathcal{X}$, and $v \in \mathcal{V}$. In what follows, we study the dynamic stability of the periodic orbit $\mathcal{O}$ for the closed-loop hybrid system. For future purposes, we assume that $\mathcal{O}_v$ denotes the projection of $\mathcal{O}$ onto the state manifold of the domain v.

The evolution of the closed-loop system during the domain $v \in \mathcal{V}$ can be described by the time-varying and periodic ordinary differential equation (ODE)

$$\dot{x} = f_v^{\text{cl}}(\tau, x) := f_v(x) + g_v(x)\,\Gamma_v(\tau, x). \tag{4.5}$$

Let $\varphi_v(t, x_0)$ represent the state solution of $\dot{x} = f_v^{\text{cl}}(\tau, x)$ with the initial condition x_0 for all $t \geq 0$ in the maximal interval of existence. From [80, Theorem 4.3], one can present an equivalent single-domain hybrid model for the closed-loop hybrid system as follows:

$$\Sigma^{\text{cl}} : \begin{cases} \begin{bmatrix} \dot{x} \\ \dot{\tau} \end{bmatrix} = \begin{bmatrix} f_v^{\text{cl}}(\tau, x) \\ \frac{1}{T_v} \end{bmatrix}, & x^- \notin \mathcal{S}_e \\ \begin{bmatrix} x^+ \\ \tau^+ \end{bmatrix} = \begin{bmatrix} \Delta_e^{\text{cl}}(x^-) \\ 0 \end{bmatrix}, & x^- \in \mathcal{S}_e, \end{cases} \tag{4.6}$$

where $e = (v \to v+1)$ is the discrete transition after the domain v. Furthermore, Δ_e^{cl} represents the equivalent discrete-time dynamics that are composed of the flows of the remaining continuous-time domains as well as the discrete-time transitions. We note that since τ resets at the beginning of each domain, $\Delta_e^{\text{cl}}(x)$ does not depend on τ. In order to maintain compact notation, we define the augmented state variables as

$$x_a := \text{col}(x, \tau) \in \mathcal{X}_a := \mathcal{X} \times \mathbb{R}^+. \tag{4.7}$$

Using this notation, the augmented hybrid system can be represented by

$$\Sigma^{\text{cl}} : \begin{cases} \dot{x}_a = f_a^{\text{cl}}(x_a), & x_a^- \notin \mathcal{S}_a \\ x_a^+ = \Delta_a^{\text{cl}}\left(x_a^-\right), & x_a^- \in \mathcal{S}_a, \end{cases} \tag{4.8}$$

with the following definitions:

$$f_a^{\text{cl}}(x_a) : = \text{col}(f_v^{\text{cl}}(\tau, x), \frac{1}{T_v}) \tag{4.9}$$

$$\Delta_a^{\text{cl}}(x_a) : = \text{col}(\Delta_e^{\text{cl}}(x), 0) \tag{4.10}$$

$$\mathcal{S}_a : = \mathcal{S}_e \times \mathbb{R}^+. \tag{4.11}$$

Equations (4.9),(4.10), and (4.11) represent the augmented closed-loop vector field, augmented discrete-time transition, and augmented switching surface, respectively. We are now in a position to define the Poincaré map for the augmented system as $P_a : \mathcal{S}_a \to \mathcal{S}_a$ by

$$P_a(x_a) := \varphi_a\left(T_I\left(\Delta_a^{\text{cl}}(x_a)\right), \Delta_a^{\text{cl}}(x_a)\right), \tag{4.12}$$

where φ_a is the flow of the augmented ODE and $T_I(x_a(0))$ is the time elapsed for the augmented state solution to intersect $\mathcal{S}_a$, that is,

$$T_I(x_a(0)) := \inf\{t > 0 \,|\, \varphi_a(t, x_a(0)) \in \mathcal{S}_a\}. \tag{4.13}$$

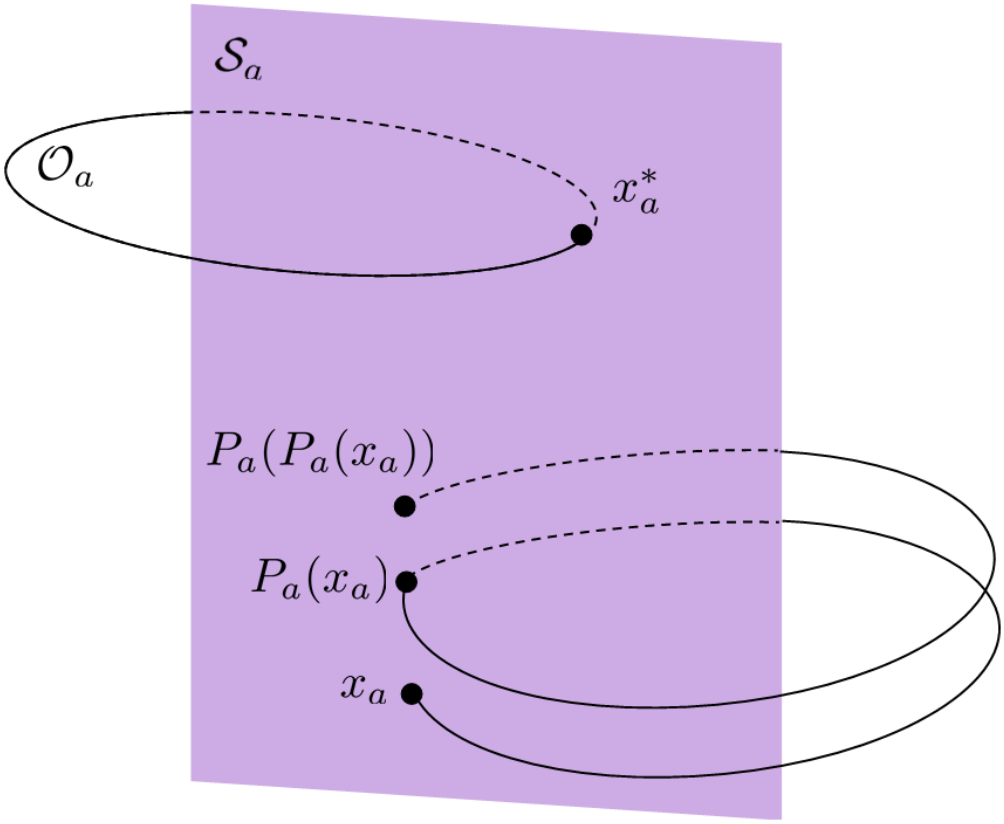

Figure 4.1: Illustration of the augmented Poincaré return map. An arbitrary point x_a has a Poincaré return mapping of $P_a(x_a)$ denoting the next location the orbit will intersect the augmented switching surface $\mathcal{S}_a$. The fixed point x_a^* uniquely defines a periodic orbit $\mathcal{O}_a$ by having a return mapping of $P_a(x_a^*) = x_a^*$.

As per the above construction, there is a fixed point corresponding to the periodic orbit of the augmented system, that is,

$$P_a(x_a^*) = x_a^*, \tag{4.14}$$

where $x_a^* = \text{col}(x^*, 1)$, and x^* is the intersection of the closure of the periodic orbit with the switching surface, i.e., $\{x^*\} := \bar{\mathcal{O}} \cap \mathcal{S}_e$. The local exponential stability of the periodic orbit for the augmented system is equivalent to having all the eigenvalues of the Jacobian matrix of the Poincaré map inside the complex unit circle, i.e.,

$$\left| \text{eig} \left\{ \frac{\partial P_a}{\partial x_a} (x_a^*) \right\} \right| < 1. \tag{4.15}$$

Figure 4.1 illustrates the augmented Poincaré return map for both a general point x_a and the fixed point x_a^*.

4.3 Extended Exponential Stability Analysis

The augmented Poincaré map defined in (4.12) can be considered as an $n+1$-dimensional discrete-time system. The following theorem reduces the exponential stability problem of the corresponding fixed point into that of an n-dimensional system.

Theorem 1. ***(Poincaré Analysis for Periodic Orbits of Time-Varying Hybrid Systems):*** *Consider the time-varying state feedback laws* (4.1)*, in which the time-based phasing variable evolves according to* (4.2) *and resets on the switching manifolds as* $\tau^+ = 0$*. Then, the following statements hold.*

1. *The Jacobian linearization of the Poincaré map for the augmented system takes the following structure*
$$\frac{\partial P_a}{\partial x_a}(x_a^*) = \begin{bmatrix} \frac{\partial P_x}{\partial x}(x^*, 1) & 0 \\ \frac{\partial P_\tau}{\partial x}(x^*, 1) & 0 \end{bmatrix}, \tag{4.16}$$
where $P_a =: col(P_x, P_\tau)$ *is a decomposition corresponding to* (x, τ)*, i.e.,* $P_x \in \mathbb{R}^n$ *and* $P_\tau \in \mathbb{R}$*.*

2. *The periodic orbit* $\mathcal{O}$ *is orbitally exponentially stable for the closed-loop hybrid system, if, and only if,*
$$\left| eig\left\{ \frac{\partial P_x}{\partial x}(x^*, 1) \right\} \right| < 1. \tag{4.17}$$

Proof. From [146, Theorem D.1] and chain rule, the Jacobian linearization of the Poincaré map can be expressed in a closed-form solution as follows:
$$\frac{\partial P_a}{\partial x_a}(x_a^*) = \underbrace{\left(I_{n+1} - \frac{f_a^{\text{cl}}(x_a^*) \frac{\partial s_a}{\partial x_a}(x_a^*)}{\frac{\partial s_a}{\partial x_a}(x_a^*) f_a^{\text{cl}}(x_a^*)} \right)}_{:=\Pi(x_a^*)} \Phi_a(T_v) \frac{\partial \Delta_a^{\text{cl}}}{\partial x_a}(x_a^*), \tag{4.18}$$
where I_{n+1} is the identity matrix of dimension $n+1$, $\Pi(x_a^*)$ is referred to as the saltation matrix, and
$$\Phi_a(t) := \frac{\partial \varphi_a}{\partial x_0}(t, x_0) \in \mathbb{R}^{(n+1)\times(n+1)} \tag{4.19}$$
represents the trajectory sensitivity matrix. In addition, the augmented switching surface $\mathcal{S}_a = \mathcal{S}_e \times \mathbb{R}^+$ can be considered as a zero-level set of a differential function $s_a(x_a)$ that only depends on x, that is, $s_a(x_a) = s_a(x)$. Since both the following expressions hold:
$$f_a^{\text{cl}}(x_a^*) = \text{col}(f_v^{\text{cl}}(x_a^*), \frac{1}{T_v}) \tag{4.20}$$
$$\frac{\partial s_a}{\partial x_a}(x_a^*) = [\frac{\partial s_a}{\partial x}(x_a^*)\ 0], \tag{4.21}$$

one can simplify the saltation matrix $\Pi(x_a^*)$ as follows:

$$\Pi(x_a^*) = \begin{bmatrix} I_n & 0 \\ 0 & 1 \end{bmatrix} - \frac{1}{\frac{\partial s_a}{\partial x}(x_a^*) f_a^{\mathrm{cl}}(x_a^*)} \begin{bmatrix} f_v^{\mathrm{cl}}(x_a^*) \frac{\partial s_a}{\partial x}(x_a^*) & 0 \\ \frac{\partial s_a}{\partial x}(x_a^*) \frac{1}{T_v} & 0 \end{bmatrix} \tag{4.22}$$

which can be decomposed into (x, τ) coordinates as

$$\Pi(x_a^*) = \begin{bmatrix} \Pi_{xx} & 0 \\ \Pi_{\tau x} & 1 \end{bmatrix} \tag{4.23}$$

From the variational equation [146, Appendix B], the state trajectory sensitivity matrix satisfies the following matrix differential equation

$$\begin{aligned} \dot{\Phi}_a(t) &= A_a(t)\, \Phi_a(t) \\ \Phi_a(0) &= I_{n+1} \\ A_a(t) :&= \frac{\partial f_a^{\mathrm{cl}}}{\partial x_a}(\varphi_a^*(t)), \end{aligned} \tag{4.24}$$

in which $\varphi_a^*(t)$ denotes the augmented periodic trajectory. The trajectory sensitivity matrix as well as the Jacobian linearization of the augmented vector field along the periodic trajectory can be decomposed into (x, τ) coordinates as follows:

$$\begin{aligned} \Phi_a(t) &= \begin{bmatrix} \Phi_{xx}(t) & \Phi_{x\tau}(t) \\ \Phi_{\tau x}(t) & \Phi_{\tau\tau}(t) \end{bmatrix} \\ A_a(t) &= \begin{bmatrix} \frac{\partial f_v^{\mathrm{cl}}}{\partial x}(\tau, x) & \frac{\partial f_v^{\mathrm{cl}}}{\partial \tau}(\tau, x) \\ 0 & 0 \end{bmatrix} := \begin{bmatrix} A_{xx}(t) & A_{x\tau}(t) \\ 0 & 0 \end{bmatrix}. \end{aligned} \tag{4.25}$$

Equation (4.25) reduces the variational equation into the following matrix differential equations

$$\dot{\Phi}_{xx}(t) = A_{xx}(t)\, \Phi_{xx}(t), \qquad \Phi_{xx}(0) = I_n \tag{4.26}$$

$$\dot{\Phi}_{x\tau}(t) = A_{xx}(t)\, \Phi_{x\tau}(t) + A_{x\tau}(t), \quad \Phi_{x\tau}(0) = 0 \tag{4.27}$$

$$\Phi_{\tau x}(t) \equiv 0, \tag{4.28}$$

$$\Phi_{\tau\tau}(t) \equiv 1. \tag{4.29}$$

Combining (4.23) and (4.26)-(4.29), we can simplify the Jacobian linearization of the Poincaré map as follows:

$$\begin{aligned} \frac{\partial P_a}{\partial x_a}(x_a^*) &= \begin{bmatrix} \Pi_{xx} & 0 \\ \Pi_{\tau x} & 1 \end{bmatrix} \begin{bmatrix} \Phi_{xx}(T_v) & \Phi_{x\tau}(T_v) \\ 0 & 1 \end{bmatrix} \underbrace{\begin{bmatrix} D_{xx} & 0 \\ 0 & 0 \end{bmatrix}}_{\frac{\partial \Delta_a^{\mathrm{cl}}}{\partial x_a}(x_a^*)} \\ &= \begin{bmatrix} \Pi_{xx}\, \Phi_{xx}(T_v)\, D_{xx} & 0 \\ \Pi_{\tau x}\, \Phi_{xx}(T_v)\, D_{xx} & 0 \end{bmatrix}, \end{aligned} \tag{4.30}$$

in which $D_{xx} := \frac{\partial \Delta_e^{\text{cl}}}{\partial x}(x^*)$. This completes the proof of Part (1). With the above structure of the Jacobian matrix, the eigenvalues become

$$\begin{aligned} \text{eig}\left\{\frac{\partial P_a}{\partial x_a}(x_a^*)\right\} &= \text{eig}\left\{\Pi_{xx}\,\Phi_{xx}(T_v)\,D_{xx}\right\} \cup \{0\} \\ &= \text{eig}\left\{\frac{\partial P_x}{\partial x}(x_a^*)\right\} \cup \{0\} \end{aligned} \tag{4.31}$$

which completes the proof of Part (2). □

4.4 Poincaré for Hybrid Models with Gait Symmetry

Theorem 1 will be utilized to synthesize stabilizing HZD controllers for dynamic quadrupedal gaits in Chapter 6. In practice, the controlled dynamics are allowed to repeatedly evolve through one full cycle of the directed graph $\mathcal{G}$ after initializing slightly perturbed from the fixed point. After the discrete transition which brings the hybrid system back to its initial domain, the eigenvalues of the Jacobian matrix of the Poincaré section are evaluated. Intuitive adjustments can be made to the parameters by observing which changes increase or lower the largest eigenvalue magnitudes.

For analyzing the controllers developed in Chapter 3, the Poincaré section is taken at $\tau = 1$ for the domain v_1 of the respective hybrid gait (see Figs. 2.4-2.6). While the results of Theorem 1 consider the Poincaré map as an $n+1$-dimensional map to simplify the presentation, it is an n-dimensional partial map from $\mathcal{S}_a$ back to $\mathcal{S}_a$. To take this point into account, a dependent coordinate from the state vector must be removed. Without loss of generality, we eliminate the q_z component which represents the height of the base frame $\mathcal{B}$ as it can be uniquely determined from the configuration of a stance leg. We also remark that as the robot travels in the x-direction, it lacks periodicity in the q_x component, and thus there will be an eigenvalue 1 for the Jacobian matrix $\frac{\partial P_x}{\partial x}(x_a^*)$. Consequently, all remaining eigenvalues must lie inside the complex unit circle in order to verify exponential stability for each gait controller.

Poincaré sections analysis is defined for a full periodic orbit, but the trotting and walking hybrid gaits for Minitaur are each composed of a pair of reflected half orbits. For general orbits with half symmetry, the exponential stability of the reflected half orbit is related to the full orbit by the equation

$$\frac{\partial P}{\partial x}(x^*) = \left(\frac{\partial P_{\text{half}}}{\partial x}(x^*)\right)^2 \tag{4.32}$$

from [83, Remark 9], where $\frac{\partial P_{\text{half}}}{\partial x}$ represents the Jacobian matrix of the half orbit. Thus, the exponential stability of the half orbit ensures the exponential stability of the full orbit and

vice-versa. The selection of either method is arbitrary, and the Poincaré sections analysis for the symmetric trotting and walking gaits corresponds to the full 8 domain orbit for each gait.

Once the designs of the tuneable virtual constraints are selected (see (3.11)-(3.13)), the trajectory of the constrained dynamics is simulated for one cycle and the eigenvalues of the Jacobian matrix of the Poincaré section are evaluated. If the eigenvalues are not within the unit circle as required to verify stability, the parameters α_v and β_v are adjusted offline to drive the eigenvalues within the unit circle. The resulting eigenvalues for each gait controller are provided in the details of the closed-loop simulations in Chapter 6.

Chapter 5

Optimal Gait Planning

Table 5.1: Definitions of terms introduced in Chapter 5

Term	Definition
α_b	bezier polynomial terms
C_{eq}	equality constraints i
C_{ineq}	inequality constraints
μ	coefficient of static friction
F_v	vertical GRF
F_h	horizontal GRF
$F_x \backslash F_y$	horizontal GRF components
J	cost function
W	weighting matrix
ξ	decision variables
γ	homotopy parameter
λ_{eq}	Lagrianian multipliers of C_{eq}
z	Lagrianian multipliers of bounds
k	current step
p_k	search direction
α_k	search step size
B	hessian approximation
$\circ_c$	of the current iterate
$\circ_+$	of the next iterate

5.1 Background

The HZD control approach described in Chapter 3 requires a desired periodic trajectory to define the holonomic virtual constraints. The high DOF complexity inherent to quadrupedal locomotion necessitates formulating the generation of an optimal gait as a Nonlinear Programming (NLP) problem. This section details the formulation of the NLPs designed for each gait and the direct collocaiton methods used to solve them. In this chapter, we describe and utilize the software package FROST [144, 154] and the optimization algorithm IPOPT. The key results of each optimal gait are also presented, including limit cycles, coordinate trajectories, torque profiles, and additional constraint verification data. Table 5.1 provides definitions of the terms and symbols introduced in this section.

5.2 Gait Optimization as an NLP

To be implemented as an NLP, the requirements for optimization must be formatted into a set of decision variables, equality constraints, inequality constraints, and cost functions. The following sections define the formulation of these quantities for compatibility with the software package FROST.

5.2.1 Decision Variables

The set of parameters modified by the optimization algorithm to solve the NLP are referred to as the "decision variables." An initial condition of these variables is supplied to the NLP solver at the beginning of optimization. A robust solver may incorporate thousands of decision variables into the gait optimization process, however these variables can be separated into distinct categories. The direct collocation approach used by FROST discretizes each continuous-time domain into a set of discrete-time points. A set of decision variables is introduced to denote the values of the generalized position q, generalized velocities $\dot{q}$, generalized acceleration $\ddot{q}$, control inputs u, and the GRFs λ on all nodes. The desired evolution of the state trajectory subject to the virtual constraints is expressed as a Bézier polynomial [77, 80]. The coefficient matrix of the Bézier polynomial represents a set of control points which shape the curve of the dynamics and forms an additional set of decision variables denoted by α_b. The elapsed times T_v for each continuous-time domain are also considered as decision variables. These terms define the main decision variables considered when designing the NLP to implement in FROST, however the software and algorithms implemented by FROST may add additional decision variables to increase the performance of the solver.

5.2.2 Equality Constraints and Inequality Constraints

The desired behavior of the optimal gait is mathematically described by a series of equality constraints C_{eq} and inequality constraints C_{ineq}, which are a series of expressions that must meet the following restrictions respectively:

$$C_{eq} = 0 \tag{5.1}$$

$$C_{ineq} \leq 0. \tag{5.2}$$

It should be noted that the distinction between equality constraints and inequality constraints is for clarity in definition and implementation. An equality constraint can be accurately modeled by two inequality constraints, and an inequality constraint may be formulated as an equality constraint through the implementation of slack variables [155]. In practice, equality constraints are given a small threshold of variance due to the nature of numerical simulation. Just as with the decision variables, certain constraints may be added to account for desirable mathematical properties of the NLP separate from conditions related to the gait optimization itself. The key constraints for gait optimization are described below.

Continuity Constraints

The optimized periodic trajectory of the simulated model must have continuity in all internal and absolute degrees of freedom during continuous-time domains. During discrete-time transitions, velocity coordinates may experience discontinuities due to impact dynamics [151], but position coordinates must maintain continuity. All degrees of freedom must also have periodicity within the entire orbit except for the horizontal x position of the floating base, which increases over the course of the gait. The optimized limit cycles of these coordinates are provided in Figs. 5.7-5.12 to demonstrate periodicity of the coordinate vector. A sampling of the internal and absolute DOF trajectories for optimized gaits are provided in Figs. 5.1-5.6 to demonstrate continuity of position.

Torque Feasibility

In order for a gait to be considered practically feasible for implementation on Minitaur outside of simulation, the torques sent to the actuators must be within acceptable bounds. However, these bounds must be considered with respect to the true configuration of Minitaur (motor space) rather than the simulation model (leg space). For the gait design and subsequent simulations, a hard upper bound magnitude of 20 Nm was placed on the actuators of Minitaur. However, this represents the absolute upper bound of what Minitaur's direct drive motors are capable of, so gait design targeted motor torques well under the limitations. Figures 5.13-5.15 display the bounded actuation for each optimized gait trajectory.

Physical Holonomic Constraints

Each domain of a hybrid gait is defined by a set of physical holonomic constraints which denote properties which remain static over the course of a domain and enact corresponding forces on the dynamic system. While dynamics evolving according to (2.6) maintain

holonomic constraints through the constraint Jacobian, holonomic constraints are treated as unilateral constraints in FROST implementations [144]. This applies to both the foot contact constraints which define each continuous-time domain and the planar restrictions for the bounding gait.

Ground Reaction Forces and Friction Cone

The forces required to maintain the foot contact constraints are also considered at this stage of gait development. For a gait to be feasible, the vertical component of the GRF on any given foot must not exceed the corresponding horizontal static friction force. This relational constraint is defined by the following friction cone equation:

$$\begin{aligned} \frac{F_h}{\mu\, F_v} &\leq 1, \quad F_v > 0 \\ F_h &:= \sqrt{(F_x)^2 + (F_y)^2} \\ F_v &:= F_z, \end{aligned} \tag{5.3}$$

where F_v is the vertical normal force, F_x and F_y are the components of the horizontal static friction force F_h, and μ is the coefficient of static friction, defined as 0.6 for these simulations. This condition validates the contact constraints enforced by the Jacobian of (2.6) by providing a mathematical validation for the lack of slippage of the contact feet. Figures 5.16-5.18 demonstrate that the GRF ratio for each gait satisfies (5.3).

Foot Position

In addition to basic feasibility constraints on the model's configuration, constraints are also placed specifically on the trajectories of each foot. In addition to guiding the optimization solver to desirable trajectories, these constraints ensure that feet never penetrate the simulated walking surface or encounter an unacceptable early impact. Plots of the foot clearance of the optimized gaits are provided in Figs. 5.19-5.21.

5.2.3 Cost Function

While a gait trajectory needs only to satisfy the above constraints to be implemented in the controller design, the NLP optimization also utilizes a cost minimization to generate actuator efficient trajectories. The cost J is minimized according to the weighted least-squares cost function defined below.

$$J = \int_0^T u^\top(t)\, W\, u(t)\, \mathrm{d}t \tag{5.4}$$

where W is a weighting matrix which scales the cost of each element of the vector u. For each of the 3 gaits, the torques corresponding to the simulated knee actuators were weighted by a factor of 100 compared to the hip actuators, as it was observed that the knee joints were producing the highest torques for the simulated model.

5.2.4 Full NLP

With the relevant quantities defined, we can now formalize the gait optimization NLP for FROST as follows

$$\begin{aligned} \min_{\xi} \ & J(\xi) \\ \text{s.t. } & C_{eq}(\xi) = 0 \\ & \xi \geq 0. \end{aligned} \tag{5.5}$$

Here, inequality constraints are characterized as equality constraints and bounds on the decision variables ξ are structured into the form $\xi \geq 0$ for notation simplicity when analyzing FROST and IPOPT's implementation.

5.3 Direct Collocation in FROST

The Fast Robot Optimization and Simulation Toolkit (FROST) is an open-source MATLAB toolkit designed expressly for addressing hybrid gait planning of legged robotic systems [144, 154]. FROST supports a variety of direct collocation methods, but for this analysis the default Hermite-Simpson approach was used. Each continuous-and discrete-time domain is framed as its own trajectory optimization problem. The continuous time phases for each gait is discritized into 15 nodes. The state variables and input variables are added as optimization variables to the NLP, and if defects at the interior nodes are eliminated and the input and state variable satisfy the dynamics, there is a piecewise function of cubic polynomials which can accurately approximate the continuous dynamics [156].

The key differentiation of FROST from other direct collocation trajectory optimization toolboxes is that FROST avoids computing the dynamics explicitly [144]. Utilizing slack variables, the dynamics are enforced in the raw form of the differential equations (see (2.6)). The slack variables decouple a constraint of the form $a(b(x)) = 0$ into

$$a(b(x)) = 0 \rightarrow b(x) = y, a(y) = 0, \tag{5.6}$$

where y is the appropriate slack variable. The final NLP construction is then formatted to the solver which will be used to perform the final optimization. In this case, that solver is IPOPT.

5.4 IPOPT and Hessian Approximation

The following section contains an abridged summary of IPOPT as described in [155], providing a brief overview of the structure of the algorithm and its use of the hessian. As an

interior-point method, IPOPT restructures the NLP into a set of equations using a homotopy method [157].

$$\begin{aligned} \nabla f(x) + \nabla C_{eq}(x)\lambda - z &= 0 \\ C_{eq}(x) &= 0 \\ XZe - \gamma e &= 0 \end{aligned}$$

where the homotopy parameter γ is driven to 0. λ and z are the Lagrangian multipliers for the equality constraints and bound constraints, respectively. At a step k, this system of equations is solved to determine the search directions $p_k = (p_k^x, p_k^\lambda, p_k^z)$ for a given constant u_j.

$$\begin{bmatrix} W_k & A_k & -I \\ A_k^T & 0 & 0 \\ Z_k & 0 & X_k \end{bmatrix} \begin{pmatrix} p_k^x \\ p_k^\lambda \\ p_k^z \end{pmatrix} = - \begin{pmatrix} \nabla f(x_k) + A_k\lambda_k - z_k \\ C_{eq}(x_k) \\ X_k Z_k e - u_j e \end{pmatrix} \tag{5.7}$$

$$W_k := \nabla^2_{xx}[f(x) + C_{eq}(z)^T\lambda - z] \tag{5.8}$$

$$A_k := \nabla C_{eq}(x_k) \tag{5.9}$$

The left hand side square matrix is referred to as the "Iteration Matrix" in this context. The terms α_k and α_k^z determine the step size once the step directions p_k are determined. The step size for the z variables are determined separately. A filter then rejects the step if the current iterate k has a constraint violation larger than a defined threshold.

The method used to approximate the hessian of the NLP is the Limited Broyden-Fletcher-Goldfarb Shanno-Algorithm (L-BFGS) [158], which is an implementation of the BFGS method utilizing a limited memory constraint. This method approximates the inverse hessian with a history of past updates to handle large variable systems. This method distinguishes itself from other methods by discarding the information of a previous iteration upon reaching its full memory for approximating the hessian, rather than throwing out the entire matrix approximation every defined number of steps. The generic update equation for BFGS (5.10) is provided below

$$B_+ = B_c + \frac{y_c y_c^T}{y_c^T y_c} + \frac{B_c s_c s_c^T B_c}{s_c^T y_c}, \tag{5.10}$$

$$s_c := x_+ - x_c \tag{5.11}$$

$$y_c := \nabla f(x_+) - \nabla f(x_c) \tag{5.12}$$

where B is the hessian approximation, and the subscripts $+$ and c represent the next and current iterate, respectively.

5.5 Optimization Results

This section presents the relevant gait specific results of the optimized trajectories for bounding, trotting, and walking. The eight-domain gaits are presented as a series of four-domain

orbit pairs to highlight the corresponding symmetries of the gaits. Further results of the corresponding closed-loop simulations are provided in Chapter 6.

5.5.1 Computational Results

Table 5.2 provides data on the scale of each gait NLP. The optimization was run on a 64-bit installation of Windows 10 with 16GB of RAM and an 8-core Intel i7-9800X 3.8GHz processor.

Table 5.2: Properties of NLP optimization for each gait

Gait	Bound	Trot	Walk
Decision Variables	8208	9770	10481
Equality Constraints	3996	5276	5636
Inequality Constraints	6684	6470	7514
Optimization Time (s)	282.27	404.08	230.51

5.5.2 Limit Cycles and Coordinate Trajectories

The costs and constrains outlined above produce the sampling of absolute and internal coordinate limit cycles displayed in Figs. 5.7-5.12. Time evolution of the corresponding coordinates are also provided in Figs. 5.1-5.6. Discontinuities in these limit cycles represent the discrete dynamics that occur during impact phases. If the constrained dynamics of each gait are exponentially stable, the gait trajectories will converge to these limit cycles when the initial state is perturbed off of the limit cycle. This criteria will be explored in the closed-loop simulations of Chapter 6.

5.5.3 Torque Profiles

Over the course of the evolution of the constrained dynamics, the torques sent to the actuators must be limited to ensure the feasibility. Unlike the cost functions, torque feasibility considers constraints on each actuator individually. Figures 5.13-5.15 display the torques corresponding to the optimal trajectory converted to the motor space model from the simulated leg space model. Since FROST acts on the simulated model, constraints must be placed on the leg space actuators which correspond to constraints for the motor space model. For each trajectory, torque magnitudes are generally below 15 Nm with only short periods above, which has been determined to be acceptable for implementation on Minitaur.

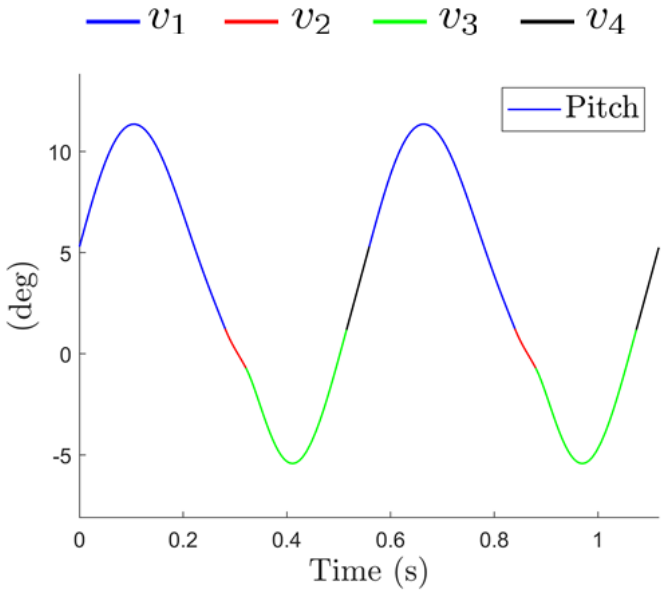

Figure 5.1: Trajectory of the absolute pitch DOF for the bounding gait. As the gait is planar, yaw and roll are held at 0.

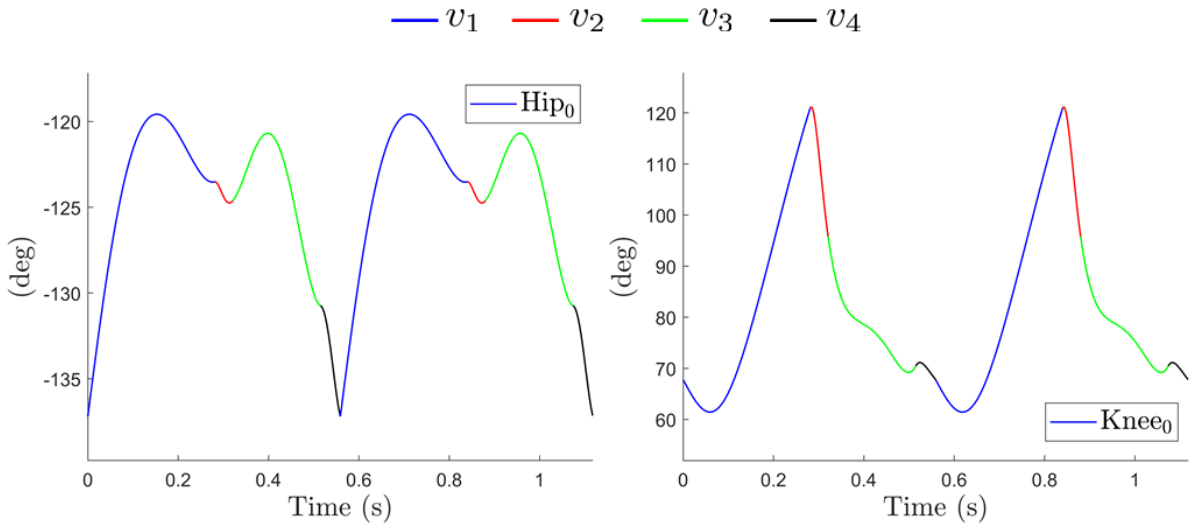

Figure 5.2: Trajectory of the internal Hip_0 and $Knee_0$ DOFs for the bounding gait.

5.5.4 Friction Cone Constraint Validation

Figures 5.16, 5.17, and 5.18 provide validation of the friction cone constraint for the bounding, trotting, and walking gaits respectively. In addition to adhering to (5.3), the vertical component of each liftoff foot goes to zero at the end of the appropriate domain. A liftoff is represented by the respective GRF ratio of (5.3) dropping to 0 N at the end of the appro-

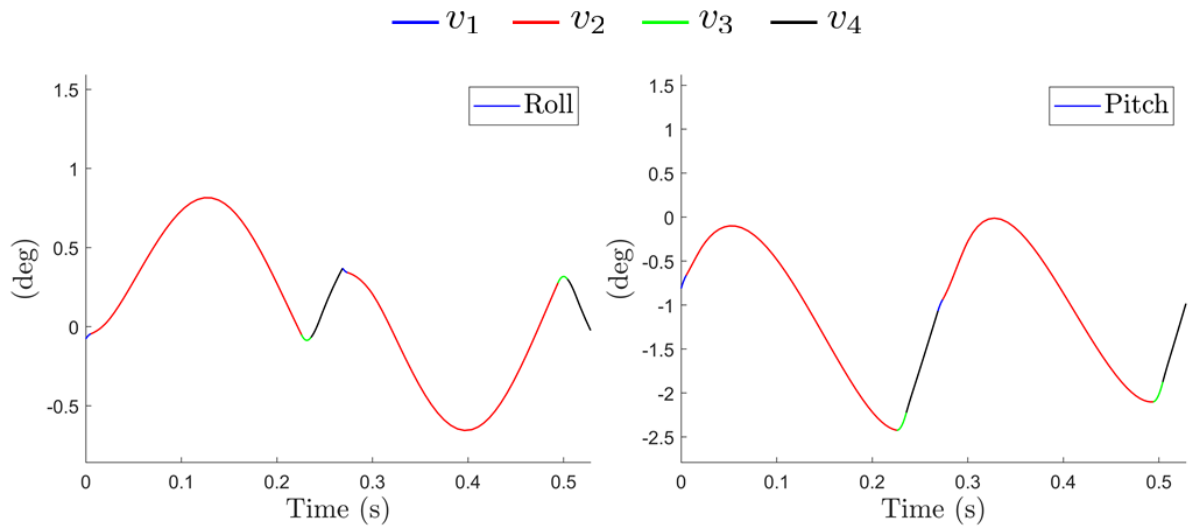

Figure 5.3: Trajectory of the absolute pitch and roll DOFs for the trotting gait.

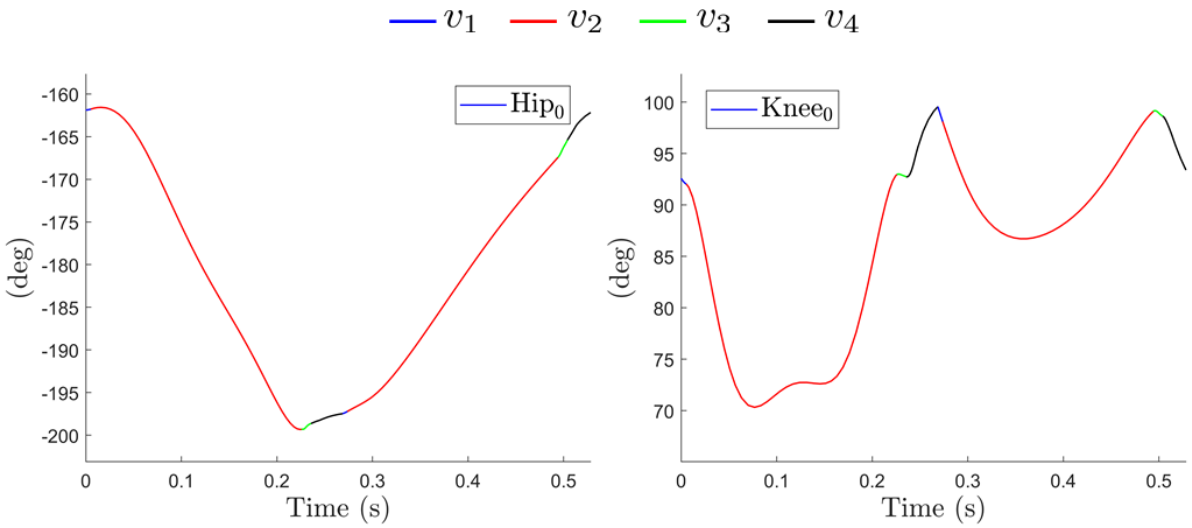

Figure 5.4: Trajectory of the internal Hip_0 and Knee_0 DOFs for the trotting gait.

priate domain, as both the horizontal and vertical components of the force disappear upon liftoff. Also note that the ratio may also approach zero if the tangential force vector F_h goes to zero.

5.5.5 Foot Placement Validation

The trajectories of each point foot and their optimization bounds are provided for the bounding (Fig. 5.19), trotting (Fig. 5.20), and walking (Fig. 5.21) gaits. In each case, it is shown

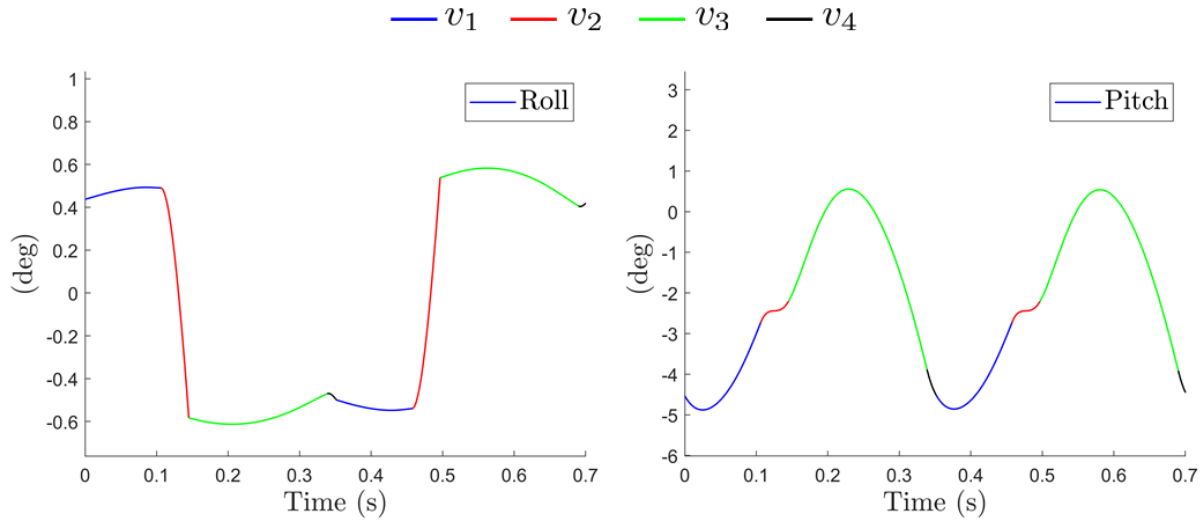

Figure 5.5: Trajectory of the absolute pitch and roll DOFs for the walking gait.

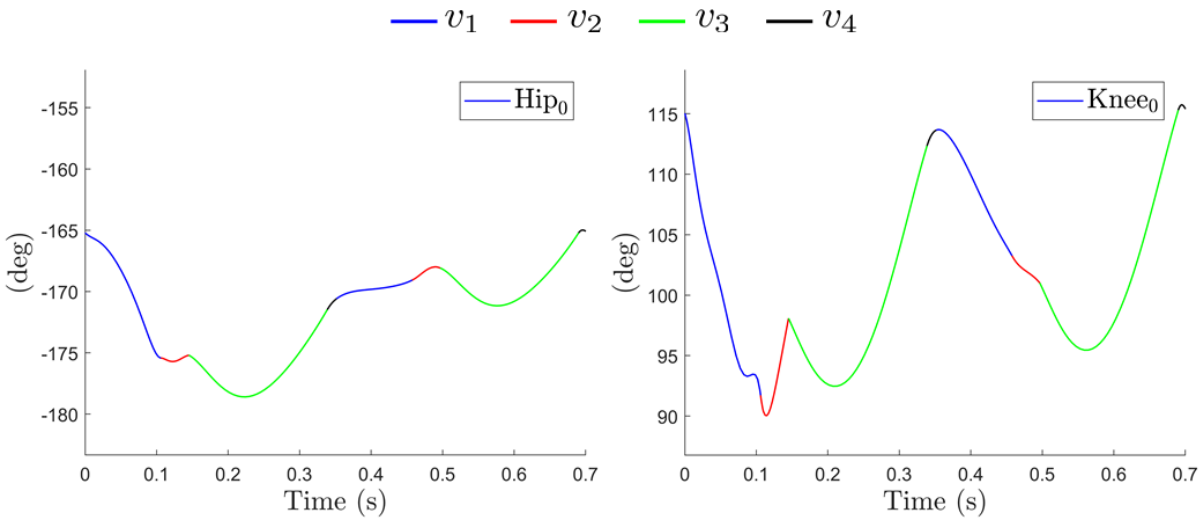

Figure 5.6: Trajectory of the internal Hip_0 and Knee_0 DOFs for the walking gait.

that the feet do not penetrate the walking surface and do not impact before the corresponding domain begins. The foot position is continuous between domains with a threshold of 1mm. For the trotting and walking gaits, the first four domains are shown with the understanding that the latter four domains have identical trajectories corresponding to their respective coordinate reflection.

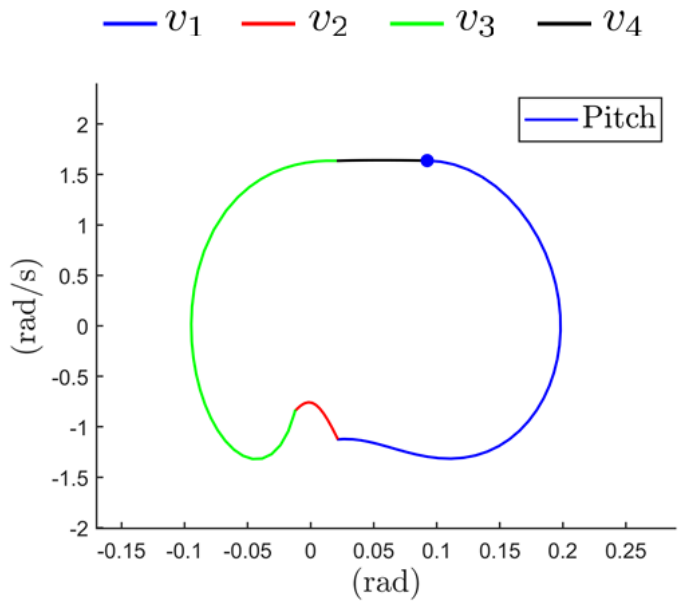

Figure 5.7: Limit cycle of the absolute pitch DOF for the bounding gait. As the gait is planar, yaw and roll are held at 0.

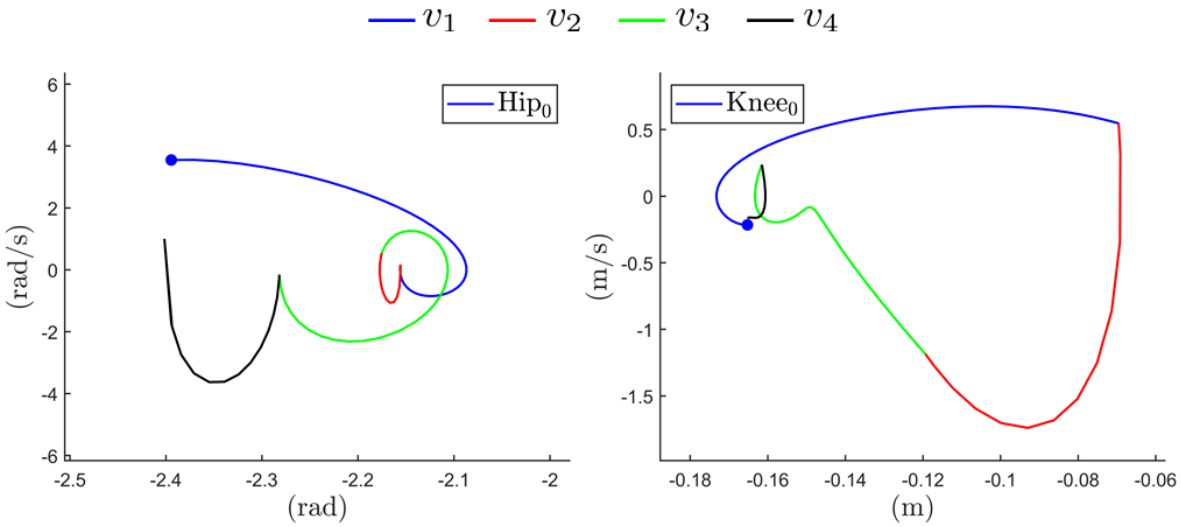

Figure 5.8: Limit cycles of the internal Hip_0 and Knee_0 DOFs for the bounding gait.

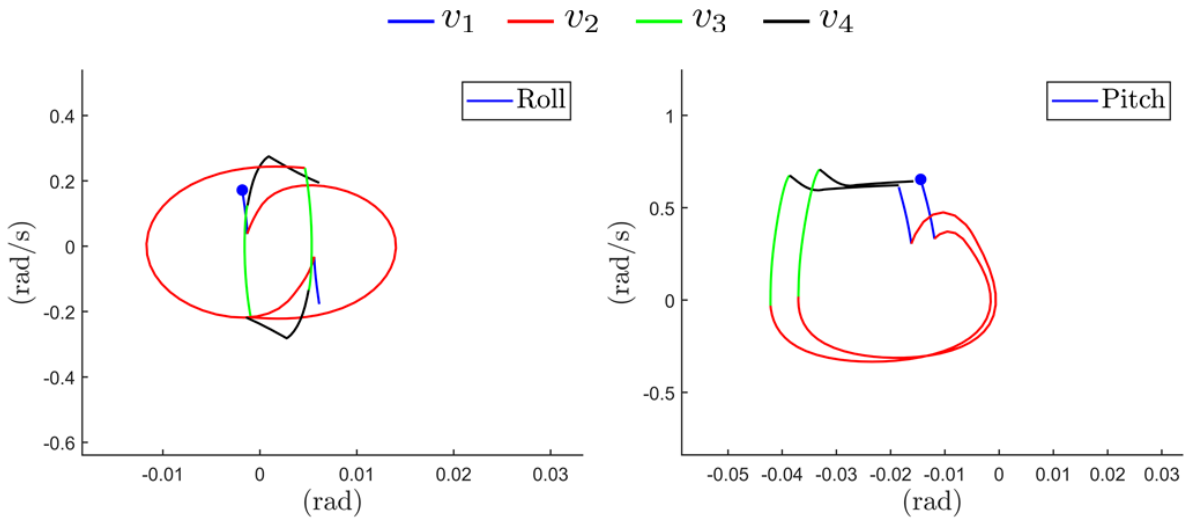

Figure 5.9: Limit cycles of the absolute roll and pitch DOFs for the trotting gait.

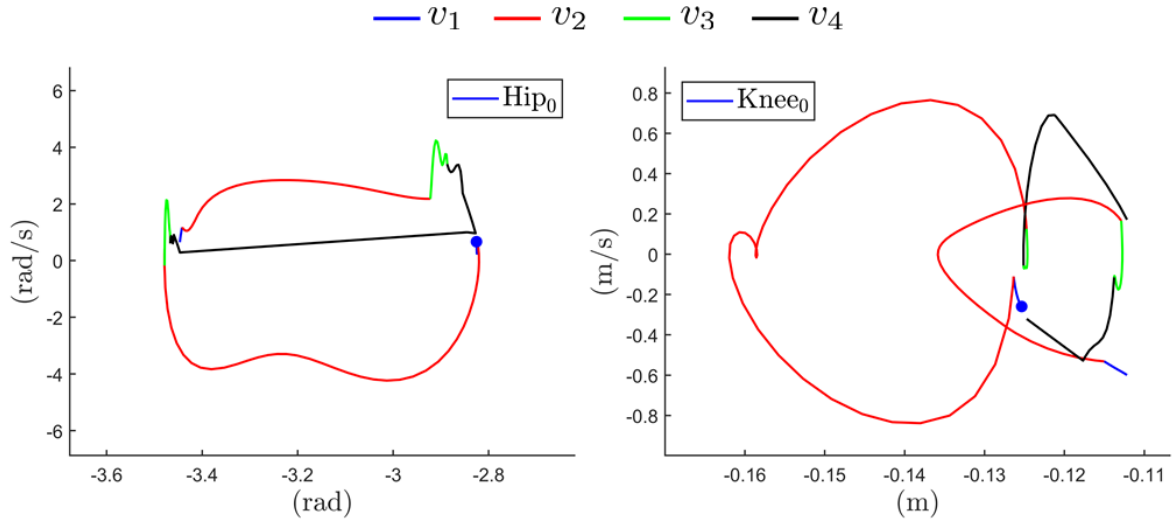

Figure 5.10: Limit cycles of the internal Hip_0 and Knee_0 DOFs for the trotting gait.

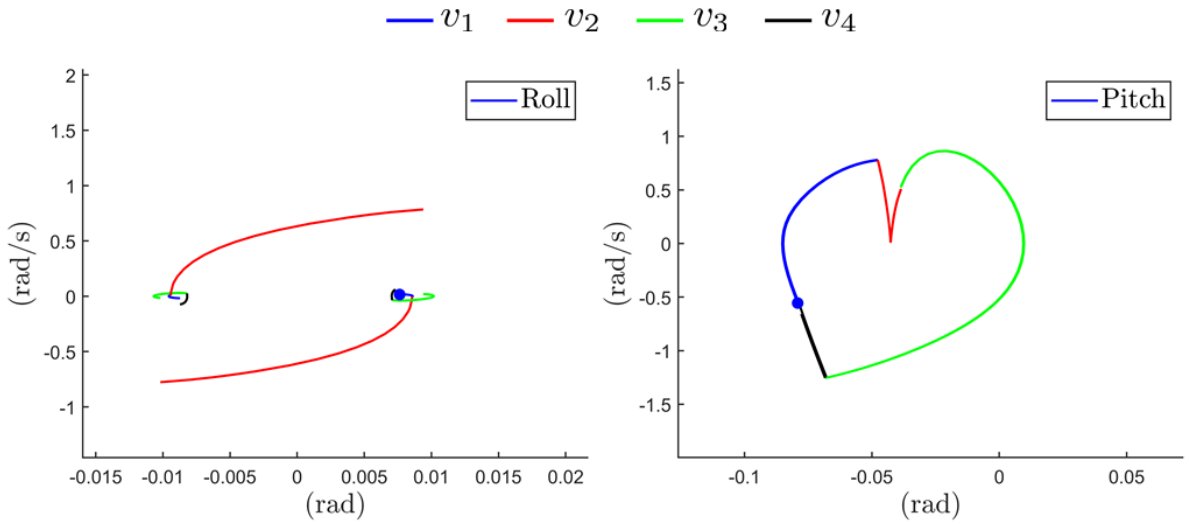

Figure 5.11: Limit cycles of the absolute roll and pitch DOFs for the walking gait.

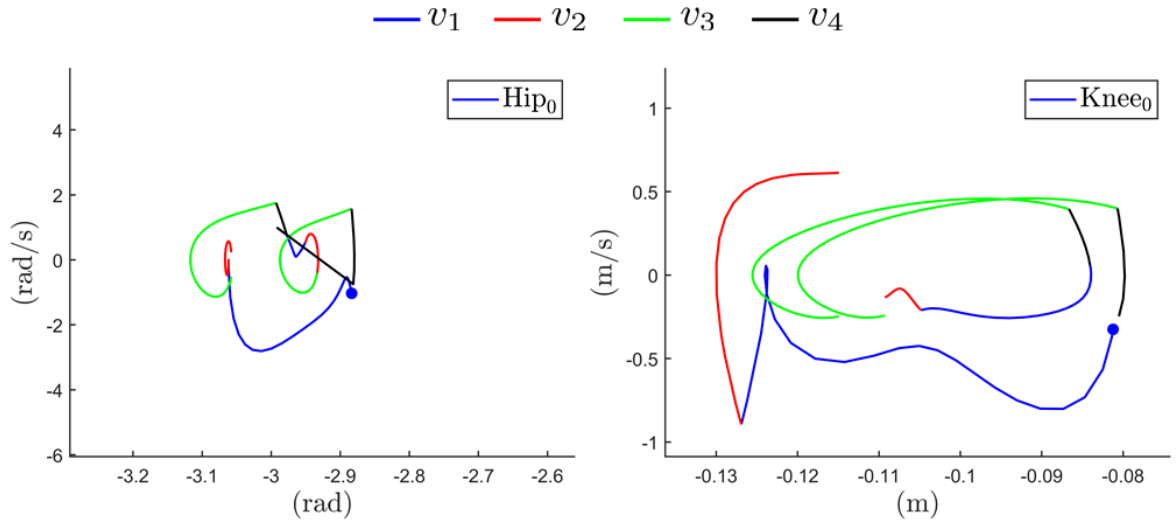

Figure 5.12: Limit cycles of the internal Hip_0 and Knee_0 DOFs for the walking gait.

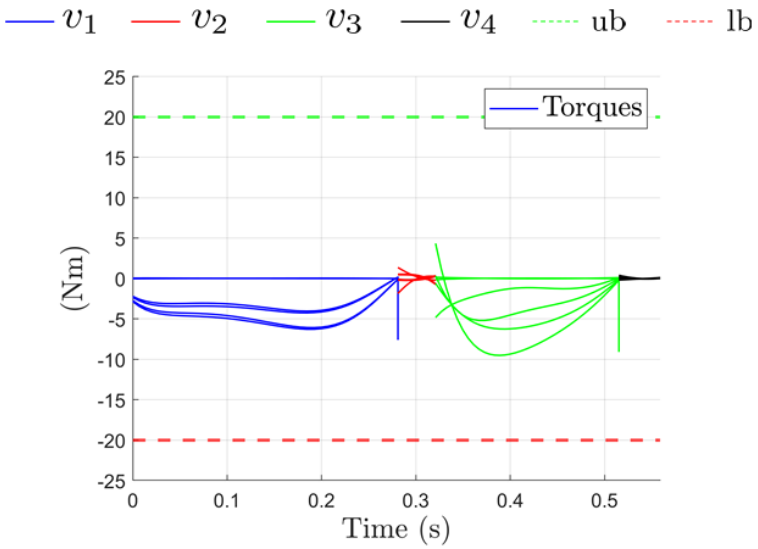

Figure 5.13: Actuator inputs for the first four domains of the optimized bounding gait. Inputs are converted from the leg space simulation model to the corresponding torques for the motor space model.

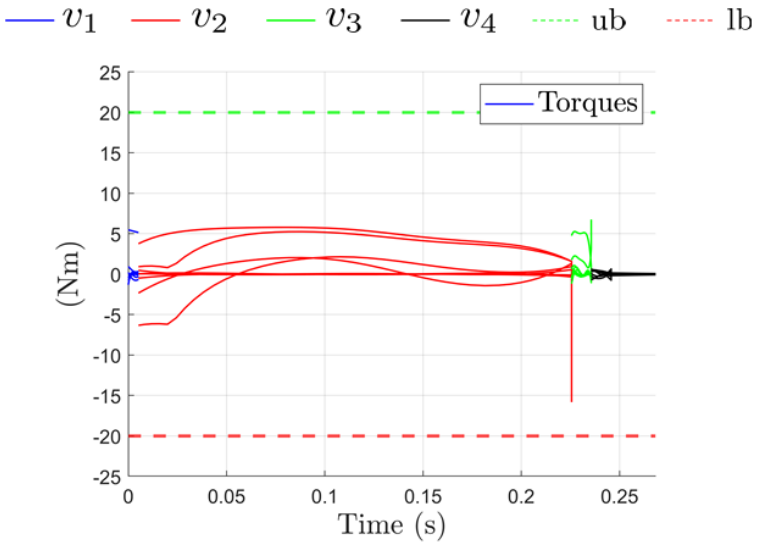

Figure 5.14: Actuator inputs for the first four domains of the optimized trotting gait. Inputs are converted from the leg space simulation model to the corresponding torques for the motor space model.

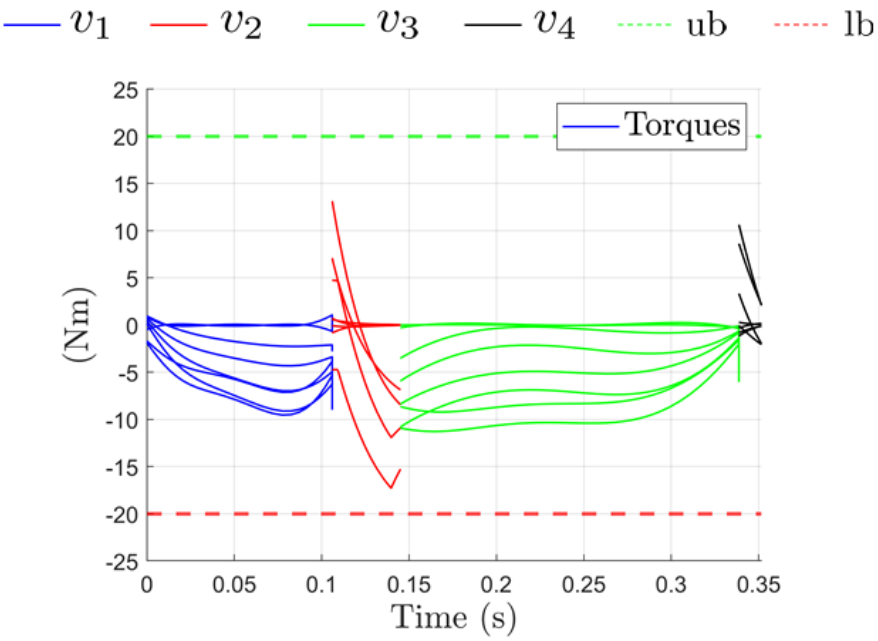

Figure 5.15: Actuator inputs for the first four domains of the optimized walking gait. Inputs are converted from the leg space simulation model to the corresponding torques for the motor space model.

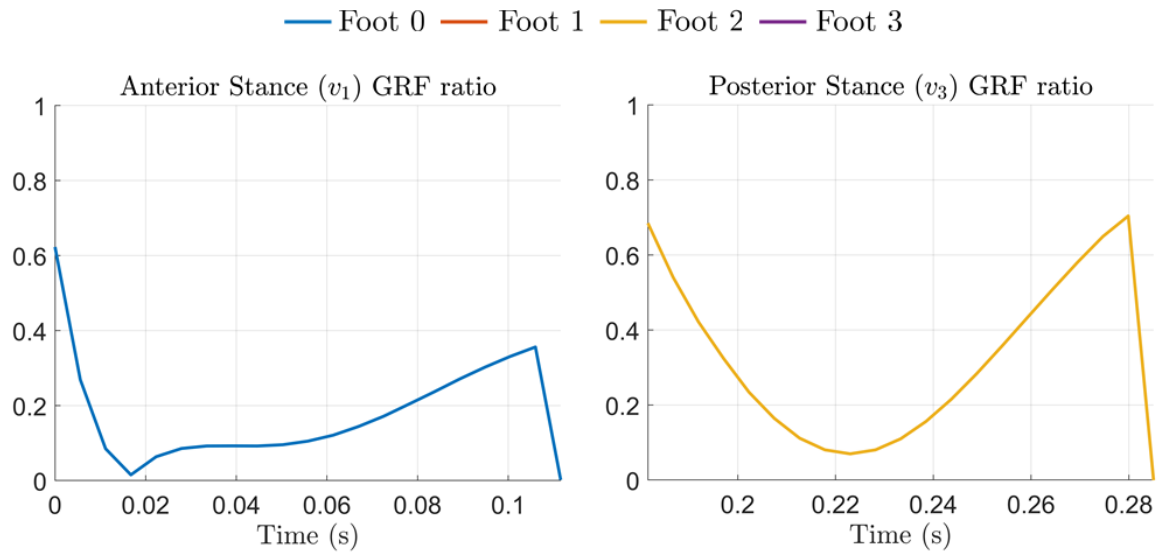

Figure 5.16: Friction cone validation for the bounding gait. Since the gait is planar, Foot 1 and Foot 3 have identical profiles to Foot 2 and Foot 4 respectively. Flight phases have no friction cone restraint, and are thus omitted.

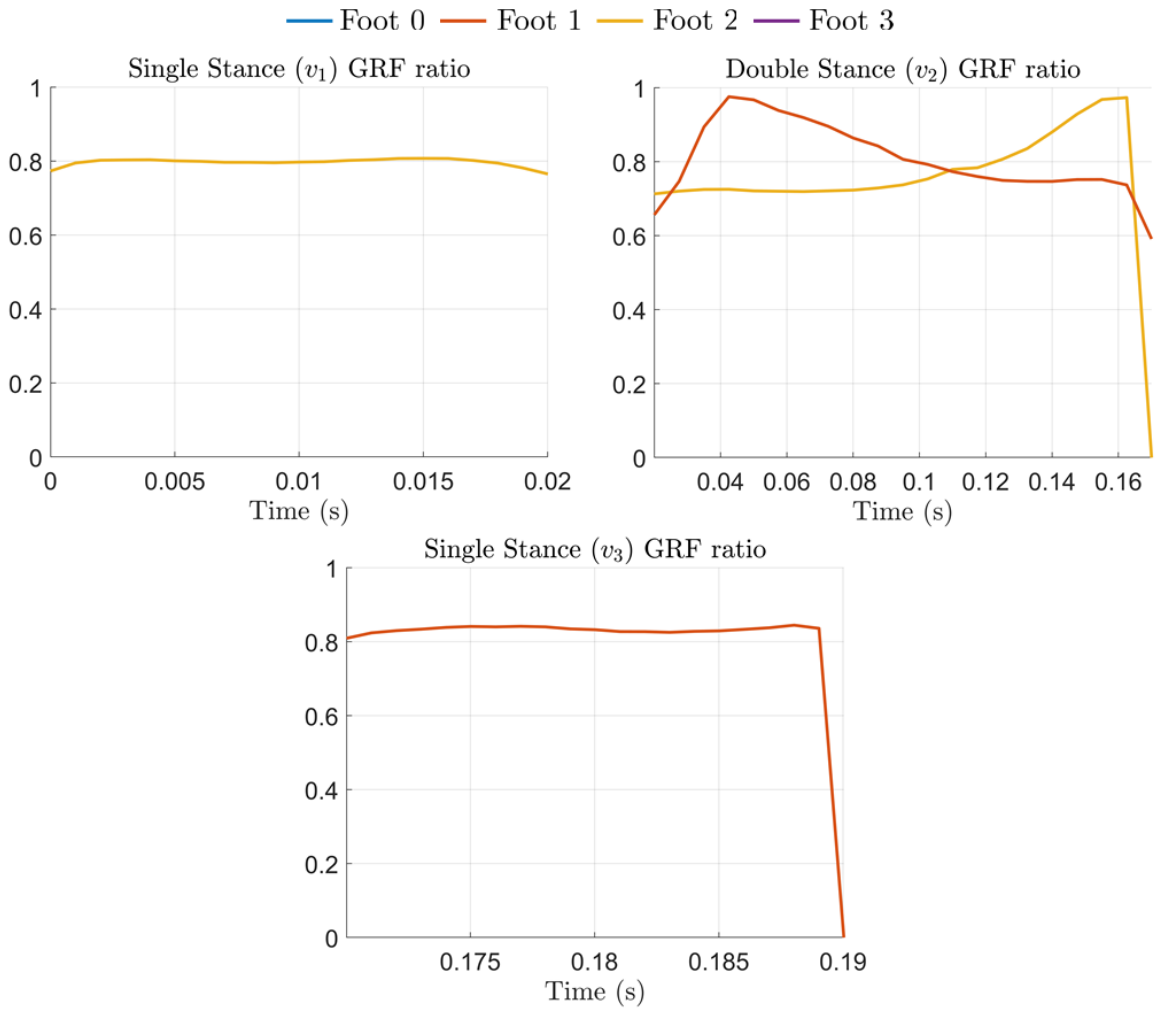

Figure 5.17: Friction cone validation for the trotting gait. Flight phases have no friction cone restraint, and are thus omitted.

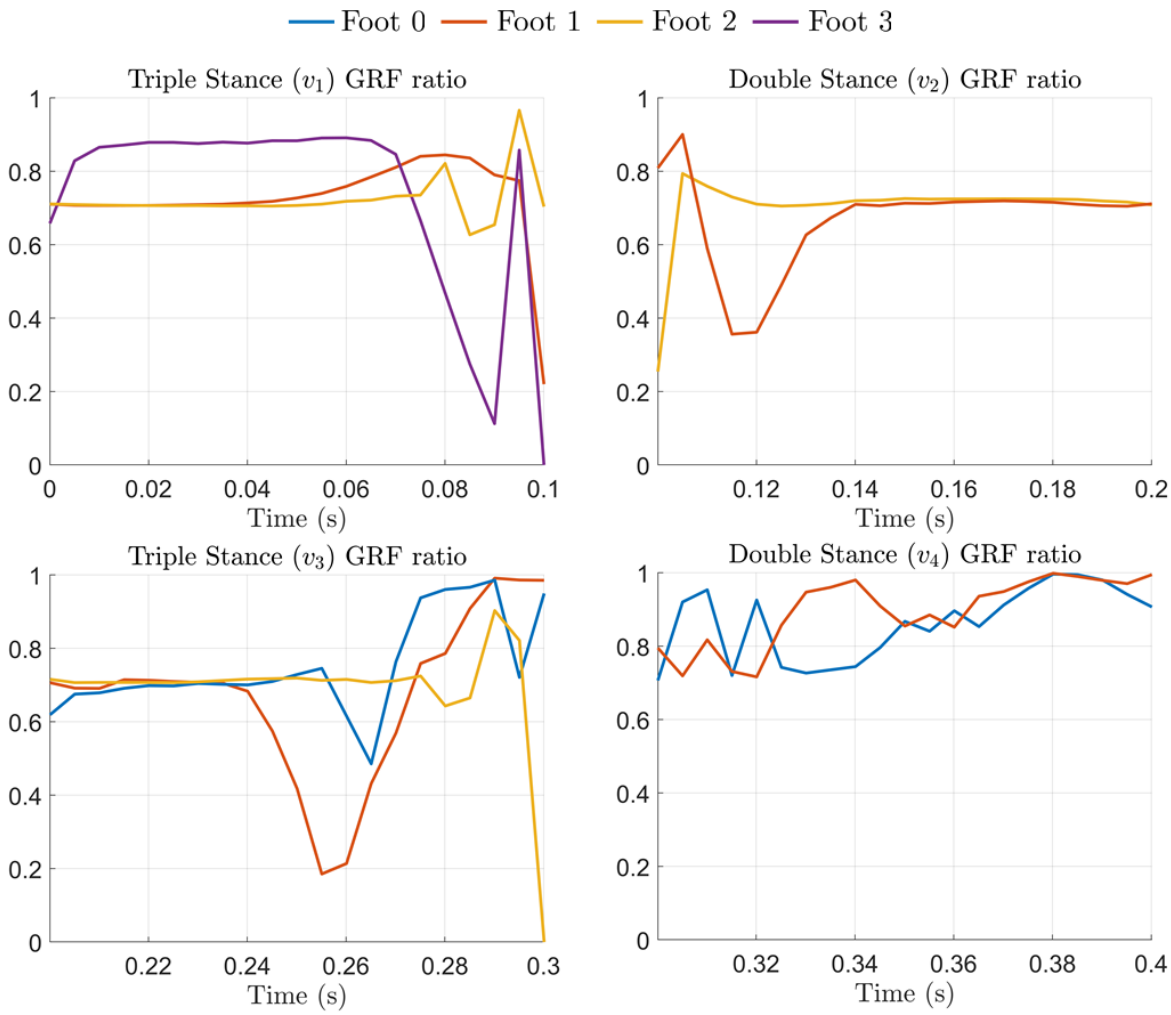

Figure 5.18: Friction cone validation for the walking gait.

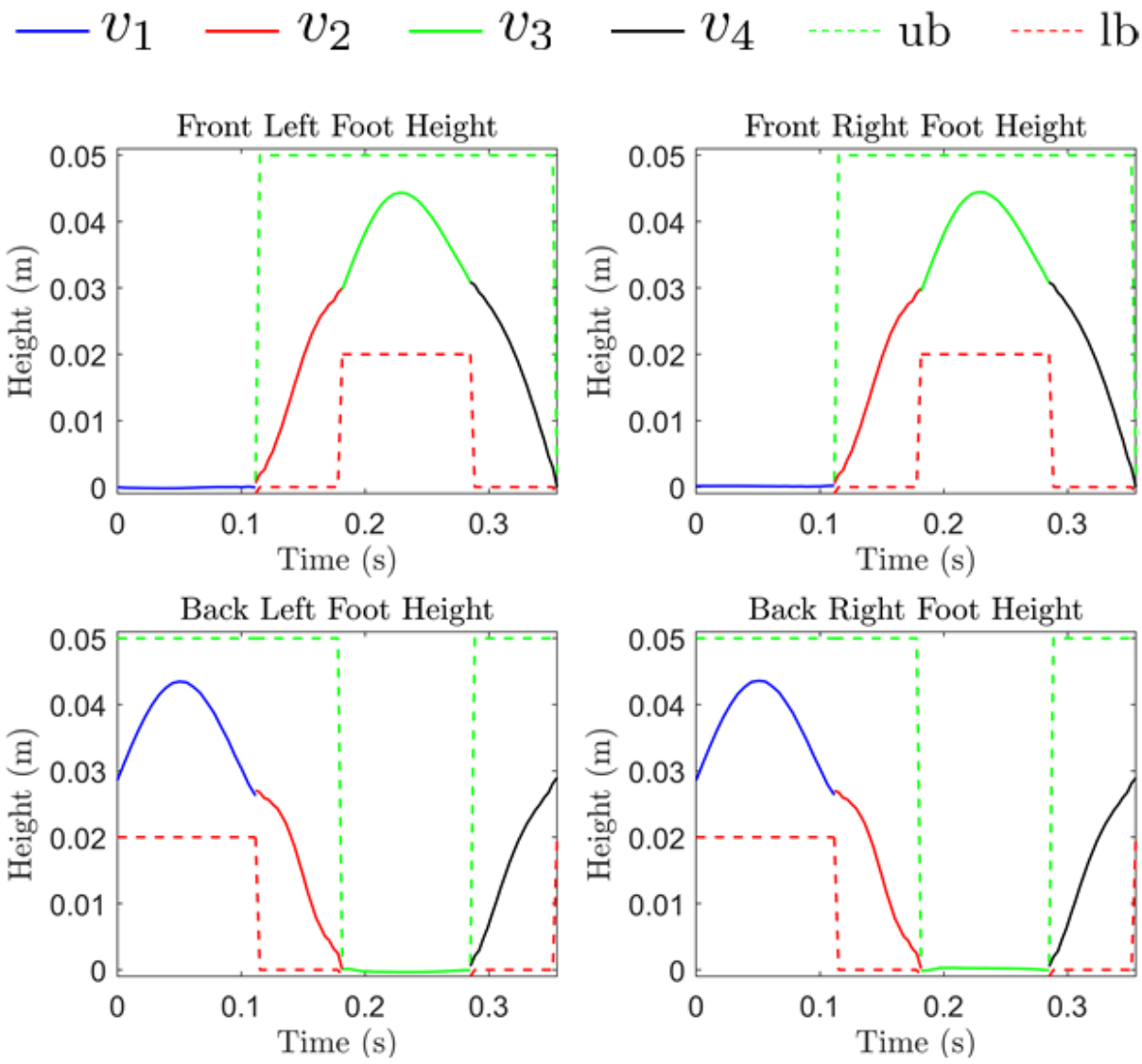

Figure 5.19: Foot height during the bounding gait.

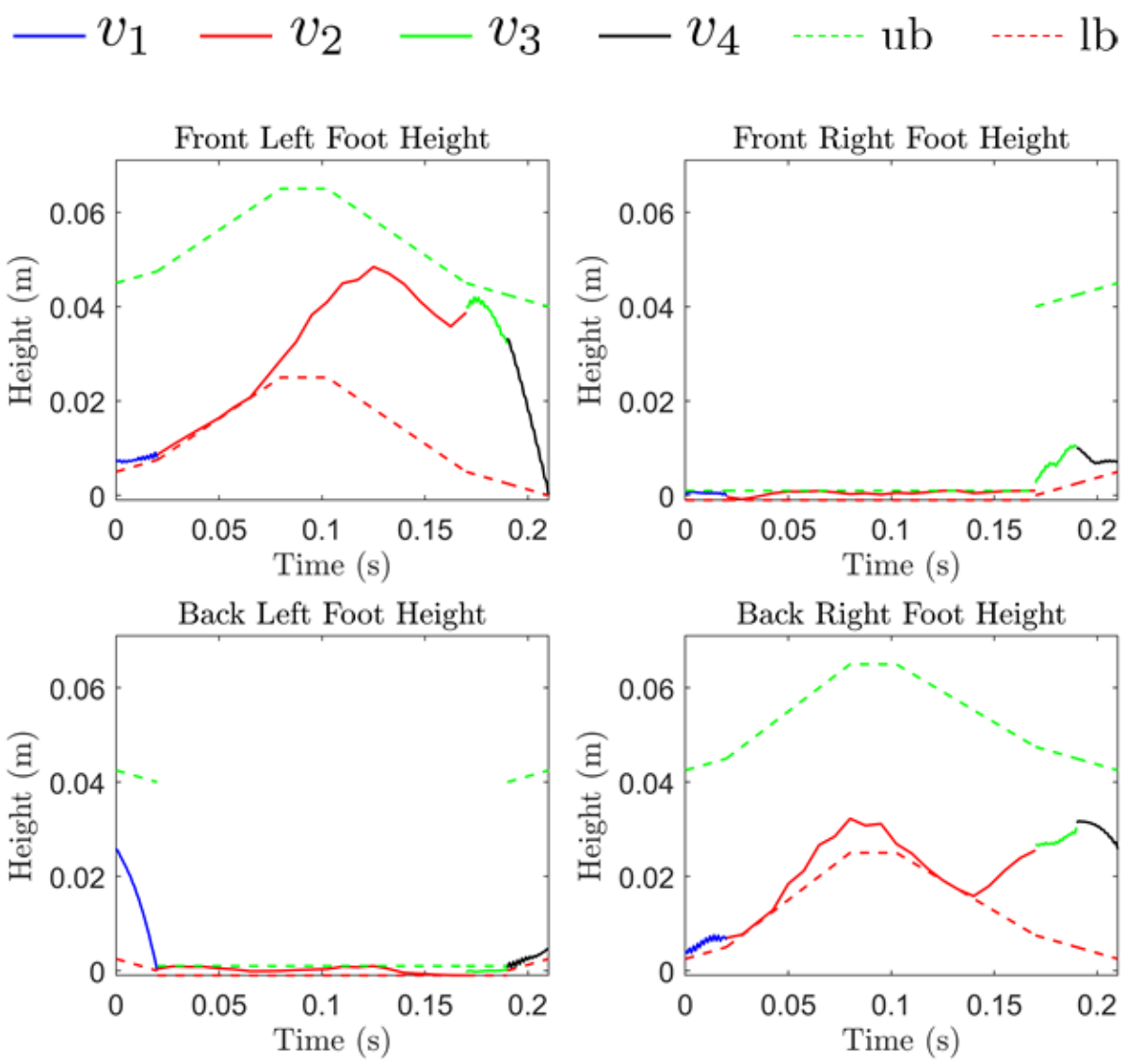

Figure 5.20: Foot height during the trotting gait.

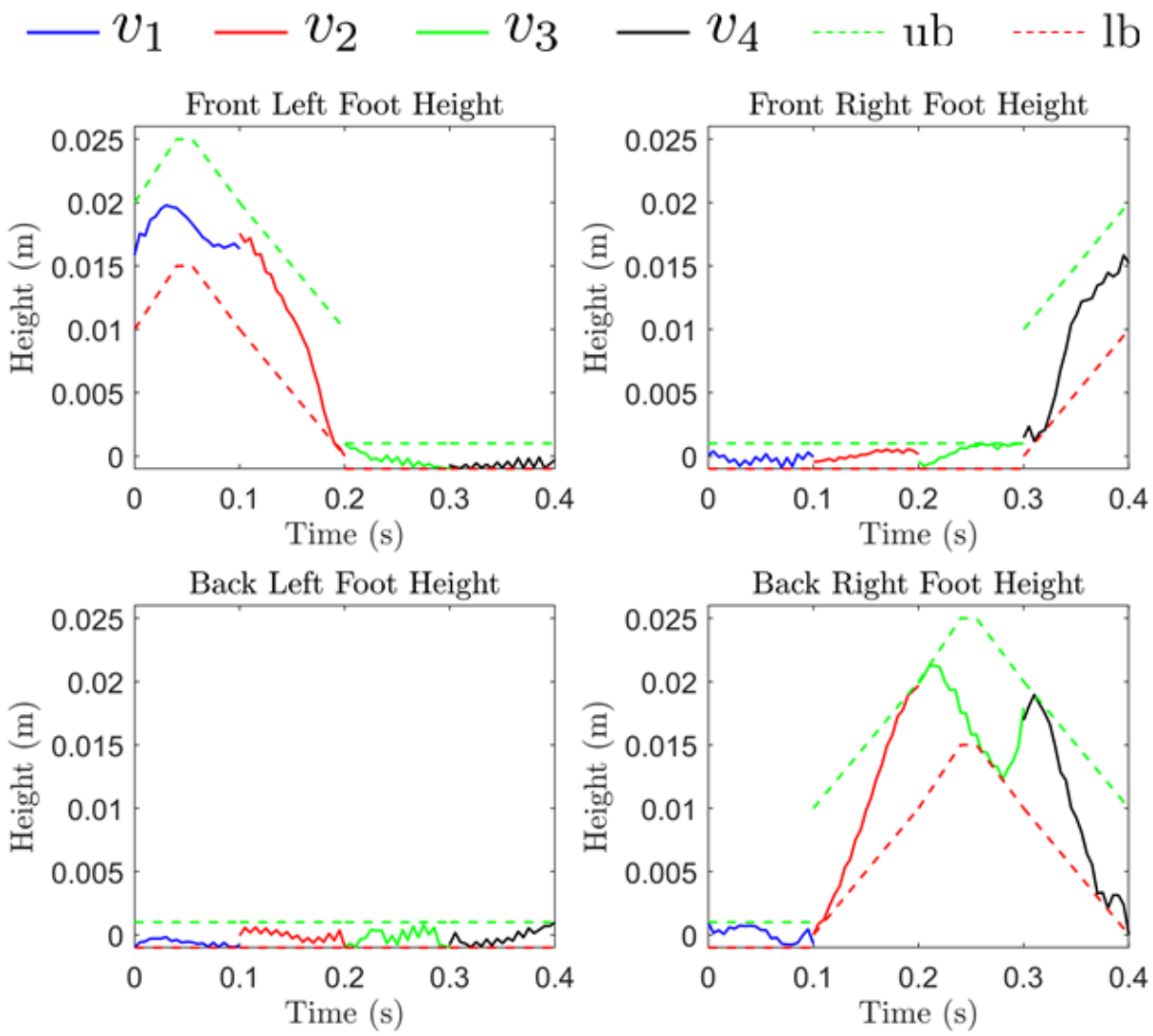

Figure 5.21: Foot height during the walking gait.

Chapter 6

Closed-Loop Simulations

6.1 Background

The objective of this chapter is to numerically verify the effectiveness of the proposed time-varying HZD controllers to achieve exponentially stable and dynamic gaits. The chapter provides the results of the MATLAB closed-loop simulation of the full-order model of Minitaur for the bounding, trotting, and walking gaits. The robot model and feedback controllers are implemented with ODE solvers to simulate the continuous-time dynamics, with proper event functions designed to account for the discrete-time dynamics. Since the optimization process of FROST approximates the state solution, small deviations from the predicted optimized trajectory are expected. With this simulation methodology, adjustments were made to the tuning parameters of each controller until exponential stability was achieved. The simulations data visualized within this chapter represent trials initialized from a point off the gait's optimized limit cycle to observe the asymptotic stability. The Poincaré sections analysis described in Chapter 4 confirms the stability of each gait, and the optimal tuned parameters that stabilized the gait trajectories are provided as well. Phase portraits of the different gaits are presented to demonstrate asymptotic convergence to limit cycles. Additional plots are provided to fully describe the stability and feasibility of the resulting gaits. Snapshots of the simulated gaits are illustrated in Figs. 6.1-6.3.

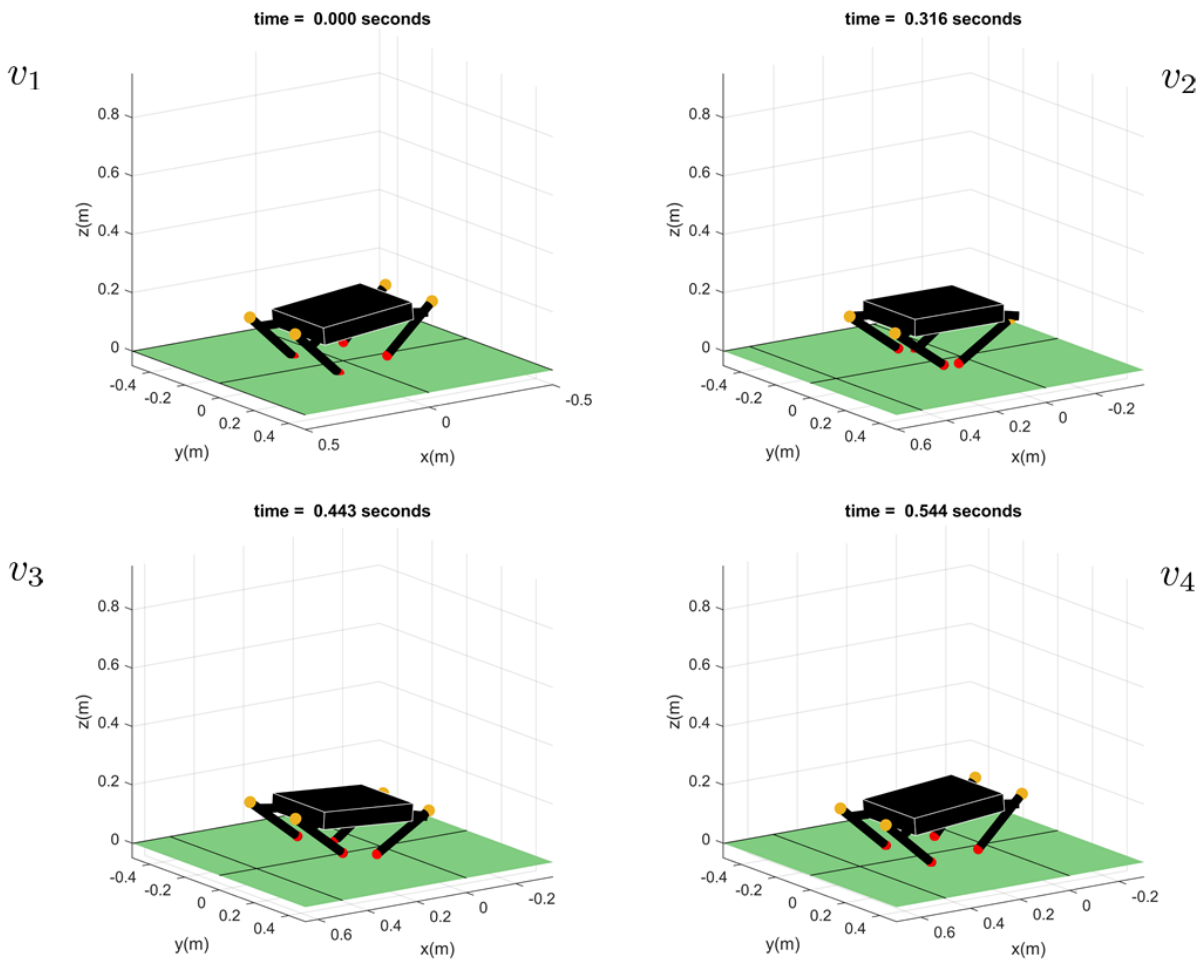

Figure 6.1: Snapshots of the first four domains of the simulated bounding gait.

6.2 Tuning Parameters and Eigenvalues

Using the Poincaré sections criteria of (4.17), the output matrices of (3.11), (3.12), and (3.13) were tuned to produce exponentially stable locomotion orbits. For each gait, it was determined that tuning was necessary to provide exponential stability. In the case of $\alpha_v = \beta_v = 0$, each gait was unable to complete even a full cycle. The instabilities are confirmed by observing the largest eigenvalues of the Jacobian of the Poincaré return maps for the gait trajectories subject to the untuned virtual constraints. The dominant eigenvalues for this case are 15.015, 3.6349, and 58.2245 for bounding, trotting, and walking respectively, which are all outside the unit circle and therefore predict the instability of the corresponding periodic orbits. In order to achieve properly tuned virtual constraints, adjustments to the parameters were made to increase the number of gait cycles the robot could complete before a fail state occurred, such as an impact foot crossing the switching surface during the incorrect

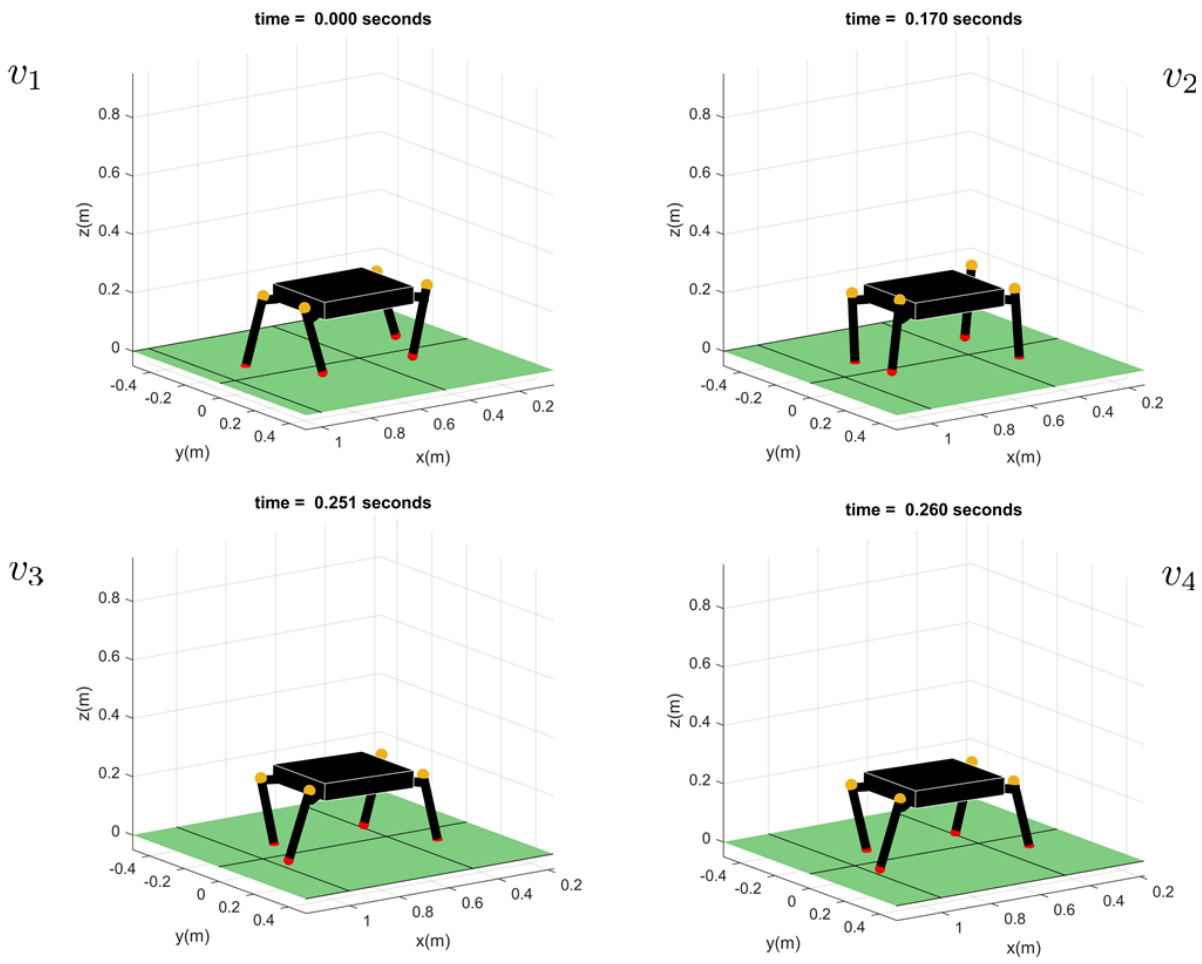

Figure 6.2: Snapshots of the first four domains of the simulated trotting gait. Note that v_3, and v_4 are two short domains in sequence and are therefore visually similar.

domain. This strategy emphasized driving the position of the incoming contact foot toward or away from the switching surface based on whether an early or late impact was predicted by the divergence of the absolute pitch and roll from the periodic orbit. Once the robot could maintain its gait trajectory from an ideal initial condition indefinitely, adjustments to the tuning parameters were then guided by lowering the magnitudes of the eigenvalues of the Jacobian of the Poincaré return map for the respective gait. Here, one can also make use of the iterative optimization algorithm that was developed in [83, 135] based on linear and bilinear matrix inequalities (LMIs and BMIs) to search for stabilizing parameters. Table 6.1 displays the values of the tuned parameters α_v and β_v for each gait.

Table 6.2 shows the three largest eigenvalues of the Jacobian of the Poincaré return map after virtual constraint tuning. As expected, the largest eigenvalue for each gait is 1, corresponding to the non-cyclical evolution of the x body coordinate. All other values are within the

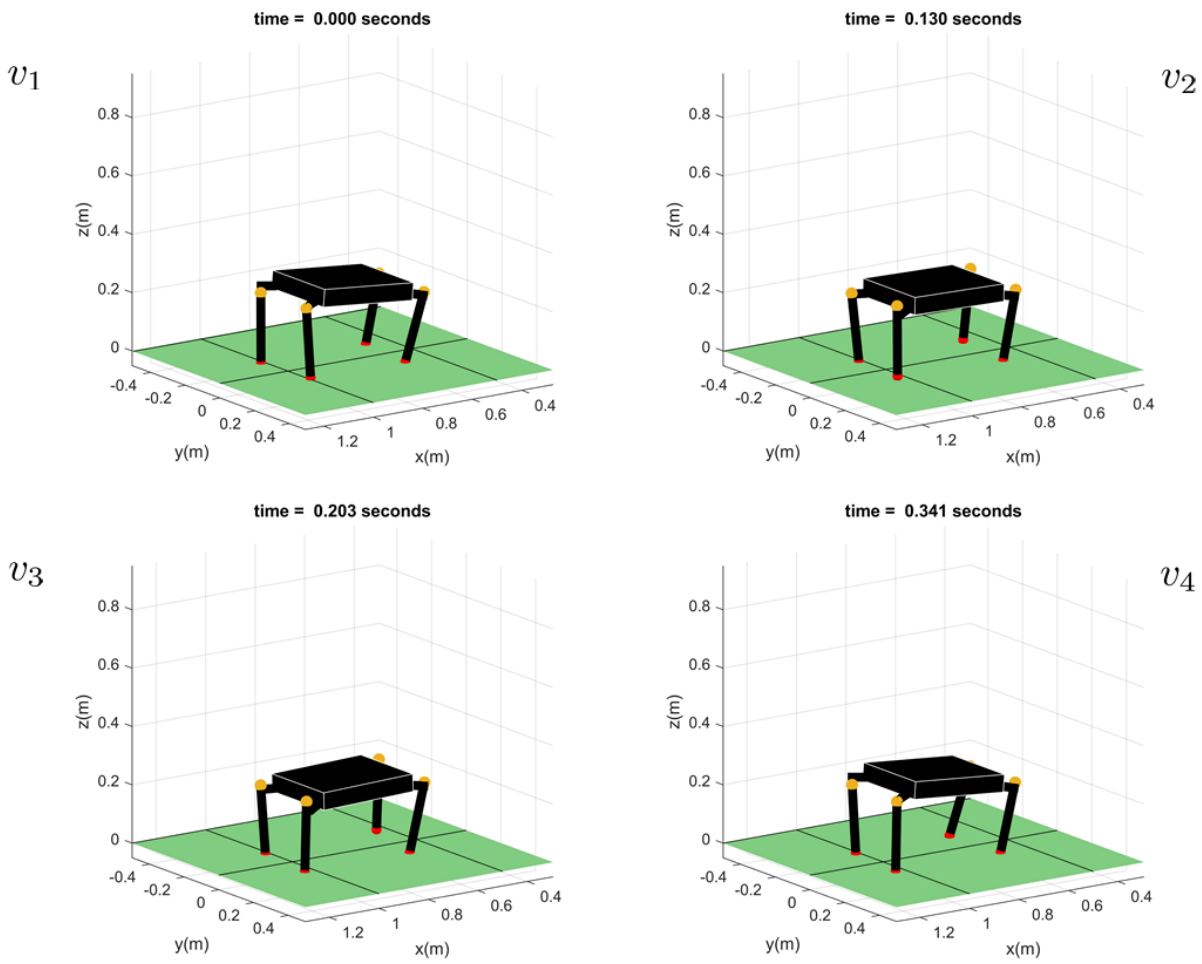

Figure 6.3: Snapshots of the first four domains of the simulated walking gait.

complex unit circle, validating the exponential stability of the virtually constrained dynamics. Here, we make use of a finite-difference approach similar to [83, 55, 120] to numerically compute the Jacobian matrix of the Poincaré return map. It is worth noting that lower eigenvalue magnitudes do not necessarily correspond to an increased domain of attraction. The resulting gait trajectories have average velocities of 0.3692 (m/s), 0.6014 (m/s), and 0.2045 (m/s) for the bounding, trotting, and walking gaits respectively.

6.3 Numerical Simulations of the Full-Order Models

The phase portraits in Figs. 6.4-6.9 give a visual representation of the exponential stability verified by the eigenvalues of Table 6.2. For these simulations, the initial condition of the state vector is perturbed off of the optimized limit cycle. As the simulation evolves, the

Table 6.1: Gait parameters α_v and β_v tuned to produce exponentially stable constrained gait trajectories.

Gait	Bound	Trot	Walk
α_1	0.8072	0.385	1.554
α_2	2.7925	0.288	1.280
α_3	-0.9384	0.172	-0.149
α_4	1.1633	0.0368	4.230
β_1	-0.1027	0.0665	1.692
β_2	-1.8087	0.483	1.358
β_3	-0.0005	-0.283	-0.958
β_4	0.7405	0.334	-2.426

Table 6.2: Dominant eigenvalues of the Jacobians of the Poincaré return maps for each gait. The largest value corresponds to the non-cyclical horizontal x position of the body frame, while all other eigenvalues are within the complex unit circle.

Gait	Bound	Trot	Walk
Eigenvalue 1	1.0000	1.0000	1.0000
Eigenvalue 2	$-0.0509 \pm 0.6145i$	0.6670	0.5095
Eigenvalue 3	-0.0621	$-0.4305 \pm 0.3041i$	0.3369

HZD controller drives the state trajectory to the limit cycle. Discontinuities in the phase portraits correspond to the discrete dynamics of impact phases. A sampling of body roll and pitch along with the parameters of leg 0 demonstrate the convergence in both absolute and internal DOFs. For Fig. 6.4, only the body pitch is displayed as the roll is held at zero by a holonomic constraint.

From visual analysis, it appears that the internal DOFs converge close to the limit cycle in fewer gait cycles than the absolute DOFs, which have a more gradual approach. This aligns with the output design philosophy, as the absolute DOFs are unactuated and can only be controlled indirectly. In particular, they are only factored into the outputs during select domains in combination with actuated internal terms in the corresponding output. As it is a very dynamic gait, the bounding gait is most sensitive to perturbation from its periodic orbit and thus has a notably smaller domain of attraction than the trotting and walking gaits.

Another means to visualize the effectiveness of the controller is to observe the evolution of the outputs defined by (3.11)-(3.13). As Figs. 6.10-6.12 demonstrate, the outputs asymptotically converge to zero over the course of each domain. Discontinuities in the output trajectories

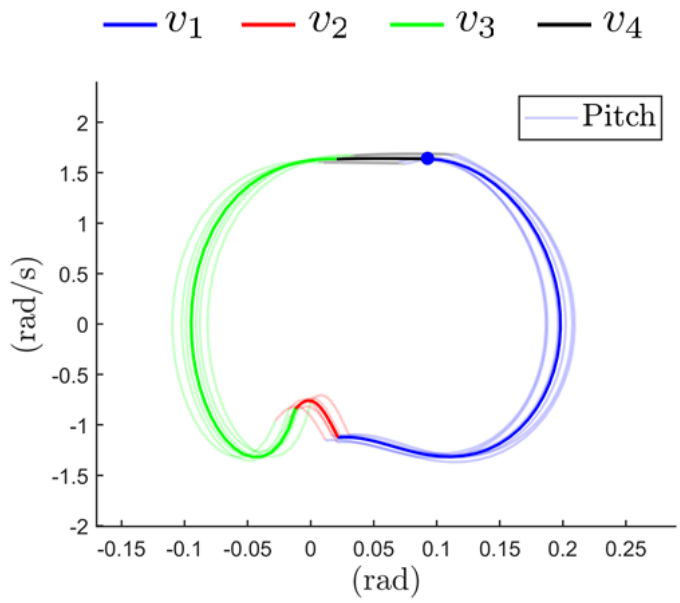

Figure 6.4: Phase portrait for the absolute pitch motion of the bounding gait starting from a perturbed initial condition. Convergence to the limit cycle is clear.

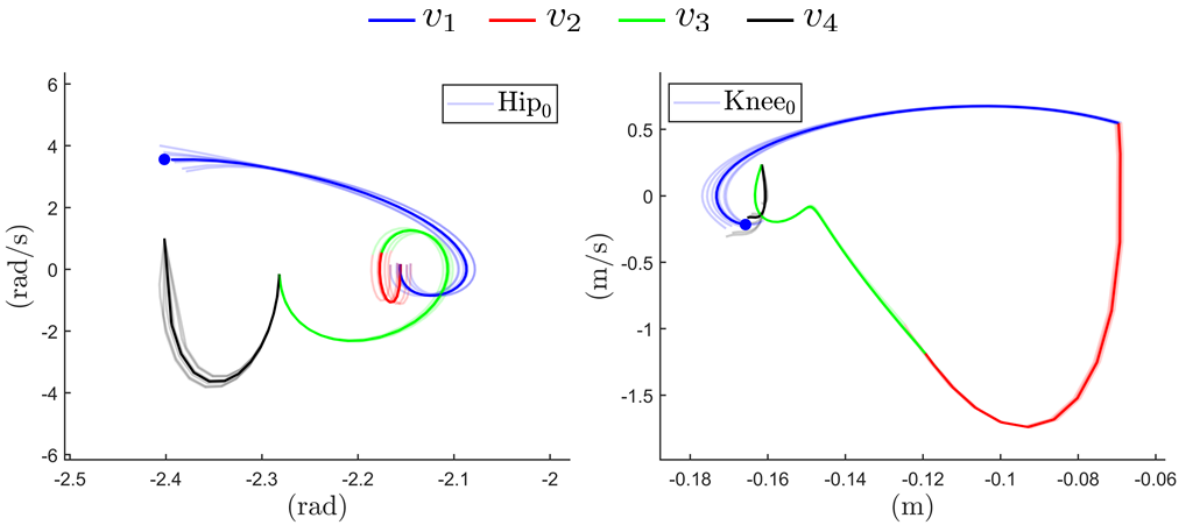

Figure 6.5: Phase portraits for the internal Hip_0 and Knee_0 DOFs of the bounding gait starting from a perturbed initial condition.

reflect the discrete change of the set of measured outputs between domains. Observation of the figures shows that at each domain transition there are coordinates which drift from the optimized trajectory during domains which do not explicitly control for them, but most terms are quickly driven to the orbit during the domains they are controlled for. Certain terms may take more than one domain to converge, and others may have low impact on the

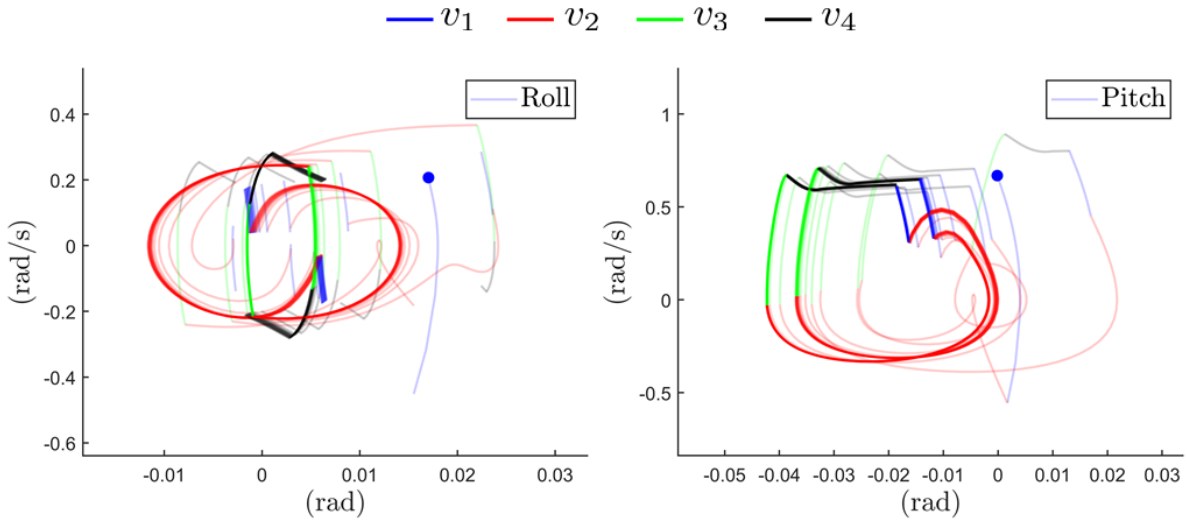

Figure 6.6: Phase portraits for the absolute roll and pitch motions of the trotting gait starting from a perturbed initial condition. Convergence to the limit cycle is clear.

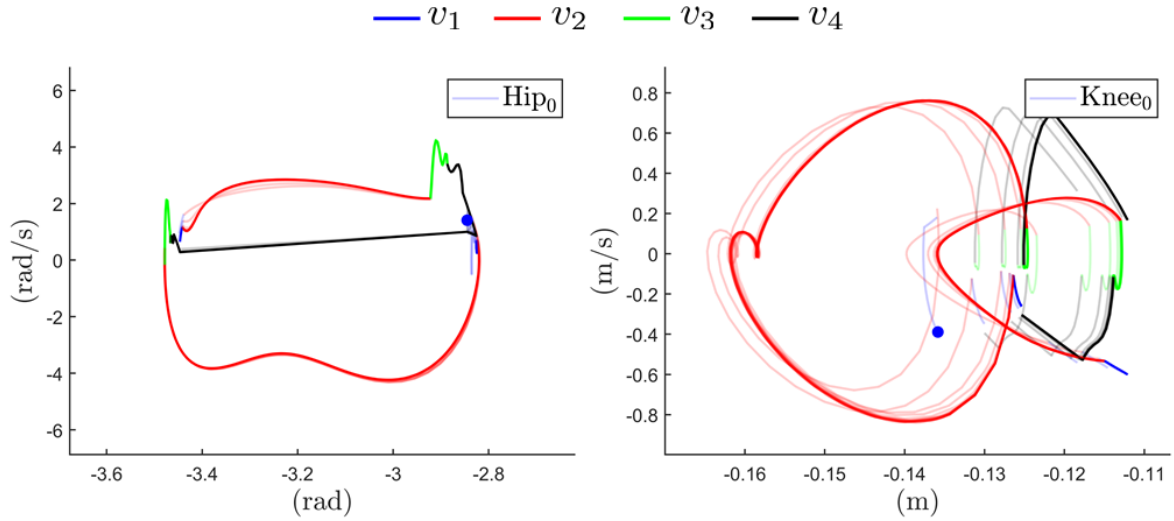

Figure 6.7: Phase portraits for the internal Hip_0 and Knee_0 DOFs of the trotting gait starting from a perturbed initial condition.

overall trajectory of the system, particularly during the short flight phases of the bounding and trotting gaits.

Figures 6.13-6.15 finally show the action of the simulated motors during the converging gaits. The ideal gait optimization does not provide any guarantees of torque feasibility when the state trajectory is off the optimized limit cycle. Therefore, the optimization bounds are implemented as saturation bounds during simulation. In particular, 20 Nm is designated as the saturation limits, but the design process targeted torque profiles which remained below a

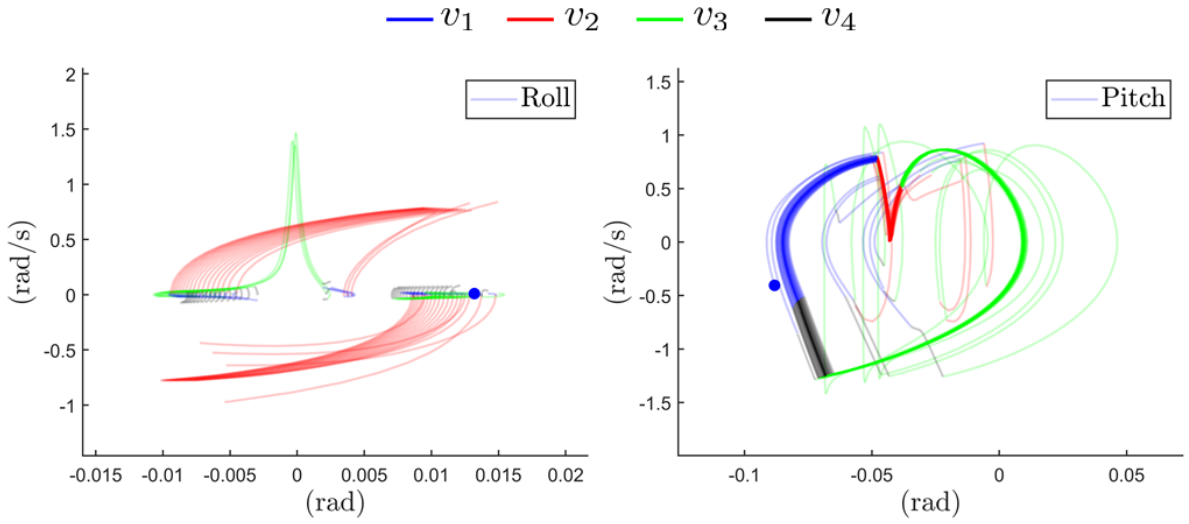

Figure 6.8: Phase portraits for the absolute roll and pitch motions of the walking gait starting from a perturbed initial condition. Convergence to the limit cycle is clear.

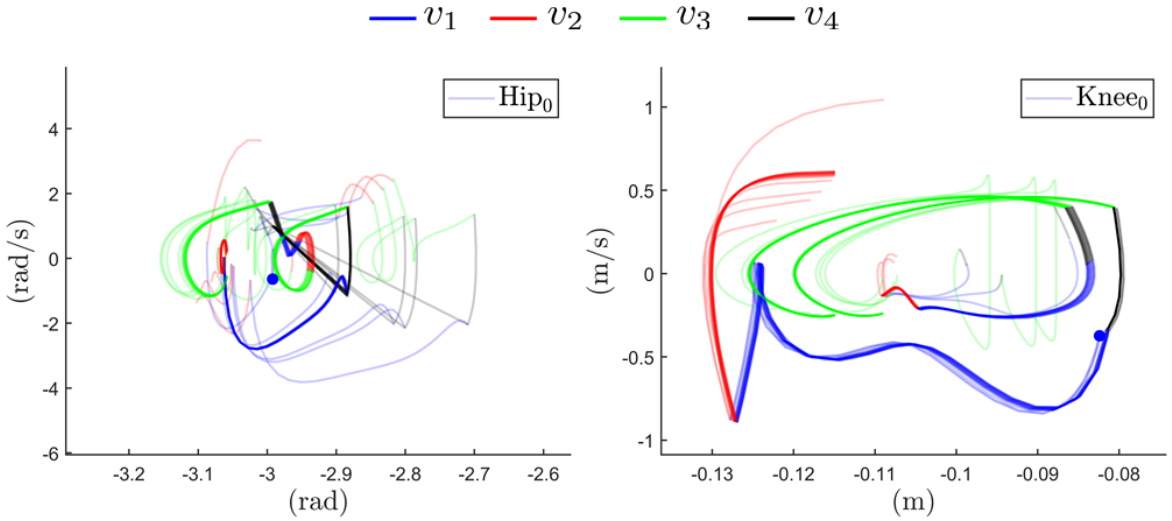

Figure 6.9: Phase portraits for the internal Hip_0 and Knee_0 DOFs of the walking gait starting from a perturbed initial condition.

magnitude of 15 Nm over the majority of the gait. Each of the displayed gaits clearly meets this criteria. With stability and feasibility criteria validated, the controllers developed for the bounding, trotting, and walking gaits are determined to be successful.

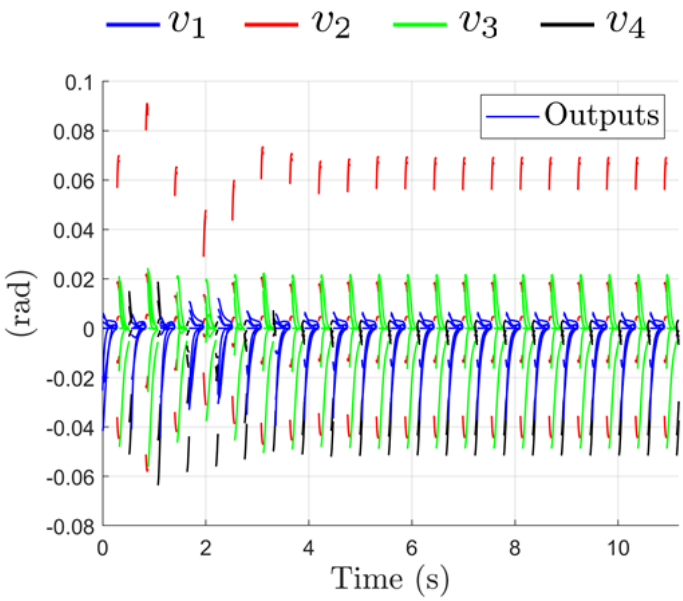

Figure 6.10: Time profile of the virtual constraints for the bounding gait starting from a perturbed initial condition.

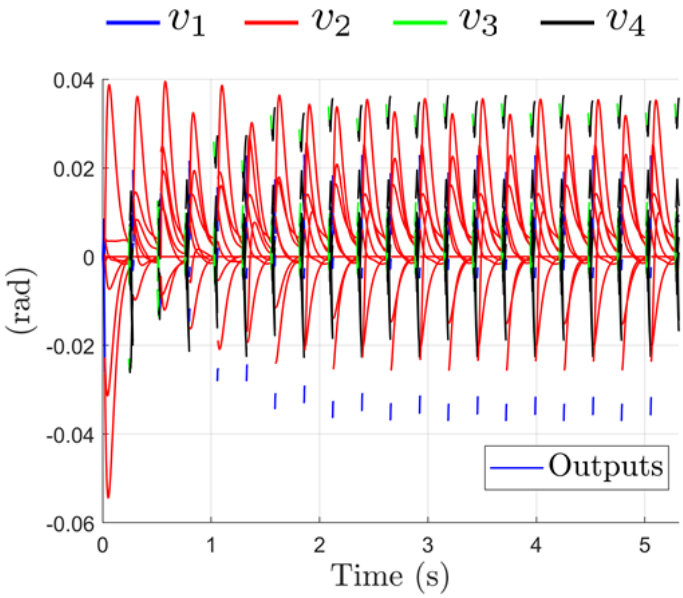

Figure 6.11: Time profile of the virtual constraints for the trotting gait starting from a perturbed initial condition.

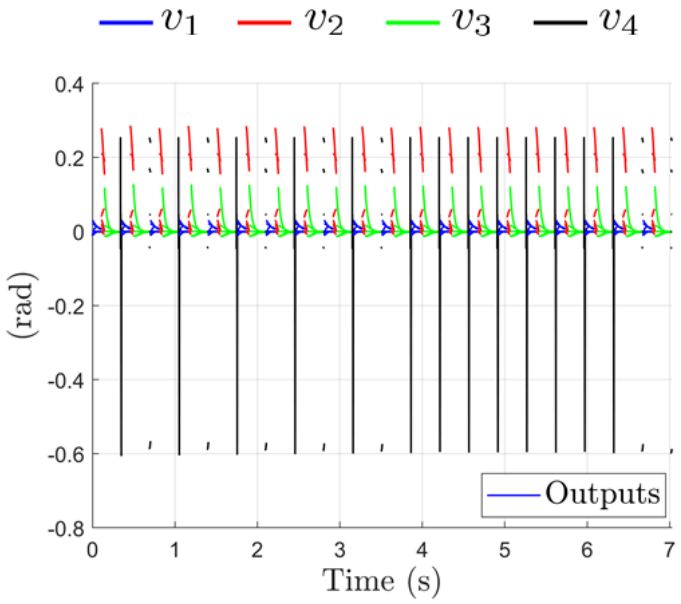

Figure 6.12: Time profile of the virtual constraints for the walking gait starting from a perturbed initial condition.

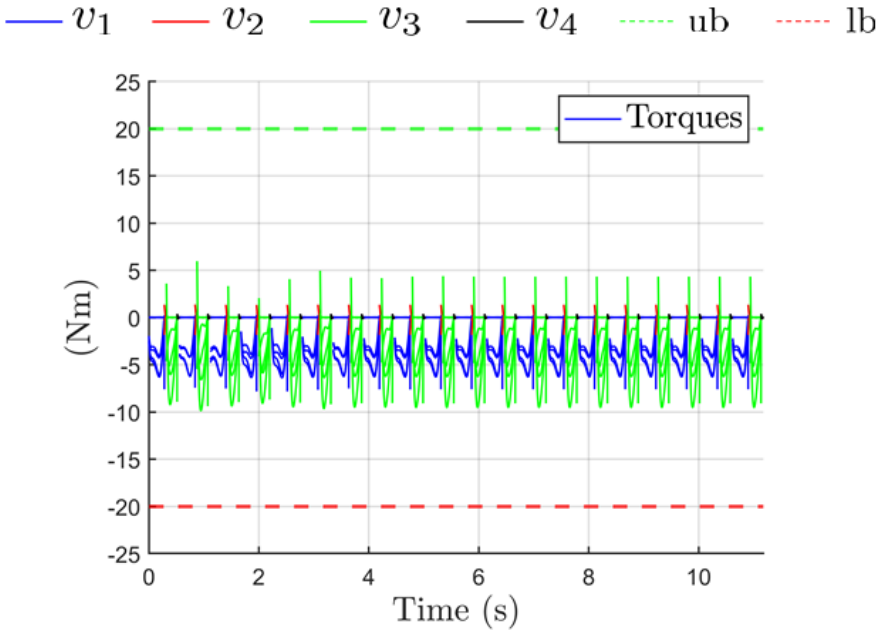

Figure 6.13: Time profile of the torque inputs over 20 consecutive cycles of the bounding gait.

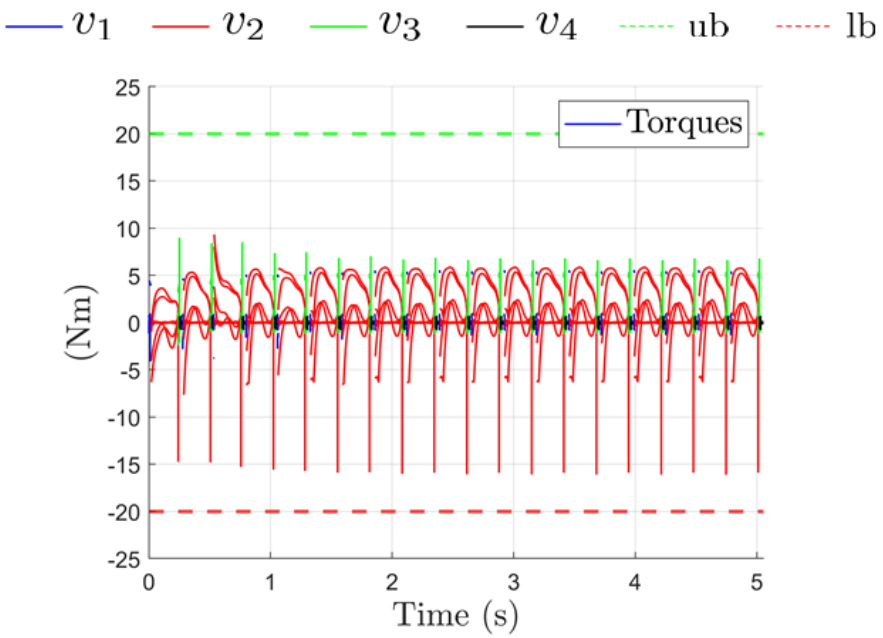

Figure 6.14: Time profile of the torque inputs over 10 consecutive cycles of the trotting gait.

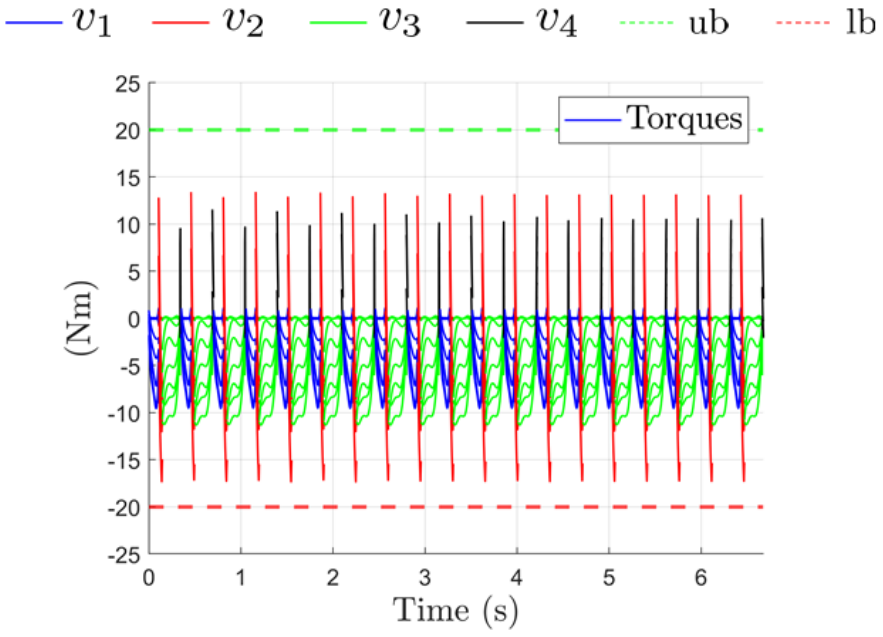

Figure 6.15: Time profile of the torque inputs over 10 consecutive cycles of the walking gait.

Chapter 7

Conclusion

While there have been great advancements in the relatively burgeoning field of robotic quadrupeds, there are still challenges to overcome when extending controller design philosophies of bipedal locomotion to the high-DOF systems of quadrupedal locomotion. A significant contribution to the field of hybrid zero dynamics is a formalized addition of a series of single-level and time-varying controllers that can exponentially stabilize dynamic gaits without a need for higher-level event-based controllers. When implemented, such controllers are able to address full-order models of high-DOF quadrupeds with added benefits of producing gaits which can start from rest and do not have to rely on sensor data to estimate gait phasing variables. The general efficacy of this design strategy is exemplified by the exponentially stable bounding, trotting, and walking gaits achieved for the simulated model of the robot Minitaur.

Stable quadrupedal locomotion patterns were achieved on a full-order model of Minitaur using a series of single-level, time-varying HZD controllers. After a formal methodology was presented for designing effective time-varying HZD controllers, the stability of each gait was verified using an extension of the Poincaré sections analysis to time-varying systems and through simulation trials. The end result is a set of time-varying virtual constraint controllers which successfully stabilize dynamic quadrupedal locomotion.

7.1 Summary of Contributions

Extension of the Poincaré sections analysis to exponentially stabilize dynamic gaits via time-varying nonlinear controllers

The Poincaré sections analysis was extended to general periodic and time-varying systems in order for the powerful mathematical tool to be utilized in verifying the stability of the time-varying HZD gait controllers. The Poincaré sections analysis is perfectly suited for

addressing the inherently periodic nature of hybrid locomotion, and an extension to time-varying systems serves to improve the versatility of the tool even further. The mathematical proof provides necessary and sufficient conditions to show that the criteria for exponential stability is identical for systems under time-varying and time-invariant systems: the eigenvalues of the Jacobian linearization of the Poincaré return map of the state trajectory must be within the complex unit circle. With this understanding, the exponential stability of any time-varying controller acting on a periodic gait can be explicitly verified.

Time-varying virtual constraint design for full-order quadrupedal gaits

This thesis presents a formal mythology for properly developing, selecting, and tuning virtual constraints for time-varying HZD controllers. The direct collocation software FROST is utilized to generate a desired trajectory orbit for the controller. This optimized trajectory must meet feasibility requirements including continuity of dynamics and the limits on external ground reaction forces and actuator torques. Proper selection of controlled variables which account for the dimension of the zero dynamics manifold provides a solid baseline structure for the desired controller which can then be tuned by a selection of variable parameters, which aids in reducing the scale of the design problem. Virtual constraint design is guided by intuition, in particular by guiding the trajectories of incoming impact feet to account for drift in the pitch and roll of the model's body frame.

Numerical verification of the analytical results using full-order simulations

Full-order simulations of the Minitaur model subject to the virtual constraint controllers designed for each gait show the stability and feasibility of the resulting gait trajectories, even when perturbed from the optimized limit cycle. The time-varying Poincaré sections analysis confirms the exponential stability of the gaits for the hybrid models of locomotion by demonstrating that the eigenvalues of the Jacobian of the Poincaré return map are all within the unit circle. Phase portraits visually confirm convergence to the limit cycles, while outputs and closed-loop torque profiles further confirm the stability and feasibility of the gaits. These simulations of Minitaur are the first to successfully implement and validate single-level time-varying HZD controllers on full-order models of quadrupedal locomotion.

7.2 Future extensions of research

Robustness analysis

The simulations conducted for this thesis focus primarily on validating the mathematics and design strategies used in developing time-varying HZD controllers. Further analysis can be performed to analyze the robustness of the controller design. Such robustness simulations would include factors such as simulating response to noisy sensor input, and evaluating the controllers' efficacy with regards to parametric and nonparametric uncertainties in the model as well as the ground profile.

Extensions to other hybrid models of locomotion

The sampling of gaits on a single platform provided in this thesis lays the groundwork for extending this controller design practice to other hybrid models of locomotion and other robotic platforms. The advantages of this controller methodology provide particular benefit to agile gaits which cannot easily define a strictly monotonic combination of states for the gait phasing parameter and which may have significant noise factors contributing to sensor input, such as aggravations from strong impacts or high velocity maneuvers. Such agile gaits may include ambling and galloping, but need not be strictly limited to quadrupedal locomotion. There is also benefit when applying this controller design to less dynamic gaits which may have an initial condition of being at rest within their domain of attraction. Aside from these particular advantages, the versatility of time-varying HZD control is such that it can be applied to a wide variety of legged locomotion structures and integrated with the same multi-level control approaches as any previously developed time-invariant controller.

Physical experiments

For future work, we will experimentally evaluate the effectiveness of the proposed time-varying HZD controllers on the Minitaur platform. Computational considerations must be taken into account in addition to the modeling and feasibility considerations described within this work. In particular, an appropriate method for approximating the Lie derivative terms must be developed to accommodate the limitations of Minitaur's on-board processor. Additional considerations must also be made for the means by which Minitaur detects impacts, as the legs are too small and light to have dedicated impact sensors and must rely on the detection of discrete changes in the measured velocities of the on-board IMU and actuated terms.

Bibliography

[1] BostonDynamics, https://www.bostondynamics.com/.

[2] MIT News: Cheetah 3, http://news.mit.edu/2018/blind-cheetah-robot-climb-stairs-obstacles-disaster-zones-0705.

[3] IEEE Spectrum, https://spectrum.ieee.org/automaton/robotics/humanoids/durus-brings-humanlike-gait-and-fancy-shoes-to-hyperefficient-robots.

[4] ATRIAS, https://mime.oregonstate.edu/research/drl/atrias/.

[5] Ghost Robotics, https://www.ghostrobotics.io/.

[6] MIT News: Mini Cheetah, http://news.mit.edu/2019/mit-mini-cheetah-first-four-legged-robot-to-backflip-0304.

[7] Dynamic Legged Systems, https://dls.iit.it/robots1/hyqreal.

[8] Terrestrial Robotics Engineering and Controls (TREC) Lab, http://www.me.vt.edu/research/laboratories/trec/.

[9] Agility Robotics, http://www.agilityrobotics.com/.

[10] ANYmal ETH Zurich, https://www.anybotics.com/anymal-legged-robot/.

[11] M. Raibert, K. Blankespoor, G. Nelson, and R. Playter, "Bigdog, the rough-terrain quadruped robot," *IFAC Proceedings Volumes*, vol. 41, no. 2, pp. 10 822 – 10 825, 2008, 17th IFAC World Congress. [Online]. Available: http://www.sciencedirect.com/science/article/pii/S1474667016407020

[12] M. H. Raibert, *Legged Robots That Balance*. The MIT Press, 1986.

[13] V. A. Tucker, "The energetic cost of moving about: Walking and running are extremely inefficient forms of locomotion. much greater efficiency is achieved by birds, fish—and bicyclists," *American Scientist*, vol. 63, no. 4, pp. 413–419, 1975. [Online]. Available: http://www.jstor.org/stable/27845576

[14] H.-W. Park, P. M. Wensing, and S. Kim, "High-speed bounding with the MIT Cheetah 2: Control design and experiments," *The International Journal of Robotics Research*, vol. 36, no. 2, pp. 167–192, 2017. [Online]. Available: https://doi.org/10.1177/0278364917694244

[15] Dynamic Legged Systems, https://www.iit.it/research/lines/dynamic-legged-systems.

[16] M. Vukobratović, B. Borovac, and D. Surla, *Dynamics of Biped Locomotion.* Springer, 1990.

[17] M. Vulobratocić and B. Borovac, "Zero-moment point — thirty five years of its life," *International Journal of Humanoid Robotics*, vol. 01, no. 01, pp. 157–173, 2004. [Online]. Available: http://www.worldscientific.com/doi/abs/10.1142/S0219843604000083

[18] B. Ugurlu and A. Kawamura, "ZMP-based online jumping pattern generation for a one-legged robot," *Industrial Electronics, IEEE Transactions on*, vol. 57, no. 5, pp. 1701–1709, May 2010.

[19] K. Hirai, M. Hirose, Y. Haikawa, and T. Takenaka, "The development of Honda humanoid robot," in *Robotics and Automation. Proceedings IEEE International Conference on*, vol. 2, May 1998, pp. 1321–1326 vol.2.

[20] H.-O. Lim, Y. Yamamoto, and A. Takanishi, "Control to realize human-like walking of a biped humanoid robot," in *Systems, Man, and Cybernetics, IEEE International Conference on*, vol. 5, 2000, pp. 3271–3276 vol.5.

[21] J. Yamaguchi, E. Soga, S. Inoue, and A. Takanishi, "Development of a bipedal humanoid robot-control method of whole body cooperative dynamic biped walking," in *Robotics and Automation. Proceedings IEEE International Conference on*, vol. 1, 1999, pp. 368–374 vol.1.

[22] J. Park and K. Kim, "Biped robot walking using gravity-compensated inverted pendulum mode and computed torque control," in *Robotics and Automation. Proceedings IEEE International Conference on*, vol. 4, May 1998, pp. 3528–3533 vol.4.

[23] K. Erbatur and O. Kurt, "Natural ZMP trajectories for biped robot reference generation," *Industrial Electronics, IEEE Transactions on*, vol. 56, no. 3, pp. 835–845, March 2009.

[24] B.-J. Lee, D. Stonier, Y.-D. Kim, J.-K. Yoo, and J.-H. Kim, "Modifiable walking pattern of a humanoid robot by using allowable ZMP variation," *Robotics, IEEE Transactions on*, vol. 24, no. 4, pp. 917–925, Aug 2008.

[25] N. Motoi, M. Ikebe, and K. Ohnishi, "Real-time gait planning for pushing motion of humanoid robot," *Industrial Informatics, IEEE Transactions on*, vol. 3, no. 2, pp. 154–163, May 2007.

[26] S. Kajita, T. Nagasaki, K. Kaneko, and H. Hirukawa, "ZMP-based biped running control," *Robotics Automation Magazine, IEEE*, vol. 14, no. 2, pp. 63–72, June 2007.

[27] T. Sato, S. Sakaino, E. Ohashi, and K. Ohnishi, "Walking trajectory planning on stairs using virtual slope for biped robots," *Industrial Electronics, IEEE Transactions on*, vol. 58, no. 4, pp. 1385–1396, April 2011.

[28] P. Sardain and G. Bessonnet, "Forces acting on a biped robot. center of pressure-zero moment point," *Systems, Man and Cybernetics, Part A: Systems and Humans, IEEE Transactions on*, vol. 34, no. 5, pp. 630–637, Sept 2004.

[29] K. Loffler, M. Gienger, F. Pfeiffer, and H. Ulbrich, "Sensors and control concept of a biped robot," *Industrial Electronics, IEEE Transactions on*, vol. 51, no. 5, pp. 972–980, Oct 2004.

[30] E. Kim, T. Kim, and J.-W. Kim, "Three-dimensional modelling of a humanoid in three planes and a motion scheme of biped turning in standing," *Control Theory Applications, IET*, vol. 3, no. 9, pp. 1155–1166, September 2009.

[31] H. Dai and R. Tedrake, "Planning robust walking motion on uneven terrain via convex optimization," in *2016 IEEE-RAS 16th International Conference on Humanoid Robots (Humanoids)*, Nov 2016, pp. 579–586.

[32] T. Akbas, S. Eskimez, S. Ozel, O. Adak, K. Fidan, and K. Erbatur, "Zero moment point based pace reference generation for quadruped robots via preview control," *International Workshop on Advanced Motion Control, AMC*, 03 2012.

[33] A. Goswami, "Postural stability of biped robots and the foot-rotation indicator (FRI) point," *The International Journal of Robotics Research*, vol. 18, no. 6, pp. 523–533, 1999.

[34] R. J. Full and D. E. Koditschek, "Templates and anchors: Neuromechanical hypotheses of legged locomotion on land," *Journal of Experimental Biology*, vol. 202, pp. 3325–3332, December 1999.

[35] C. R. Lee and C. T. Farley, "Determinants of the center of mass trajectory in human walking and running." *Journal of Experimental Biology*, vol. 201, no. 21, pp. 2935–2944, 1998. [Online]. Available: https://jeb.biologists.org/content/201/21/2935

[36] M. DeDonato, V. Dimitrov, R. Du, R. Giovacchini, K. Knoedler, X. Long, F. Polido, M. A. Gennert, T. Padır, S. Feng, H. Moriguchi, E. Whitman, X. Xinjilefu, and C. G. Atkeson, "Human-in-the-loop control of a humanoid robot for disaster response: A report from the DARPA robotics challenge trials," *Journal of Field Robotics*, vol. 32, no. 2, pp. 275–292. [Online]. Available: https://onlinelibrary.wiley.com/doi/abs/10.1002/rob.21567

[37] S. Kuindersma, R. Deits, M. Fallon, A. Valenzuela, H. Dai, F. Permenter, T. Koolen, P. Marion, and R. Tedrake, "Optimization-based locomotion planning, estimation, and control design for the Atlas humanoid robot," *Autonomous Robots*, vol. 40, no. 3, pp. 429–455, Mar 2016. [Online]. Available: https://doi.org/10.1007/s10514-015-9479-3

[38] M. Johnson, B. Shrewsbury, S. Bertrand, T. Wu, D. Duran, M. Floyd, P. Abeles, D. Stephen, N. Mertins, A. Lesman, J. Carff, W. Rifenburgh, P. Kaveti, W. Straatman, J. Smith, M. Griffioen, B. Layton, T. Boer, T. Koolen, P. Neuhaus, and J. Pratt, "Team IHMC's lessons learned from the DARPA robotics challenge trials," *Journal of Field Robotics*, vol. 32, no. 2, pp. 192–208. [Online]. Available: https://onlinelibrary.wiley.com/doi/abs/10.1002/rob.21571

[39] U. Saranli, W. J. Schwind, and D. E. Koditschek, "Toward the control of a multi-jointed, monoped runner," in *Proceedings. 1998 IEEE International Conference on Robotics and Automation (Cat. No.98CH36146)*, vol. 3, 1998, pp. 2676–2682 vol.3.

[40] I. Poulakakis and J. Grizzle, "The spring loaded inverted pendulum as the hybrid zero dynamics of an asymmetric hopper," *Automatic Control, IEEE Transactions on*, vol. 54, no. 8, pp. 1779–1793, Aug 2009.

[41] X. Xiong and A. D. Ames, "Bipedal hopping: Reduced-order model embedding via optimization-based control," in *IEEE/RSJ International Conference on Intelligent Robots and Systems (IROS), arXiv preprint arXiv:1807.08037*, Accepted to Appear, 2018.

[42] J. Di Carlo, P. M. Wensing, B. Katz, G. Bledt, and S. Kim, "Dynamic locomotion in the MIT Cheetah 3 through convex model-predictive control," in *2018 IEEE/RSJ International Conference on Intelligent Robots and Systems (IROS)*, Oct 2018, pp. 1–9.

[43] Y. Ding, A. Pandala, and H. Park, "Real-time model predictive control for versatile dynamic motions in quadrupedal robots," in *2019 International Conference on Robotics and Automation (ICRA)*, May 2019, pp. 8484–8490.

[44] Q. Cao and I. Poulakakis, "Quadrupedal running with a flexible torso: control and speed transitions with sums-of-squares verification," *Artificial Life and Robotics*, vol. 21, no. 4, pp. 384–392, Dec 2016.

[45] O. Villarreal, V. Barasuol, P. Wensing, and C. Semini, "MPC-based controller with terrain insight for dynamic legged locomotion," *arXiv preprint arXiv:1909.13842*, 2019.

[46] G. Bledt, P. M. Wensing, and S. Kim, "Policy-regularized model predictive control to stabilize diverse quadrupedal gaits for the mit cheetah," in *2017 IEEE/RSJ International Conference on Intelligent Robots and Systems (IROS)*, Sep. 2017, pp. 4102–4109.

[47] M. Neunert, M. Stäuble, M. Giftthaler, C. D. Bellicoso, J. Carius, C. Gehring, M. Hutter, and J. Buchli, "Whole-body nonlinear model predictive control through contacts for quadrupeds," *IEEE Robotics and Automation Letters*, vol. 3, no. 3, pp. 1458–1465, July 2018.

[48] D. Lehmann, E. Henriksson, and K. H. Johansson, "Event-triggered model predictive control of discrete-time linear systems subject to disturbances," in *2013 European Control Conference (ECC)*, 2013, pp. 1156–1161.

[49] F. Borrelli, A. Bemporad, and M. M., *Predictive Control for Linear and Hybrid Systems*. Cambridge University Press, 2017.

[50] Y. Wang and S. Boyd, "Fast model predictive control using online optimization," *IEEE Transactions on Control Systems Technology*, vol. 18, no. 2, pp. 267–278, March 2010.

[51] K. Akbari Hamed, J. Kim, and A. Pandala, "Quadrupedal locomotion via event-based predictive control and qp-based virtual constraints," *IEEE Robotics and Automation Letters*, vol. 5, no. 3, pp. 4463–4470, 2020.

[52] S. Fahmi, C. Mastalli, M. Focchi, and C. Semini, "Passive whole-body control for quadruped robots: Experimental validation over challenging terrain," *IEEE Robotics and Automation Letters*, vol. 4, no. 3, pp. 2553–2560, July 2019.

[53] S. Kuindersma, F. Permenter, and R. Tedrake, "An efficiently solvable quadratic program for stabilizing dynamic locomotion," in *2014 IEEE International Conference on Robotics and Automation (ICRA)*, May 2014, pp. 2589–2594.

[54] J. Grizzle, G. Abba, and F. Plestan, "Asymptotically stable walking for biped robots: Analysis via systems with impulse effects," *IEEE Transactions on Automatic Control*, vol. 46, no. 1, pp. 51–64, Jan 2001.

[55] C. Chevallereau, J. Grizzle, and C.-L. Shih, "Asymptotically stable walking of a five-link underactuated 3-D bipedal robot," *Robotics, IEEE Transactions on*, vol. 25, no. 1, pp. 37–50, Feb 2009.

[56] A. Ames, K. Galloway, K. Sreenath, and J. Grizzle, "Rapidly exponentially stabilizing control Lyapunov functions and hybrid zero dynamics," *IEEE Transactions on Automatic Control*, vol. 59, no. 4, pp. 876–891, April 2014.

[57] M. Spong and F. Bullo, "Controlled symmetries and passive walking," *IEEE Transactions on Automatic Control*, vol. 50, no. 7, pp. 1025–1031, July 2005.

[58] M. Spong, J. Holm, and D. Lee, "Passivity-based control of bipedal locomotion," *Robotics Automation Magazine, IEEE*, vol. 14, no. 2, pp. 30–40, June 2007.

[59] I. Manchester, U. Mettin, F. Iida, and R. Tedrake, "Stable dynamic walking over uneven terrain," *The International Journal of Robotics Research*, vol. 30, no. 3, pp. 265–279, 2011.

[60] H. Dai and R. Tedrake, "$\mathcal{L}_2$-gain optimization for robust bipedal walking on unknown terrain," in *Robotics and Automation, IEEE International Conference on*, May 2013, pp. 3116–3123.

[61] G. Song and M. Zefran, "Underactuated dynamic three-dimensional bipedal walking," in *Robotics and Automation. Proceedings IEEE International Conference on*, May 2006, pp. 854–859.

[62] R. Gregg, A. Tilton, S. Candido, T. Bretl, and M. Spong, "Control and planning of 3-D dynamic walking with asymptotically stable gait primitives," *Robotics, IEEE Transactions on*, vol. 28, no. 6, pp. 1415–1423, Dec 2012.

[63] R. Gregg and L. Righetti, "Controlled reduction with unactuated cyclic variables: Application to 3D bipedal walking with passive yaw rotation," *Automatic Control, IEEE Transactions on*, vol. 58, no. 10, pp. 2679–2685, Oct 2013.

[64] K. Byl and R. Tedrake, "Approximate optimal control of the compass gait on rough terrain," in *Robotics and Automation. IEEE International Conference on*, May 2008, pp. 1258–1263.

[65] K. Akbari Hamed and R. D. Gregg, "Decentralized event-based controllers for robust stabilization of hybrid periodic orbits: Application to underactuated 3D bipedal walking," *IEEE Transactions on Automatic Control*, vol. 64, no. 6, pp. 2266–2281, June 2019.

[66] K. Akbari Hamed and J. Grizzle, "Event-based stabilization of periodic orbits for underactuated 3-D bipedal robots with left-right symmetry," *Robotics, IEEE Transactions on*, vol. 30, no. 2, pp. 365–381, April 2014.

[67] C. Chevallereau, G. Abba, Y. Aoustin, F. Plestan, E. Westervelt, C. Canudas-de Wit, and J. Grizzle, "RABBIT: A testbed for advanced control theory," *IEEE Control Systems Magazine*, vol. 23, no. 5, pp. 57–79, Oct 2003.

[68] B. Morris and J. Grizzle, "Hybrid invariant manifolds in systems with impulse effects with application to periodic locomotion in bipedal robots," *Automatic Control, IEEE Transactions on*, vol. 54, no. 8, pp. 1751–1764, Aug 2009.

[69] K. Sreenath, H.-W. Park, I. Poulakakis, and J. W. Grizzle, "Compliant hybrid zero dynamics controller for achieving stable, efficient and fast bipedal walking on MABEL," *The International Journal of Robotics Research*, vol. 30, no. 9, pp. 1170–1193, Aug. 2011.

[70] S. Collins, A. Ruina, R. Tedrake, and M. Wisse, "Efficient bipedal robots based on passive-dynamic walkers," *Science*, vol. 307, no. 5712, pp. 1082–1085, 2005.

[71] R. Tedrake, T. Zhang, and H. Seung, "Stochastic policy gradient reinforcement learning on a simple 3D biped," in *Intelligent Robots and Systems. Proceedings 2004 IEEE/RSJ International Conference on*, vol. 3, Sept 2004, pp. 2849–2854 vol.3.

[72] K. Byl and R. Tedrake, "Metastable walking machines," *The International Journal of Robotics Research*, vol. 28, no. 8, pp. 1040–1064, 2009.

[73] A. M. Johnson, S. A. Burden, and D. E. Koditschek, "A hybrid systems model for simple manipulation and self-manipulation systems," *The International Journal of Robotics Research*, vol. 35, no. 11, pp. 1354–1392, 2016.

[74] S. A. Burden, S. S. Sastry, D. E. Koditschek, and S. Revzen, "Event–selected vector field discontinuities yield piecewise–differentiable flows," *SIAM Journal on Applied Dynamical Systems*, vol. 15, no. 2, pp. 1227–1267, 2016.

[75] R. Vasudevan, *Hybrid System Identification via Switched System Optimal Control for Bipedal Robotic Walking*. Cham: Springer International Publishing, 2017, pp. 635–650.

[76] S. Veer, Rakesh, and I. Poulakakis, "Input-to-state stability of periodic orbits of systems with impulse effects via poincaré analysis," *arXiv preprint arXiv:1712.03291*, 2017.

[77] A. Hereid, C. M. Hubicki, E. A. Cousineau, and A. D. Ames, "Dynamic humanoid locomotion: A scalable formulation for HZD gait optimization," *IEEE Transactions on Robotics*, pp. 1–18, 2018.

[78] M. Posa, M. Tobenkin, and R. Tedrake, "Stability analysis and control of rigid-body systems with impacts and friction," *IEEE Transactions on Automatic Control*, vol. 61, no. 6, pp. 1423–1437, June 2016.

[79] E. Westervelt, J. Grizzle, and D. Koditschek, "Hybrid zero dynamics of planar biped walkers," *IEEE Transactions on Automatic Control*, vol. 48, no. 1, pp. 42–56, Jan 2003.

[80] E. Westervelt, J. Grizzle, C. Chevallereau, J. Choi, and B. Morris, *Feedback Control of Dynamic Bipedal Robot Locomotion*. Taylor & Francis/CRC, 2007.

[81] K. Akbari Hamed and J. W. Grizzle, "Reduced-order framework for exponential stabilization of periodic orbits on parameterized hybrid zero dynamics manifolds: Application to bipedal locomotion," *Nonlinear Analysis: Hybrid Systems*, vol. 25, pp. 227–245, August 2017.

[82] N. Sadati, G. Dumont, K. Akbari Hamed, and G. W.A., *Hybrid Control and Motion Planning of Dynamical Legged Locomotion*. Wiley-IEEE Press, October 2012.

[83] K. Akbari Hamed, B. Buss, and J. Grizzle, "Exponentially stabilizing continuous-time controllers for periodic orbits of hybrid systems: Application to bipedal locomotion with ground height variations," *The International Journal of Robotics Research*, vol. 35, no. 8, pp. 977–999, 2016.

[84] S. Kolathaya, J. Reher, A. Hereid, , and A. D. Ames, "Input to state stabilizing control Lyapunov functions for robust bipedal robotic locomotion," in *Proceedings of the American Control Conference*, 2018. [Online]. Available: http://ames.caltech.edu/akbari2018exponentially.pdf

[85] S. Kolathaya and A. D. Ames, "Parameter to state stability of control Lyapunov functions for hybrid system models of robots," *Nonlinear Analysis: Hybrid Systems*, vol. 25, pp. 174–191, 2017. [Online]. Available: http://ames.caltech.edu/kolathaya2017parameter.pdf

[86] A. Shiriaev, L. Freidovich, and S. Gusev, "Transverse linearization for controlled mechanical systems with several passive degrees of freedom," *Automatic Control, IEEE Transactions on*, vol. 55, no. 4, pp. 893–906, April 2010.

[87] A. D. Ames, R. D. Gregg, E. D. B. Wendel, and S. Sastry, "On the geometric reduction of controlled three-dimensional bipedal robotic walkers," in *Lagrangian and Hamiltonian Methods for Nonlinear Control 2006*. Berlin, Heidelberg: Springer Berlin Heidelberg, 2007, pp. 183–196.

[88] A. Ames and S. Sastry, "Hybrid geometric reduction of hybrid systems," in *Decision and Control, 45th IEEE Conference on*, Dec 2006, pp. 923–929.

[89] A. Ames, R. W. Sinnet, and E. D. Wendel, "Three-dimensional kneed bipedal walking: A hybrid geometric approach," in *Hybrid Systems: Computation and Control*, ser. Lecture Notes in Computer Science, R. Majumdar and P. Tabuada, Eds. Springer Berlin Heidelberg, 2009, vol. 5469, pp. 16–30.

[90] R. D. Gregg and M. W. Spong, "Reduction-based control of three-dimensional bipedal walking robots," *The International Journal of Robotics Research*, vol. 29, no. 6, pp. 680–702, May 2010.

[91] I. M. L. Freidovich, A. Shiriaev, "Stability analysis and control design for an underactuated walking robot via computation of a transverse linearization," 07 2008, pp. 10 166–10 171.

[92] A. D. Ames and S. Sastry, "Hybrid routhian reduction of lagrangian hybrid systems," in *2006 American Control Conference*, 2006, pp. 6 pp.–.

[93] A. D. Ames, R. D. Gregg, E. D. B. Wendel, and S. Sastry, "On the geometric reduction of controlled three-dimensional bipedal robotic walkers," in *3rd Workshop on Lagrangian and Hamiltonian Methods for Nonlinear Control*, 2006. [Online]. Available: http://ames.caltech.edu/BipedReduction.pdf

[94] R. Gregg and M. Spong, "Reduction-based control of branched chains: Application to three-dimensional bipedal torso robots," in *Decision and Control, 2009 held jointly with the 2009 28th Chinese Control Conference. CDC/CCC 2009. Proceedings of the 48th IEEE Conference on*, Dec 2009, pp. 8166–8173.

[95] K. McGeer, "Passive dynamic walking," *Int. J. Robot. Res.*, vol. 9, no. 2, pp. 62–82, 1990.

[96] A. Goswami, B. Espiau, and A. Keramane, "Limit cycles in a passive compass gaitbiped and passivity-mimicking control laws," *Autonomous Robots*, vol. 4, pp. 273–286, 07 1997.

[97] M. Garcia, A. Chatterjee, A. Ruina, and M. Coleman, "The simplest walking model: Stability, complexity, and scaling," *Journal of biomechanical engineering*, vol. 120, pp. 281–8, 04 1998.

[98] A. Goswami, B. Thuilot, and B. Espiau, "A study of the passive gait of a compass-like biped robot: Symmetry and chaos," *The International Journal of Robotics Research*, vol. 17, no. 12, pp. 1282–1301, 1998.

[99] S. H. Collins, M. Wisse, and A. Ruina, "A three-dimensional passivedynamic walking robot with two legs and knees," *Int. J. Robot. Res.*, vol. 20, no. 7, pp. 607–615, 2001.

[100] M. W. Spong, "Bipedal locomotion, robot gymnastics, and and robot air hockey: A rapprochement," 1999, pp. 34–41.

[101] ——, "Passivity based control of the compass gait biped," *IFAC Proceedings Volumes*, vol. 32, no. 2, pp. 506 – 510, 1999, 14th IFAC World Congress 1999, Beijing, Chia, 5-9 July. [Online]. Available: http://www.sciencedirect.com/science/article/pii/S1474667017560863

[102] H. Ohta, M. Yamakita, and K. Furuta, "From passive to active dynamic walking," in *Proceedings of the 38th IEEE Conference on Decision and Control (Cat. No.99CH36304)*, vol. 4, 1999, pp. 3883–3885 vol.4.

[103] L. Freidovich, U. Mettin, A. Shiriaev, and M. Spong, "A passive 2-DOF walker: Hunting for gaits using virtual holonomic constraints," *Robotics, IEEE Transactions on*, vol. 25, no. 5, pp. 1202–1208, Oct 2009.

[104] A. Isidori, *Nonlinear Control Systems*. Springer; 3rd edition, 1995.

[105] M. Maggiore and L. Consolini, "Virtual holonomic constraints for Euler Lagrange systems," *Automatic Control, IEEE Transactions on*, vol. 58, no. 4, pp. 1001–1008, April 2013.

[106] A. Mohammadi, M. Maggiore, and L. Consolini, "Dynamic virtual holonomic constraints for stabilization of closed orbits in underactuated mechanical systems," *Automatica*, vol. 94, pp. 112 – 124, 2018.

[107] A. E. Martin, D. C. Post, and J. P. Schmiedeler, "The effects of foot geometric properties on the gait of planar bipeds walking under HZD-based control," *The International Journal of Robotics Research*, vol. 33, no. 12, pp. 1530–1543, 2014.

[108] A. Ramezani, J. Hurst, K. Akbai Hamed, and J. Grizzle, "Performance analysis and feedback control of ATRIAS, a three-dimensional bipedal robot," *Journal of Dynamic Systems, Measurement, and Control December, ASME*, vol. 136, no. 2, December 2013.

[109] H.-W. Park, A. Ramezani, and J. Grizzle, "A finite-state machine for accommodating unexpected large ground-height variations in bipedal robot walking," *Robotics, IEEE Transactions on*, vol. 29, no. 2, pp. 331–345, April 2013.

[110] C. O. Saglam and K. Byl, "Meshing hybrid zero dynamics for rough terrain walking," in *2015 IEEE International Conference on Robotics and Automation (ICRA)*, May 2015, pp. 5718–5725.

[111] K. Sreenath, H.-W. Park, I. Poulakakis, and J. Grizzle, "Embedding active force control within the compliant hybrid zero dynamics to achieve stable, fast running on MABEL," *The International Journal of Robotics Research*, vol. 32, no. 3, pp. 324–345, 2013.

[112] A. Ames, "Human-inspired control of bipedal walking robots," *Automatic Control, IEEE Transactions on*, vol. 59, no. 5, pp. 1115–1130, May 2014.

[113] K. Akbari Hamed and A. D. Ames, "Nonholonomic hybrid zero dynamics for the stabilization of periodic orbits: Application to underactuated robotic walking," *IEEE Transactions on Control Systems Technology*, pp. 1–8, 2019.

[114] K. Akbari Hamed, N. Sadati, W. Gruver, and G. Dumont, "Stabilization of periodic orbits for planar walking with noninstantaneous double-support phase," *Systems, Man and Cybernetics, Part A: Systems and Humans, IEEE Transactions on*, vol. 42, no. 3, pp. 685–706, May 2012.

[115] R. Gregg, T. Lenzi, L. Hargrove, and J. Sensinger, "Virtual constraint control of a powered prosthetic leg: From simulation to experiments with transfemoral amputees," *Robotics, IEEE Transactions on*, vol. 30, no. 6, pp. 1455–1471, Dec 2014.

[116] H. Zhao, J. Horn, J. Reher, V. Paredes, and A. Ames, "Multicontact locomotion on transfemoral prostheses via hybrid system models and optimization-based control," *IEEE Transactions on Automation Science and Engineering*, vol. 13, no. 2, pp. 502–513, April 2016.

[117] A. Agrawal, O. Harib, A. Hereid, S. Finet, M. Masselin, L. Praly, A. Ames, K. Sreenath, and J. Grizzle, "First steps towards translating HZD control of bipedal robots to decentralized control of exoskeletons," *IEEE Access*, vol. 5, pp. 9919–9934, 2017.

[118] T. Gurriet, S. Finet, G. Boeris, A. Hereid, O. Harib, M. Masselin, J. W. Grizzle, and A. D. Ames, "Towards restoring locomotion for paraplegics: Realizing dynamically stable walking on exoskeletons," in *IEEE International Conference on Robotics and Automation (ICRA), https://web.eecs.umich.edu/faculty/grizzle/papers/exo_icra_2018Gurriet.pdf*, Accepted to Appear, 2018.

[119] O. Harib, A. Hereid, A. Agrawal, T. Gurriet, S. Finet, G. Boeris, A. Duburcq, M. E. Mungai, M. Masselin, A. D. Ames, K. Sreenath, and J. W. Grizzle, "Feedback control of an exoskeleton for paraplegics: Toward robustly stable hands-free dynamic walking," *IEEE Control Systems Magazine, arXiv preprint arXiv:1802.08322*, 2019, Accepted to Appear.

[120] K. Akbari Hamed, N. Sadati, W. Gruver, and G. Dumont, "Exponential stabilisation of periodic orbits for running of a three-dimensional monopedal robot," *Control Theory Applications, IET*, vol. 5, no. 11, pp. 1304–1320, July 2011.

[121] K. A. Hamed, W. Ma, and A. D. Ames, "Dynamically stable 3d quadrupedal walking with multi-domain hybrid system models and virtual constraint controllers," in *2019 American Control Conference (ACC)*, July 2019, pp. 4588–4595.

[122] W. Ma, K. A. Hamed, and A. D. Ames, "First steps towards full model based motion planning and control of quadrupeds: A hybrid zero dynamics approach," in *2019 IEEE/RSJ International Conference on Intelligent Robots and Systems (IROS)*, Nov 2019, pp. 5498–5503.

[123] S. Kolathaya, A. Hereid, and A. D. Ames, "Time dependent control Lyapunov functions and hybrid zero dynamics for stable robotic locomotion," in *2016 American Control Conference (ACC)*, July 2016, pp. 3916–3921.

[124] W. Ma, S. Kolathaya, E. R. Ambrose, C. M. Hubicki, and A. D. Ames, "Bipedal robotic running with DURUS-2D: Bridging the gap between theory and experiment," in *Proceedings of the 20th International Conference on Hybrid Systems: Computation and Control*. ACM, 2017, pp. 265–274. [Online]. Available: http://ames.caltech.edu/ma2017bipedal.pdf

[125] E. Aranda-Escolástico, M. Guinaldo, R. Heradio, J. Chacon, H. Vargas, J. Sánchez, and S. Dormido, "Event-based control: A bibliometric analysis of twenty years of research," *IEEE Access*, vol. 8, pp. 47 188–47 208, 2020.

[126] M. M. Ankarali and U. Saranli, "Control of underactuated planar pronking through an embedded spring-mass hopper template," *Autonomous Robots*, vol. 30, no. 2, pp. 217–231, February 2011.

[127] M. Buehler, D. E. Koditschek, and P. J. Kindlmann, "Planning and control of robotic juggling and catching tasks," *International Journal of Robotics Research*, vol. 13, no. 12, pp. 101–118, April 1994.

[128] S. G. Carver, N. J. Cowan, and J. M. Guckenheimer, "Lateral stability of the spring-mass hopper suggests a two-step control strategy for running," *Chaos*, vol. 19, no. 2, p. 026106, 2009.

[129] M. H. Raibert, "Legged robots," *Communications of the ACM*, vol. 29, no. 6, p. 499–514, 1986.

[130] C. D. Remy, "Optimal exploitation of natural dynamics in legged locomotion," Ph.D. dissertation, ETH Zurich, 2011.

[131] J. Seipel and P. Holmes, "A simple model for clock-actuated legged locomotion," *Regular and Chaotic Dynamics*, vol. 12, no. 5, pp. 502–520, October 2007.

[132] A. Seyfarth, H. Geyer, and H. Herr, "Swing-leg retraction: a simple control model for stable running," *The Journal of Experimental Biology*, vol. 206, no. 15, pp. 2547–2555, 2003.

[133] J. W. Grizzle, "Remarks on event-based stabilization of periodic orbits in systems with impulse effects," in *Second International Symposium on Communication, Control and Signal Processing*, 2006.

[134] M. Diehl, K. Mombaur, and D. Noll, "Stability optimization of hybrid periodic systems via a smooth criterion," *Automatic Control, IEEE Transactions on*, vol. 54, no. 8, pp. 1875–1880, Aug 2009.

[135] K. Akbari Hamed and R. D. Gregg, "Decentralized feedback controllers for robust stabilization of periodic orbits of hybrid systems: Application to bipedal walking," *Control Systems Technology, IEEE Transactions on*, vol. 25, no. 4, pp. 1153–1167, July 2017.

[136] A. Ames, E. Cousineau, and M. Powell, "Dynamically stable bipedal robotic walking with nao via human-inspired hybrid zero dynamics," 04 2012.

[137] H. Bock and K. Plitt, "A multiple shooting algorithm for direct solution of optimal control problems*," *IFAC Proceedings Volumes*, vol. 17, no. 2, pp. 1603 – 1608, 1984, 9th IFAC World Congress: A Bridge Between Control Science and Technology, Budapest, Hungary, 2-6 July 1984. [Online]. Available: http://www.sciencedirect.com/science/article/pii/S1474667017612059

[138] A. Hereid, C. M. Hubicki, E. A. Cousineau, J. W. Hurst, and A. D. Ames, "Hybrid zero dynamics based multiple shooting optimization with applications to robotic walking," in *2015 IEEE International Conference on Robotics and Automation (ICRA)*, 2015, pp. 5734–5740.

[139] A. Hereid, E. A. Cousineau, C. M. Hubicki, and A. D. Ames, "3d dynamic walking with underactuated humanoid robots: A direct collocation framework for optimizing hybrid zero dynamics," in *IEEE International Conference on Robotics and Automation (ICRA). IEEE*, 2016.

[140] M. Posa, S. Kuindersma, and R. Tedrake, "Optimization and stabilization of trajectories for constrained dynamical systems," in *2016 IEEE International Conference on Robotics and Automation (ICRA)*, May 2016, pp. 1366–1373.

[141] J. Carpentier, S. Tonneau, M. Naveau, O. Stasse, and N. Mansard, "A versatile and efficient pattern generator for generalized legged locomotion," in *2016 IEEE International Conference on Robotics and Automation (ICRA)*, May 2016, pp. 3555–3561.

[142] M. Kelly, "An introduction to trajectory optimization: How to do your own direct collocation," *SIAM Review*, vol. 59, no. 4, pp. 849–904, 2017. [Online]. Available: https://doi.org/10.1137/16M1062569

[143] A. Patel, S. Shield, S. Kazi, A. M. Johnson, and L. T. Biegler, "Contact-implicit trajectory optimization using orthogonal collocation," *arXiv preprint arXiv:1809.06436*, 2018.

[144] A. Hereid and A. D. Ames, "Frost: Fast robot optimization and simulation toolkit," in *IEEE/RSJ International Conference on Intelligent Robots and Systems (IROS)*. Vancouver, BC, Canada: IEEE/RSJ, Sep. 2017.

[145] H. Zhao, A. Hereid, E. Ambrose, and A. D. Ames, "3D multi-contact gait design for prostheses: Hybrid system models, virtual constraints and two-step direct collocation," in *Decision and Control (CDC), 2016 IEEE 55th Conference on*. IEEE, 2016, pp. 3668–3674.

[146] T. Parker and L. Chua, *Practical Numerical Algorithms for Chaotic Systems*. Springer, 1989.

[147] W. Haddad and V. Chellaboina, *Nonlinear Dynamical Systems and Control: A Lyapunov-Based Approach*. Princeton University Press, February 2008.

[148] W. Haddad, V. Chellaboina, and S. Nersesov, *Impulsive and Hybrid Dynamical Systems: Stability, Dissipativity, and Control*. Princeton University Press, July 2006.

[149] J. Martin, V. R. Kamidi, A. Pandala, R. Fawcett, and K. Akbari Hamed, "Exponentially stabilizing and time-varying virtual constraint controllers for dynamic quadrupedal bounding," Accepted to Appear, October 2020.

[150] J. Tan, T. Zhang, E. Coumans, A. Iscen, Y. Bai, D. Hafner, S. Bohez, and V. Vanhoucke, "Sim-to-real: Learning agile locomotion for quadruped robots," in *Robotics: Science and Systems (RSS)*, 2018.

[151] Y. Hurmuzlu and D. B. Marghitu, "Rigid body collisions of planar kinematic chains with multiple contact points," *The International Journal of Robotics Research*, vol. 13, no. 1, pp. 82–92, 1994.

[152] E. Westervelt, J. Grizzle, and C. De Wit, "Switching and pi control of walking motions of planar biped walkers," *Automatic Control, IEEE Transactions on*, vol. 48, no. 2, pp. 308–312, Feb 2003.

[153] V. Arnold, *Geometrical Methods in the Theory of Ordinary Differential Equations*. Springer; 2nd edition, November 1996.

[154] (2018) FROST: Fast Robot Optimization and Simulation Toolkit, https://ayonga.github.io/frost-dev/index.html.

[155] A. Wächter and L. T. Biegler, "On the implementation of an interior-point filter line-search algorithm for large-scale nonlinear programming," *Mathematical programming*, vol. 106, no. 1, pp. 25–57, 2006.

[156] Y. A., "Dynamic humanoid locomotion: Hybrid zero dynamics based gait optimization via direct collocation methods," Ph.D. dissertation, Georgia Institute of Technology, 2016.

[157] R. H. Byrd, G. Liu, and J. Nocedal, "On the local behavior of an interior point method for nonlinear programming," *Numerical Analysis*, pp. 37–56, 1997.

[158] J. Nocedal, "Updating quasi-newton matrices with limited storage," *Mathematics of Computation*, vol. 35, no. 151, pp. 773–782, 1980. [Online]. Available: http://www.jstor.org/stable/2006193